ADVANCED OPTICAL MATERIALS
www.advopticalmat.de

Semiconductor Thin Film Based Metasurfaces and Metamaterials for Photovoltaic and Photoelectrochemical Water Splitting Applications

*Amir Ghobadi, Turkan Gamze Ulusoy Ghobadi, Ferdi Karadas, and Ekmel Ozbay**

In both photovoltaic (PV) and photoelectrochemical water splitting (PEC-WS) solar conversion devices, the ultimate aim is to design highly efficient, low cost, and large-scale compatible cells. To achieve this goal, the main step is the efficient coupling of light into active layer. This can be obtained in bulky semiconductor-based designs where the active layer thickness is larger than light penetration depth. However, most low-bandgap semiconductors have a carrier diffusion length much smaller than the light penetration depth. Thus, photogenerated electron–hole pairs will recombine within the semiconductor bulk. Therefore, an efficient design should fully harvest light in dimensions in the order of the carriers' diffusion length to maximize their collection probability. For this aim, in recent years, many studies based on metasurfaces and metamaterials were conducted to obtain broadband and near-unity light absorption in subwavelength ultrathin semiconductor thicknesses. This review summarizes these strategies in five main categories: light trapping based on i) strong interference in planar multilayer cavities, ii) metal nanounits, iii) dielectric units, iv) designed semiconductor units, and v) trapping scaffolds. The review highlights recent studies in which an ultrathin active layer has been coupled to the above-mentioned trapping schemes to maximize the cell optical performance.

1. Introduction

The main goal in solar energy harvesting devices is to design a low-cost sustainable and efficient architecture as well as elementally earth abundant materials to have high manufacturing throughput and large-scale compatibility. The photoactive material is generally composed of single or multiple semiconductor layers responsible for harvesting solar energy. This harvested solar irradiation can be used to generate electricity using photovoltaic (PV) devices, or it can be converted to chemical energy in the form of hydrogen which is the case for photoelectrochemical water splitting (PEC-WS). In both PV and PEC-WS applications, the ultimate goal is to establish an efficient photon capturing and electron collecting scheme to generate a huge number of photocarriers (including electron–hole pairs) with rational carrier dynamics (efficient charge generation, separation, and collection). This means that the device should be optically thick enough to generate high carrier's density and electrically thin enough to collect photogenerated carrier before they recombine. When light impinges a semiconductor surface, a part of the light is reflected back due to the mismatch between the air and the semiconductor layer refractive index. The rest will propagate within the bulk until it is fully absorbed by the semiconductor slab. The optical penetration depth (LPD) is defined as the depth at which the incident power falls to $1/e$ (≈37%) of its input value. This parameter differs from one semiconductor to another and it depends on the extinction coefficient (κ) of the

A. Ghobadi, Prof. E. Ozbay
NANOTAM—Nanotechnology Research Center
Bilkent University
Ankara 06800, Turkey
E-mail: ozbay@bilkent.edu.tr
A. Ghobadi, Prof. E. Ozbay
Department of Electrical and Electronics Engineering
Bilkent University
Ankara 06800, Turkey
T. G. Ulusoy Ghobadi, Prof. F. Karadas
UNAM—National Nanotechnology Research Center
Institute of Materials Science and Nanotechnology
Bilkent University
Ankara 06800, Turkey
T. G. Ulusoy Ghobadi
Department of Energy Engineering
Faculty of Engineering
Ankara University
Ankara 06830, Turkey
Prof. F. Karadas
Department of Chemistry
Faculty of Science
Bilkent University
Ankara 06800, Turkey
Prof. E. Ozbay
Department of Physics
Bilkent University
Ankara 06800, Turkey
The ORCID identification number(s) for the author(s) of this article can be found under https://doi.org/10.1002/adom.201900028.

DOI: 10.1002/adom.201900028

material (which is the imaginary part of the complex refractive index). The values of LPD are plotted in **Figure 1**a–c, for different semiconductor materials at three different visible wavelengths of $\lambda = 400$, 500, and 600 nm. As it can be deduced from these panels, to harvest the whole penetrated light, a minimal slab thickness of a couple hundred nanometers is required, for most of semiconductors. However, to maximize the carrier collection capability of the design, the semiconductor layer should be thinner than the carrier diffusion length. The carrier diffusion length (LD) is the length that a carrier can transport without being recombined. LD is an inherent property of semiconductor material and it mainly depends on the crystallinity phase of the layer. However, for most semiconductors, LD is much smaller than LPD. Thus, it is essential to propose a design architecture to absorb light in dimensions much smaller than the LPD. However, this cannot be satisfied using a conventional design in such thin layers. Absorption coefficient, α, cannot be improved using synergetic effects; it is an inherent property of material. However, this deficiency can be significantly suppressed by using light trapping nanostructures. This could be achieved using ultrathin semiconductor based metasurface and metamaterial designs. Metamaterials refer to a class of synthetic materials comprising designed inclusions with exotic properties that cannot be attained using natural ones. The concept of light confinement and its harvesting using subwavelength architectures has been one of the most studied applications of metamaterials. These designed architectures can go beyond the inherent limitations of conventional optoelectronic devices. Semiconductor nanostructuring is an efficient way to increase the light harvesting property of the material and many great reviews have already covered these design strategies in different optoelectronic applications.[1–5] Generally speaking, in this design strategy, the nanostructured surface will simultaneously suppress light reflection and increase light coupling into the underlying bulk active layer. Thus, the above-mentioned architectures are generally bulky designs. For some of single-crystalline semiconductor materials such as Si or GaAs with LD values in the order of hundreds of micrometers, this is an efficient approach to maximize the photoconversion efficiency of the cell. However, for the most of semiconductors, the LD is much shorter than the LPD and therefore nanostructuring is the best solution. Even for semiconductors with large LD, this length is significantly shortened if we move to poly-crystalline or amorphous phases. Thus, for a wise design, it is of great importance to keep active layer thickness as thin as carrier's diffusion length. Thus, this review will not cover those bulky nanostructuring ideas. The main motivation of this review is to find the strategies in which light perfect absorption can occur in thin active layer dimensions (rather than the bulk ones). This review will provide a comprehensive study on the design of efficient light harvesting devices using thin semiconductor layers. In other words, we will study how different 2D metasurface and 3D metamaterial-based trapping schemes can efficiently couple light into a thin semiconductor layer. Near perfect harvesting of solar irradiation in a broad spectral range in such thin semiconductor layer geometries could lead to the realization of highly efficient, cost effective, and large scale compatible PV and PEC-WS devices. In the following sections, we will categorize the different trapping schemes and scrutinize their use in light

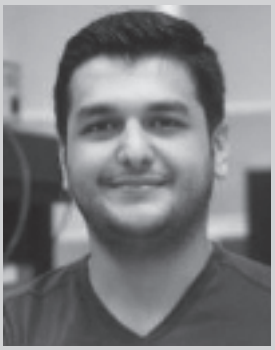

Amir Ghobadi obtained his B.S. degree in electrical engineering from the University of Tehran, Iran in 2012. He obtained his M.S. degree from the same department at Bilkent University in 2014. Currently, he is working toward his Ph.D. under the supervision of Prof. Ekmel Ozbay at Bilkent University. His research involves the design, synthesis, and characterization of novel semiconductor-based optic and photonic devices.

Turkan Gamze Ulusoy Ghobadi received her B.S. degree in chemical engineering from Ankara University, Turkey in 2012. She joined the National Nanotechnology Research Center (UNAM), Institute of Materials Science and Nanotechnology, Bilkent University, Turkey and obtained an M.S. degree in 2015. Currently, she is pursuing her Ph.D. degree in the same department under the guidance of Asst. Prof. Ferdi Karadas from the Chemistry Department. She became a research assistant in the Department of Energy Engineering at Ankara University in 2017. Her current research interests focus on the development of (photo)electrochemical materials for energy storage and conversion systems.

Ekmel Ozbay obtained M.S. and Ph.D. degrees in electrical engineering from Stanford University in 1989 and 1992, respectively. He worked as a postdoctoral research associate at Stanford University and as a scientist at Iowa State University. He joined Bilkent University (Ankara, Turkey) in 1995, where he is currently a full professor in the Physics Department and EEE Department. In 2003, he founded the Bilkent University Nanotechnology Research Center (NANOTAM) where he leads a research group working on nanophotonics, nanometamaterials, nanoelectronics, GaN/AlGaN MOCVD growth, and GaN based devices. Recently he became the CEO of a spin-off company: AB-MicroNano Inc. He has published 420+ articles in SCI journals (with an SCI h-index of 70), including a Science paper on plasmonics.

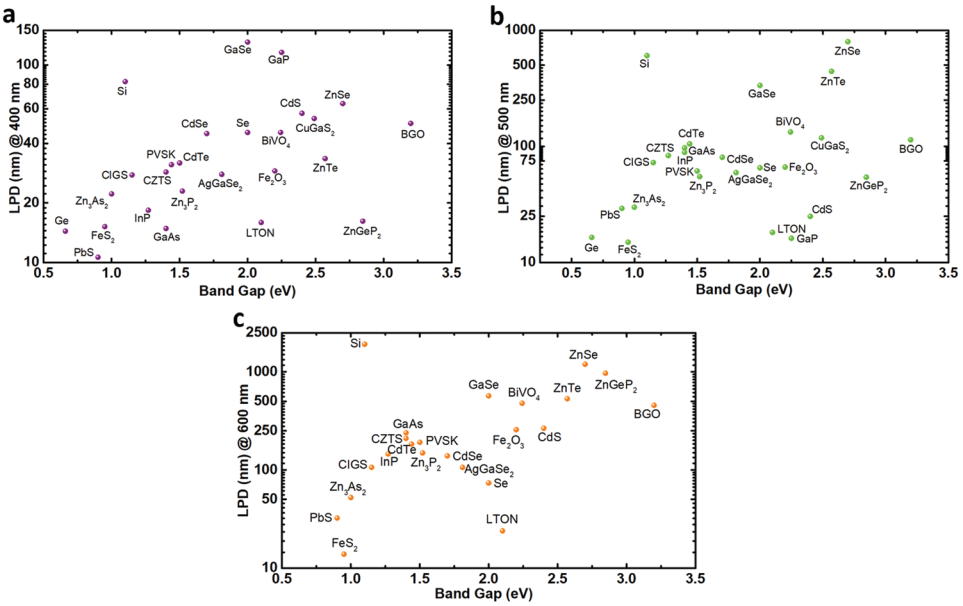

Figure 1. The light penetration depth (LPD) for different types of semiconductors at three different wavelengths of a) 400 nm, b) 500 nm, and c) 600 nm. The *x*-axis represents the optical bandgap of the semiconductors. In this figure LTON stands for $LaTiO_2N$ and BGO stands for $BiGeO_{20}$.

harvesting devices. Finally, we will provide an outlook to highlight the future direction of these ultrathin metadesigns.

2. Light Trapping Schemes

2.1. Light Trapping Based on Strong Interference in Planar Multilayer Cavities

Strong interference in metal-lossy layer interface could provide the condition to obtain perfect light absorption in dimensions much smaller than the light wavelength. This phenomenon offers the opportunity to use planar lithography-free multilayer designs for ultrathin optoelectronic applications. These multilayer resonant absorbers have been realized in different types of materials and spectral regions. The most common materials for realization of light perfect absorption are metals. It was shown that the use of lossy metals such as Cr, in a metal–insulator–metal (MIM) configuration, can provide light perfect absorption from 450 to 850 nm.[6] This absorption can be further improved by introduction of an insulator layer on top of this cavity which acts as a broadband antireflective coating. The use of metal–insulator-metal–insulator (MIMI) configuration enhances the absorption bandwidth (BW) toward longer wavelength values.[7,8] Different metal–insulator combinations were utilized to obtain ultrabroadband light absorption from these multilayer designs. W-Al_2O_3,[9] Cr-SiO_2,[8] W-SiO_2,[8] Mo-SiO_2,[8] Ag-Si,[10] Bi-LiF,[11] and Ni-SiO_2[12] are some examples of these MI pairs to obtain perfect broadband absorption. Further improvements can be also achieved using different strategies; excitation of multiple modes in a multithickness absorbing layer,[13] reducing the effective permittivity of metals via their composition with air,[14,15] the optimal selection of materials to maximize absorption BW[16] are some examples of these strategies. A recent perspective by our group reviews strong light-matter interaction in lithography-free planar perfect absorbers.[17] It was shown, upon choice of proper material and configuration, this absorbing behavior can be realized in almost all parts of electromagnetic (EM) spectrum. Although the common materials for the design of multilayer absorber metasurfaces are metals, this strong interference can also be found in semiconductors in the photon energies above their optical bandgap.[18,19]

The simplest way to increase the absorption of an ultrathin semiconductor slab is to introduce a back-reflecting metal mirror. This metal layer reflects the light back into the slab and increases the optical path of the light inside the medium. If the impedance matching condition can be satisfied, we can trap the light inside the layer and fully harvest it in the resonance wavelength. This is called Fabry-Perot (FP) resonance. The spectral position of FP resonance in metal–semiconductor (MS) configuration is a function of semiconductor's refractive index, extinction coefficient, and thickness. To gain insight on the ideal condition to obtain strong light absorption, the transfer matrix method (TMM) is utilized.[17,20,21] Using this modeling approach, the bottom layer is chosen as an optically thick metal layer. The bottom mirror is chosen as Al which has relatively flat high reflection throughout the whole visible range. Then, the ideal absorption region (absorption near unity or reflection near zero) is extracted for three different slab thicknesses (D_S) of 3, 10, and 30 nm. The threshold for absorption is chosen as 0.8 (where reflection is below 0.2). It should be noted that the upper scale of the color bar have been set as 0.25 to provide a better visualization for the borders of 0.2 reflection. These ideal regions are compared with the refractive index (n) and extinction coefficient (k) data of typical semiconductors, as shown in **Figure 2**a–c. As depicted in these panels, the reflection counter plots are made of centric circles and being located inside this colored region means an absorption above 0.8 (reflection below 0.2). These ideal regions are extracted from three visible light

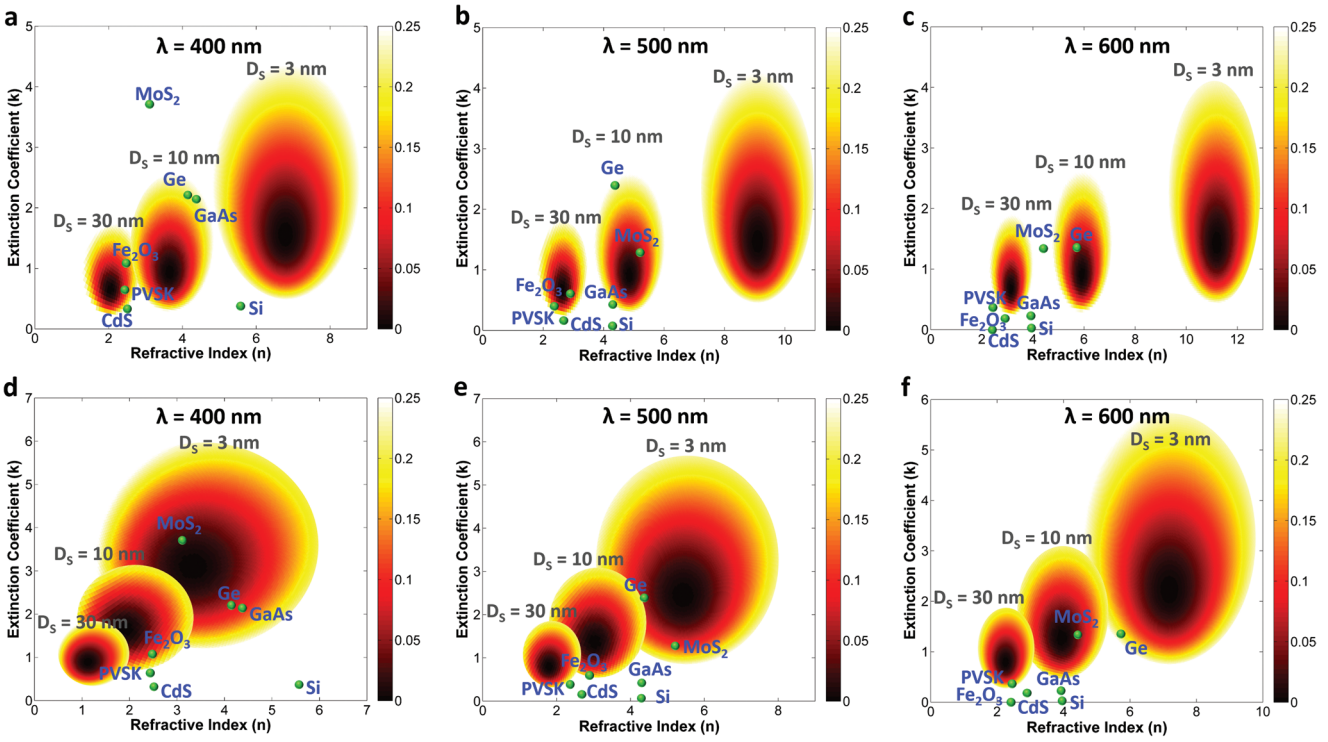

Figure 2. The reflection contour plot for an MS cavity design at three different wavelength values of a) 400 nm, b) 500 nm, and c) 600 nm. d–f) Similar plot for an MOS junction with a TiO_2 spacer layer of 20 nm. In all of the panels, the largest circle belongs to a D_S of 3 nm, the middle one is for 10 nm, and the smallest circle is the ideal data for 30 nm thick ideal absorber. These ideal *n* and *k* regions are compared with those of typical visible active semiconductors.

wavelengths of 400, 500, and 600 nm. As shown in Figure 1a–c, the ideal circular patterns for a 3 nm thick layer is located at high *n* and *k* values that cannot be satisfied with common natural semiconductors. Therefore, as can be deduced from these panels, none of the semiconductors are matched with this ideal region. By increasing the slab thickness to 10 and 30 nm, the ideal *n*, *k* circles shift toward smaller values but, in the meantime, their radii get smaller. According to these contour plots, high refractive index semiconductors, such as germanium (Ge) and molybdenum disulfide (MoS_2), can show strong interference at a relatively moderate thickness of 10 nm. However, other materials with smaller *n* and *k* values, such as oxides and organic semiconductors need a larger thickness to have strong absorption. For instance, Ge *n* and *k* data have located inside ideal region circles for a 10 nm thick layer in all three wavelengths of 400, 500, and 600 nm. While for hematite (α-Fe_2O_3), this matching is achieved for a thicker layer of 30 nm. These findings are in line with previous studies. Kats et al. showed strong interface effects in an Au-Ge MS structure in which the spectral position of reflection dip is tuned by Ge thickness.[19] It has been proven later on that this MS configuration can go beyond the Yablonovitch limit.[22] This strong absorption has been also detected in a couple of tens of nanometer thick MoS_2 layer on top of Au/Ag mirror.[23] Later, a proof-of-concept device has been made to reveal the potential of ultrathin transition metal dichalcogenides (TMDs) for energy conversion applications.[24] A 22 nm thick Fe_2O_3 on Ag mirror has also been shown to have strong light absorption at $\lambda < 450$ nm.[25] Similar optical responses have been realized for another type of metals and semiconductors.[26,27] This strong interference is not only probed in semiconductor based cavity designs but also excitonic thin films, such as dyes and organic molecules, and could also show light perfect absorption.[28,29] The optical response of these organic materials (*n* and *k* values) can be controlled with the change in the aggregate concentration. Thus, the optical response of the cavity can be easily tailored. It should be mentioned that the use of lossy metals as the reflector layer could make this interference effects stronger. This has been studied for many different MS configurations, specifically for color filter applications.[26,27,30] It was shown that an ultrathin Si layer on different metal types, such as Au, Ag, Cr, and Ti, has quite different absorption responses. In general, the low loss metals, such as Au, Ag, and Al, provide perfect absorption condition in a relatively narrow spectral range while lossy ones offer a broad absorption BW. However, when it comes to photovoltaic and photochemistry, our goal is to maximize absorption in the semiconductor layer (rather than the back metal). Therefore, the use of low loss highly reflective metals, such as Au, Ag, and Al, is desired. Moreover, the main goal in the design of an efficient semiconductor based metasurface is to achieve near unity absorption in the thinnest possible layer and broadest wavelength regime. This could be achieved by the introduction of metal–oxide–semiconductor (MOS) configuration. The spacer layer, which is the transparent oxide layer in the MOS configuration, can be counted as a new parameter to tune the absorption strength and BW of the metasurface design. Similar to the case of MS configuration, the ideal regions have been extracted for the case of MOS cavity (Figure 2d–f). The spacer layer is set

as titanium dioxide (TiO_2) with a thickness of 20 nm, which is much smaller than the incident visible light wavelength and, consequently, it could make a destructive interference between the electromagnetic fields at the top surface to trap the incident light. Compared to MS configuration, embedding a transparent oxide between metal and semiconductor coatings can shift the ideal absorbing region toward smaller refractive index values. Moreover, the circle sizes become larger and this in turn enhances the probability of matching between the ideal area and the semiconductor refractive index data. As we can see in Figure 2d–f, unlike MS cavity design, MOS configuration can provide strong light-matter interaction in thicknesses as thin as 3 nm. The matching is retained for 3 nm thick Ge in all three different wavelengths. This is in agreement with the experimental findings of an earlier study where the authors improved the absorption BW and strength by the introduction of a silicon dioxide (SiO_2) transparent oxide between Au and Ge layers.[31] As already explained, the oxide layer with a thickness much smaller than the incident light wavelength can broaden the absorption BW. In the meantime, thicker spacer layers could offer a quarter wavelength matching condition. In this case, the destructive interference only occurs in a narrow wavelength range and this can be used to obtain spectrally selective light absorption. A recent study demonstrated the realization of efficient and ultrathin MOS cavities based on single crystalline Ge for spectrally selective photodetector applications.[32] This strong light-matter interaction for an MOS design is specifically important for 2D semiconductors, such as TMDs. That is because the excitonic response of these materials is improved as they are thinned down to atomic levels. While 3 nm thick MoS_2 (which corresponds two an approximately five-layer thick) has weak matching condition with the ideal region in the MS configuration, its utilization in an MOS configuration can lead to nearly perfect absorption in both 400 and 500 nm incident lights. It has been shown that an Ag-MgF_2-(four-layer) MoS_2 cavity can have near unity absorption from 550 up to 700 nm.[33] A similar functionality has been also found in other type of semiconductors such as hematite. The optimal thickness for this material in an MOS cavity configuration is found to be 10 nm, which is much thinner compared to the optimum thickness of 30 nm for MS case. It should be noted that another resonant configuration is based on metal–semiconductor–oxide (MSO) design. In this architecture, the top oxide layer acts as an antireflective (AR) coating to match the air impedance into underneath the MS cavity. Based on the thickness and refractive index of this AR coating, one could obtain broad or narrow absorption peak. This has been explored in a previous study for the case of Ge and the monolayer of MoS_2.[34,35] Therefore, all of these aforementioned theoretical findings can be viewed from two main perspectives; first, the MOS structure, with one more degree of freedom, could be designed in a way to obtain a stronger and broader absorption response that is necessary for energy conversion applications. Second, the absorption of light in thinner semiconductor thicknesses (as in the case of MOS cavity) could promote the collection probability of the carriers. As an instance, the main limiting factor for α-Fe_2O_3 based water splitting photoanodes is their short hole diffusion length (below 20 nm).[36] Therefore, the absorption of the light in dimensions smaller than this thickness could significantly enhance photogenerated holes participation in water oxidation reaction. In addition, this oxide layer could act as an electron (or hole) transport layer. The proper band alignment at the interface of the top semiconductor and the oxide spacer can spatially separate carriers and consequently prolong their lifetime. This ultrathin spacer layer has also been found to enhance the efficiency of the organic solar cells by its simultaneous role in improving the electrical and optical behavior of the cell.[37]

Similar to the former design, a part of the incident light power can be consumed in the metal layer. This could be mitigated by using photonic crystal (PC) based back reflector. A PC is made of an alternative arrangement of lossless high and low index transparent multilayers. This architecture has been used as the mirror layer to maximize the light absorption inside the semiconductor slab.[38,39] However, this is not the only way to use PCs for efficient light trapping. With such a hybrid multilayer structure, optical Tamm resonance (which is also called surface state) can be excited near the PC and absorbing layer interface.[40] The intense Tamm resonance modes can bring a strong field localization to the incident photon energy, enabling light perfect absorption in sub-nanometer thick semiconductor layers. This design has been intensively employed for 2D semiconductors, such as TMDs. It was found that a 1D PC on top of an MoS_2 monolayer, with a back reflecting mirror, can efficiently couple the incident light into MoS_2 monolayer within a narrow wavelength range.[41] The coupled field is harvested by MoS_2 layer with an amplitude as high as 96%. The use of finite all-dielectric random PC has also been proven to provide strong field localization which enables about 99.9% light perfect absorption by MoS_2 monolayer in its resonance wavelength, due to Anderson localization.[42] As already proven, in the theoretical section, both MS and MOS junctions cannot satisfy the strong interference effects for semiconductor thicknesses as thin as a monolayer TMD. In other words, realization of light perfect absorption in single TMD layer is not possible using these design cavities. Therefore, for the application of 2D PV and photodetection, the use of PC based design architecture could be of great interest. However, PC designs operate in a narrow spectral range and a broadening in the absorption BW of the design is required to maximize the utilization of solar spectrum. A photodetector based on the monolayer of MoS_2 embedded in chirped Bragg reflectors exhibit broadband coherent light absorption that can harvest 33% of incident visible light over a 300 nm BW.[43] Wu and co-workers have theoretically demonstrated a broadband near unity light absorption, covering the whole visible range, in a graphene-monolayer MoS_2 photovoltaic cell.[44] The absorbing monolayer is located inside a wedge-shaped microcavity with a spectrum-splitting. Although this PC based design can be envisioned as a promising strategy to maximize 2D photovoltaic efficiency, it has a complex fabrication route due to the required multiple processing steps. At the expense of losing the absorption strength, a more feasible way was recently proposed where this atomically thin double layer cell is placed inside a metal-based wedge-shape cavity.[45]

Employing these simple resonant designs, other innovative planar and lithography-free structures have been utilized for PV and PEC-WS applications. In one of the pioneer studies, it was proven that a predesigned cavity with an impedance

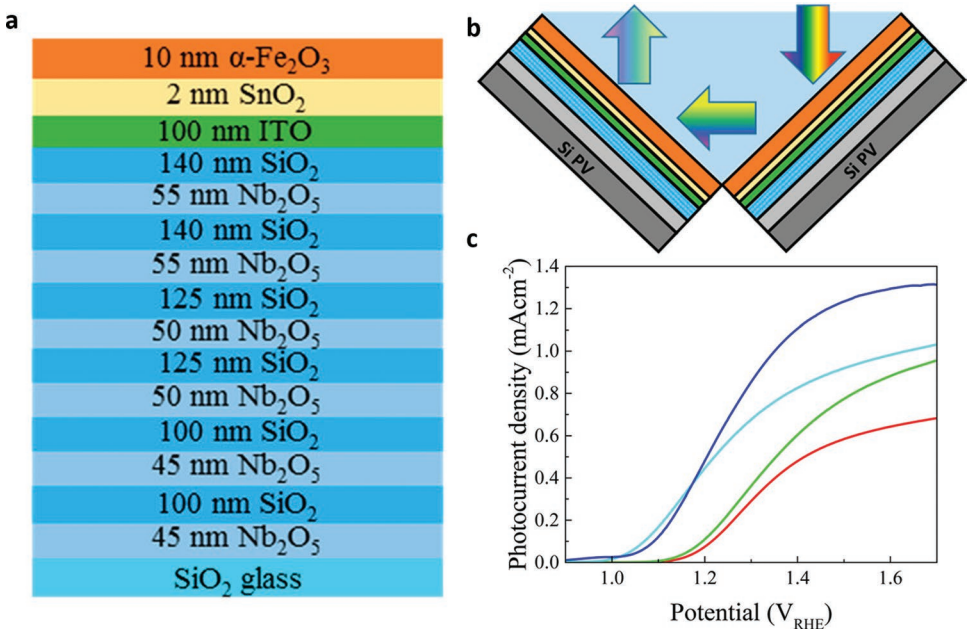

Figure 3. a) Schematic representation of the proposed PC based photoanode. b) The 90° V-shaped cell configuration for enhancing light absorption. c) The Photocurrent voltammograms of photoanodes in planar configuration (red), with PC mirror in planar configuration (green), with PC mirror and cocatalyst overlayer in planar configuration (cyan), and two photoanodes with PC mirror and cocatalyst overlayer facing each other in the 90° V-shaped cell configuration. Reproduced with permission.[49] Copyright 2018, American Chemical Society.

match reflector can significantly enhance light absorption in the ultrathin α-Fe_2O_3 layer.[46] Employing this design strategy, a 71% above bandgap absorption can be attained in a layer as thin as 50 nm. The authors substantiated the photoresponse of the cell by Ti doping. Atomic layer deposition (ALD) of 25 nm thick α-Fe_2O_3 on Pt substrate with a thin TiO_2 protection layer has been also demonstrated as an ultrathin efficient photoanode.[47] It was found that the proposed design can have a photocurrent density as high as 1.014 mA cm^{-2} at 1.4 V (vs RHE) and a maximum external quantum efficiency (EQE) of 20.1% at 370 nm for an applied bias of 1.23 V_{RHE}. Similar performance enhancement was recorded for an Au-Fe_2O_3 heterostructure.[48] A most recent paper proved an efficient design based on PC mirror in 10 nm thick α-Fe_2O_3 based MOS cavity. The proposed multilayer structure is depicted in **Figure 3**a.[49] In this study, the authors were able to obtain highly efficient PEC-WS photoanode using an active layer dimensions smaller than the hole diffusion length. To further improve the activity of the design, two photoanodes were placed face to face with an angle of 90°, as shown in Figure 3b, to harvest incident light as strongly as possible. In this case, the optical path of the light is significantly increased and more photons are captured. A substantial improvement was also achieved by introducing a cocatalyst on top of the active layer. The photocurrent spectra for all the different design configurations have been depicted in Figure 3c. As this figure implies, the use of bottom PC mirror has increased the photocurrent of reference bare sample, mainly in the plateau region (at 1.6 V_{RHE}). Adding the cocatalyst has improved both photocurrent value and shifts the onset potential by 130 mV. Finally, combination of PC mirror, cocatalyst, and wedge configuration has increased the photocurrent by an order larger than two (compared to reference cell) at 1.6 V_{RHE}. This improvement is as high as four folds at the reversible potential of water oxidation, 1.23 V_{RHE}. Apart from ALD and other similar processes that are conducted in low temperatures, the common fabrication route for narrow bandgap oxide semiconductors involves a high temperature process to improve layer crystallinity.[50] For instance, the annealing temperature for α-Fe_2O_3 is typically around 800 °C which is close to the melting point of most noble metals. Therefore, the specular reflectivity of the bottom mirror can be diminished during this annealing step. Recently, a film flip and transfer process was adopted to enable the deposition of bottom mirror after the annealing process.[51] This process has been schematically depicted in **Figure 4**a. Similar to the above-mentioned study, homogeneous Ti doping was employed to further improve the electrical properties of the α-Fe_2O_3 layer. As shown in the Figure 4b,c, the BW of the spectral region with near zero reflection is widened as we increase the α-Fe_2O_3 layer thickness. This is in line with our theoretical findings in Figure 2. Moreover, as these panels imply, the adding of cocatalyst does not significantly change the absorption property of the design. While the theoretical results estimated the highest absorption in a 20 nm thick semiconductor layer, the highest photocurrent values were obtained for an 8 nm thick layer, see Figure 4b. This was mainly due to the short hole diffusion length of the hematite layer where photocarriers generated far from the surface cannot participate in the water oxidation process. The response was gradually improved by adding a cocatalyst into the system. This deficiency was further lessened by heterogeneous doping with the 1 cat% Zn—undoped—1 cat% Ti profile (cat.; cation fraction). As shown in Figure 4c, this modification led to a 1.01 mA cm^{-2} photocurrent in reversible potential of water oxidation (1.23 V vs RHE) for a 14 nm thick active layer. The Spalling process has also been

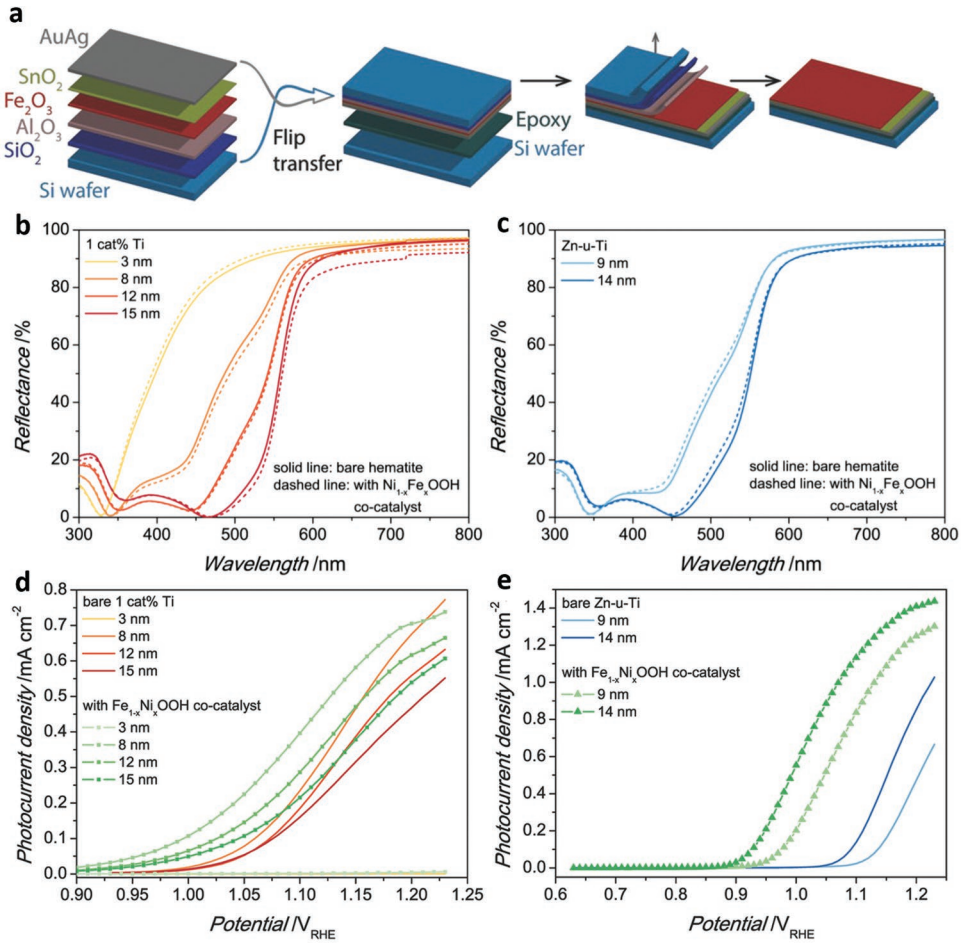

Figure 4. a) The steps to fabricate Hematite based MOS cavity, b,c) the reflection spectra for MS cavities with different Hematite layer thicknesses, and d,e) the photocurrent values of the photoanode for different semiconductor layer thicknesses and doping conditions. Reproduced with permission.[51] Copyright 2018, Wiley-VCH.

demonstrated as an efficient way to make metal backed single crystalline ultrathin semiconductor layers. The use of Si and GaAs, as single crystalline semiconductor layers, in this configuration could offer a high efficiency photocathode.[52]

A similar story can be followed for these impedance matching metasurfaces in PV applications. In an earlier study on the application of these resonant designs in PV, a 13 nm thick amorphous germanium (a-Ge) layer was sandwiched between two ultrathin n- and p-doped amorphous silicon (a-Si) coatings,[53] see **Figure 5**a. As can be clearly seen in Figure 5b, it was found that the conversion efficiency in such an ultrathin solar cell design can be as high as 3.6%. Considering the small k values for the silicon layer (compared to its refractive index *n*) in the visible range, this configuration can be considered as an MOS cavity that has been capped with an AR coating (a-Si/TCO/glass). Therefore, based on our theoretical findings, the strong interference is achieved in a specific active layer thickness. Simulated EQE data reveals that the optimal a-Ge layer thickness of 15 nm can provide an EQE of ≈80% in a broad range of 500–800 nm, see Figure 5c. The experimental data also show a maximum EQE of 60% at around 600 nm wavelength (Figure 5d). Another common semiconductor material for PV applications is a-Si that has a compatible fabrication route for both MS and MOS configurations. A typical high efficiency a-Si based solar cell has an active layer thickness of 100–300 nm. However, the carrier diffusion length is much smaller than this thickness that makes the carrier collection efficiency low. Therefore, squeezing light absorption in dimensions as thin as the carrier's diffusion length could be a prominent feature for the design of high-performance solar cells. Moreover, unlike thick a-Si based solar cells that have a dark appearance, these MS pairs based metasurface designs can act as reflective or transmissive color filters. This is highly desired for decorative purposes in both interior and exterior architectural features. However, based on the findings of previous studies, visible range resonant a-Si based color filters require a semiconductor thickness smaller than 25 nm.[54] This brings up a new challenge because it is known that the typical a-Si solar cell doping layers alone already impose an equivalent thickness in the range of 40–50 nm.[55] Therefore, a colorful a-Si based solar cell should have an ultrathin nonsilicon electron and hole transport layers. Lee et al. proposed a colored ultrathin solar cell that is made of a 10 nm–27 nm thick Si sandwiched between a 10 nm indene-C_{60} bisadduct (ICBA) electron transport layer, and 8 nm V_2O_5

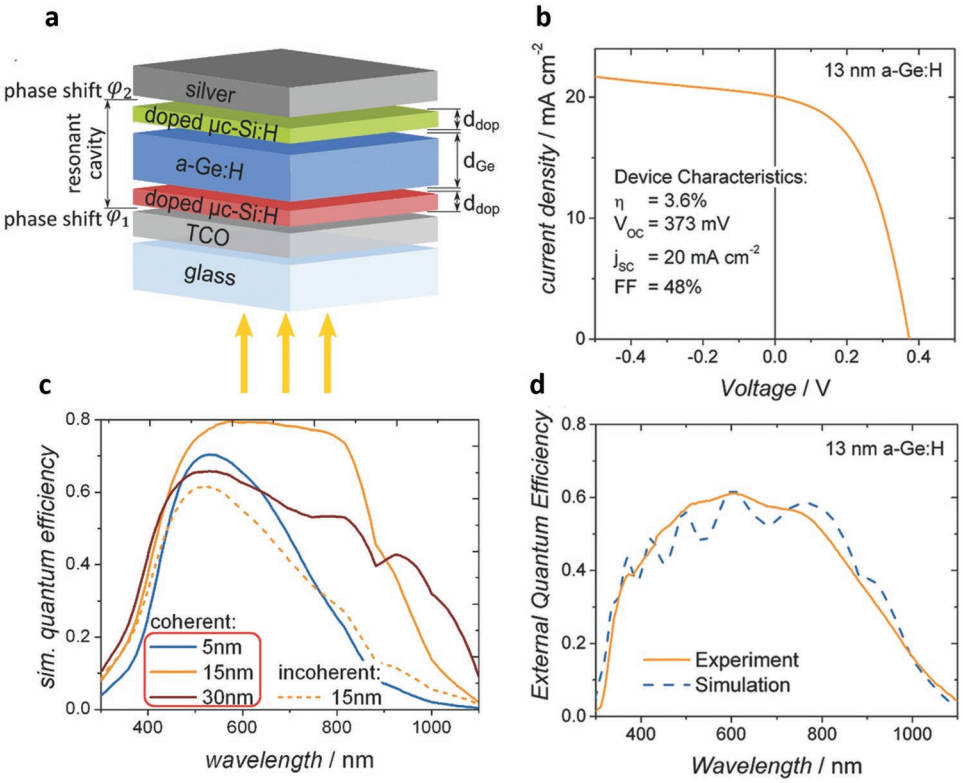

Figure 5. a) The resonant cavity based ultrathin solar cell design, and b) its current–voltage characteristic showing a photoconversion efficiency of 3.6%. c) The simulated EQE for different a-Ge layer thicknesses, and d) a comparison between simulation and measurement EQE data for a 13 nm thick a-Ge layer based solar cell. Reproduced with permission.[53] Copyright 2015, Wiley-VCH.

hole extraction coating.[56] This three-layer design has been covered with a thick (120 nm) bottom Ag layer (which acts as the bottom contact) and a semitransparent 23 nm top contact Ag. Therefore, the overall system can act as a colorful solar cell. By fixing the active a-Si layer thickness at 10, 18, and 27 nm, yellow, magenta, and cyan colors were accomplished. The highest overall efficiency of this ultrathin design was found to be 3%, which belongs to magenta. The maximum measured EQE values were found as 70%, 65%, and 40% for yellow, magenta, and cyan samples. While the above-mentioned conversion efficiencies and amorphous cell are quite remarkable, they are still much lower than the current state of the art for other similar types of thin film solar cells (e.g., 10% for a-Si).[57] This could be due to the narrow absorption spectra of the design. Moreover, although the thickness has been thinned down to a level comparable with the carrier's diffusion length, the crystallinity in such a thin layer is still a major challenge. Generally speaking, for a covalently bonded, isotropic semiconductor, reducing the thickness to the sub-100 nm range will cause significant diminishing in crystalline quality, increasing in defect and disorder trap states and so on. Thus, amorphous based solar cells have generally shorter carrier diffusion length compared to single-crystalline ones. This in turn induces an inherent limit in the performance of ultrathin amorphous based semiconductor designs. A recent study demonstrated a fabrication route for a sub-10 nm single crystalline Ge layer for photodetection application.[32] The authors claimed that this approach can also be adopted for other type of semiconductors. However, a more feasible route to realize an ultrathin single crystalline layer can be found in chemically synthesized highly absorbing organic layers. In a very recent study, Liu et al. demonstrated a magenta solar cell using a 30 nm thick perovskite ($CH_3NH_3PbI_{3-x}Cl_x$) showing remarkable efficiency as high as 11.5%.[58] The proposed colored solar cell design with its corresponding band alignments and *J*–*V* characteristics are depicted in **Figure 6**a–c. The obtained efficiency for this colorful solar cell design is 75% of that of the black thick cell (with a thickness an order of magnitude larger), which highlights the promising potential of metasurface design for colorful and efficient organic based solar cells. These results can be understood by looking at the reflection spectra of thick black cell and colored cells, Figure 6d. While the black cell has a broad and strong absorption from 400 to 800 nm, the magenta cell also depicts a strong absorption up to 650 nm. However, yellow and cyan samples have narrow absorption BW and consequently much less efficiency compared to black cell. As already stated, requiring colored behavior will sacrifice the absorption BW and this is one of the reasons that limits the efficiency of nanocavity based solar cells. A way to tackle this problem is to cascade multiple cavities in a proper way to have double resonant behavior and broaden the absorption response. An elegant design made of an organic active layer was proposed by Liu and co-workers where they provide two-resonance cascaded cavities for broadband light trapping in thin-film organic solar cells, see **Figure 7**a. It was stated that the proposed design has the highest reported efficiency of 11.1% for an organic solar cell design,[59] see Figure 7b. The proposed

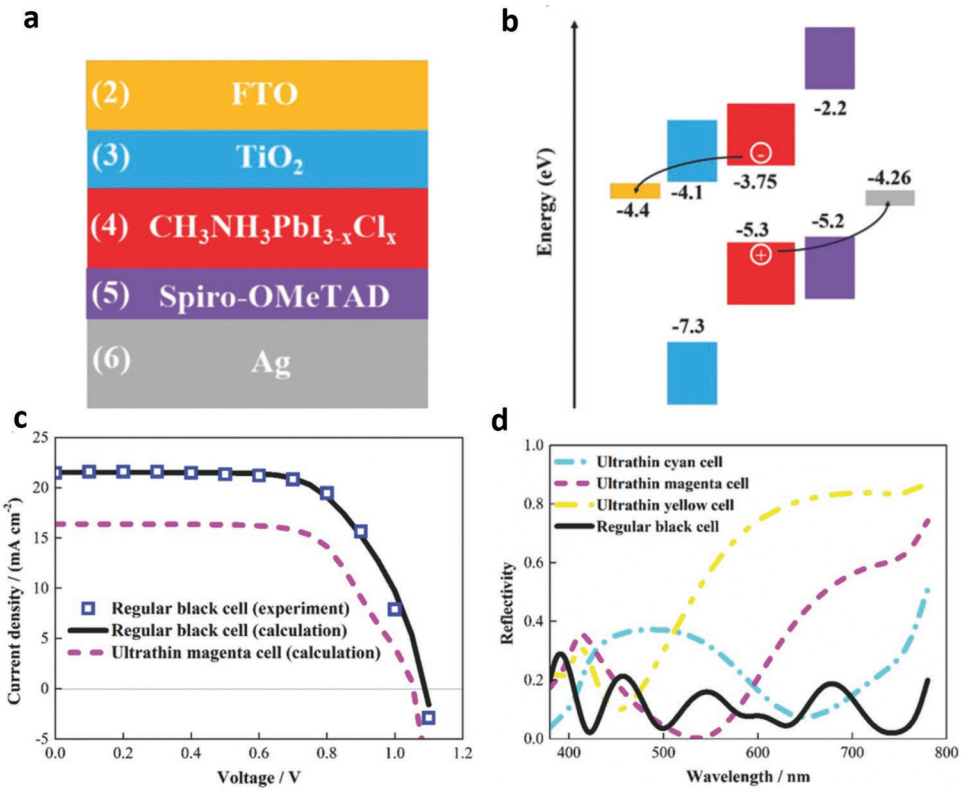

Figure 6. a) The proposed colored perovskite based solar cell design with its corresponding b) band alignments and c) *J*–*V* characteristics. d) The reflection spectra for regular thick black cell and its comparison with colored ultrathin cyan, magenta, and yellow cells. Reproduced with permission.[58] Copyright 2018, Wiley-VCH.

structure has an EQE as high as 80% from 550 to 750 nm. Thus, it is envisioned that lithography-free planar metasurface designs incorporating ultrathin highly crystalline layers could be promising options for future PV and PEC-WS applications. The proposed cavity has not only application in PV and PEC-WS, but also it can be utilized for emission applications. It is

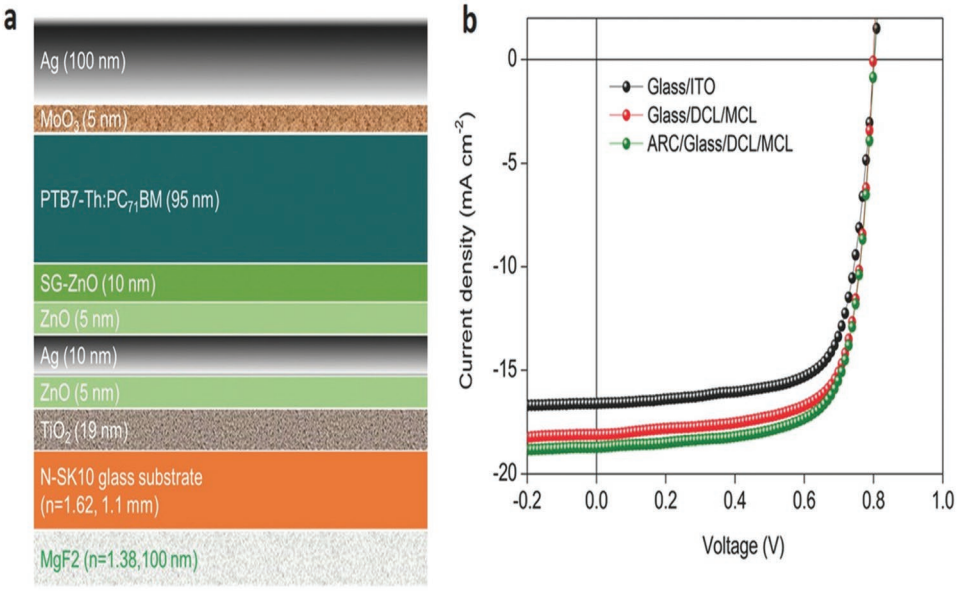

Figure 7. a) Cascaded cavity based organic solar cell and b) its current–voltage characteristic under solar irradiation. Reproduced with permission.[59] Copyright 2017, Wiley-VCH.

known that reducing the size of a semiconductor nanoparticle down to its excitonic Bohr radius can intensify its emission property.[60,61] In the other side, as demonstrated in this paper, the strong light-matter interaction in a semiconductor based cavity occurs in nanometer scale thicknesses. Therefore, it is envisioned that introduction of a thin layer of semiconductor nanoparticles into this cavity can significantly enhance its emission property. Chemical synthesis, chemical vapor deposition of 2D semiconductors (such as TMDs), and other innovative preparation and transfer routes can lead to substantial enhancement in the performance of these ultrathin optoelectronic designs. A further enhancement in the performance of these designs can be achieved by using ultrathin surface engineering where the electrical response is improved significantly while the optical response stays intact.[62–64]

2.2. Light Trapping Using Metal Nanounits

Upon the excitation of localized surface plasmons in metal–semiconductor interface, its energy can be transferred to the adjacent semiconductor via two main pathways; 1) radiative and 2) nonradiative energy transfer.[65] In the radiative energy process, the subwavelength metal particle acts like an antenna where excited hot electrons relax into lower energy states and reradiate as a secondary source. Keeping the antenna terminology in mind, this reradiated power can be coupled to the outside environment through propagating far field waves or it can be coupled to near field evanescent modes. The first process is called scattering and it is dominant in nanosphere diameters larger than 100 nm.[66] It should be noted that this property can be tuned by the refractive index of surrounding medium, composition, and the wavelength. Scattering could be found in both metal and dielectric nanostructures and it mainly improves light trapping by maximizing the optical path of the light within the semiconductor.[65] The second process is named near field coupling and it takes the main role in the energy transfer process for smaller plasmonic particles. This process imposes high field localization in the vicinity of metal particle where a high density of electron and hole pairs can be generated. But both of these processes can only intensify absorption in photon energies above the bandgap of the semiconductor. In other words, this process is to maximize the above bandgap absorption of the design. Sub-bandgap absorption could be achieved through nonradiative energy transfer routes. In this type of energy transfer, the plasmonic nanounit design contributes to enhancement in photocurrent by the direct injection of excited hot electron into the conduction band of the semiconductor. This mechanism is called hot electron injection. Upon irradiation of the metal–semiconductor junction, the localized surface plasmon resonance (LSPR) gets excited. The nonradiative decay of these LSPRs will generate hot electrons.[65] Most of these hot electrons have energetic location close to the metal Fermi level (E_f) and just a small portion of them can have required energy to overcome the Schottky barrier at the metal–semiconductor interface and contribute to the overall photocurrent.[67] Another nonradiative path is defined as plasmon-induced resonance energy transfer (PRET or PIRET). In this transfer mechanism, LSPR decay generates photocarriers directly in the semiconductor via dipole-dipole interactions with a transient exciton.[68] The energetic overlap among plasmonic metal and semiconductor bands measures the overall efficiency of the process. All of these mechanisms have been schematically depicted in **Figure 8**a.[66] Based on the type of plasmonic metals, geometry of the design, including its size, shape, and composition, and the nature of metal–semiconductor junction, some of these mechanisms can be activated or even dominant. A recent theoretical study has scrutinized the involved energy transfer processes in the plasmonic metal–semiconductor interface for photoconversion devices.[69] It has been demonstrated that in each of the plasmon energy levels (above, near edge, and below bandgap) a specific energy transfer mechanism is dominant.

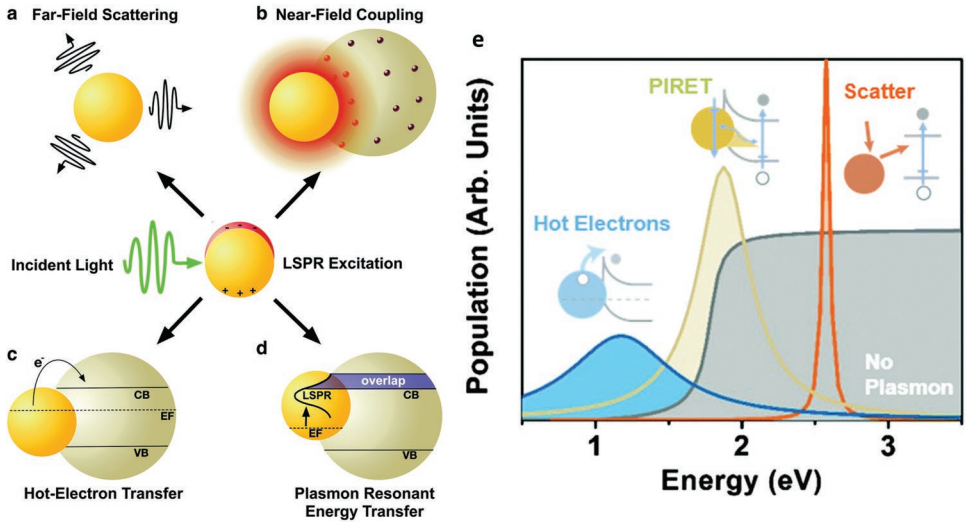

Figure 8. Upon the excitation of plasmonic in metal–semiconductor interface, its energy can be transferred to the adjacent semiconductor via a) far-field scattering, b) near-field coupling, c) hot-electron transfer, and d) plasmon resonant energy transfer. e) Schematic representation for where each plasmonic mechanism can lead to the largest enhancement in semiconductor photoconversion. a–d) Reproduced with permission.[66] Copyright 2016, Royal Society of Chemistry. e) Reproduced with permission.[69] Copyright 2015, Royal Society of Chemistry.

Scattering is the most efficient process in plasmon energy values larger than the semiconductor optical band edge, see Figure 8b. This is in line with our previous explanations that scattering could only provide absorption in above bandgap photons. The situation is the opposite for hot electron injection case. Theoretical findings predict their maximum contribution in photoconversion when bandgap is large (UV range) and the plasmon energy is below this bandgap. Although this process can open up the opportunity to use sub-bandgap photons, it has lower efficiency compared to scattering.[69] At the band edge or energy levels close to it, the PIRET process takes the dominant role. In this section, we will summarize the main strategies for enhancing light-matter interaction in a plasmonic metal–ultrathin semiconductor system. In this review, we focus on strategies for enhancement in the absorption capability of the semiconductor layer and, therefore, we will mainly consider the radiative energy transfer process rather than nonradiative ones. In other words, the motivation in this section is to highlight the trapping strategies based metal nanounits to efficiently couple the light into thin semiconductor active layers.

2.2.1. Plasmonic Nanoantennas

In ultrathin active semiconductor-based systems, to obtain strong light absorption, the optical path length of the incident plane wave should be maximized. This could be obtained by utilizing the scattering property of large metal nanoparticles. The scattering cross section of these metallic nanoparticles can be tuned by particles' type, shape, size, distance from the semiconductor and the surrounding environment permittivity.[65] For instance, it has been found that cylindrical Ag particles can scatter a higher fraction of indent light into the underlying active layer compared to spherical shapes.[70] However, from the synthetic point, spheres are more feasible designs to be fabricated. Similarly, it was shown that the spectral position of maximum scattering experiences a red shift when the particle is brought to a contact with a high refractive index medium such as Si.[71] Considering the fact that most semiconductors have small k values in long wavelength visible and NIR ranges, this is quite desired to put this trapping mechanism in longer λs to enhance their weak inherent response. The optimum particle size for light scattering into the active layer is about ≈100 nm.[66] It should be noted that larger particles will suffer from high reflection and consequently less incident power will be accessible by active layer (specifically in shorter wavelengths where particle size is comparable with the incident light wavelength). Wrapping an ultrathin dielectric shell on plasmonic nanoparticle can further increase the scattering cross section of the design.[72] From the PV application perspective, this is also a beneficiary for suppressing recombination pathways. These metallic particles, placed inside the bulk or the surface of semiconductor layer, could act as an undesired trapping center. While the use of a high bandgap oxide layer can electronically isolate them from the surrounding active area. Moreover, scattering which is also called light trapping can be more effective by the introduction of a metallic back mirror. By this way, light will transport longer distances within the semiconductor layer. In addition, an intense localized field around a plasmonic object or at the metal–semiconductor interface can substantiate the density of generated electron–hole pairs.[73] These highly confined field regions are also referred as hot spots. These phenomena are mostly seen in deep subwavelength particle dimensions. These intense fields are not only for absorption enhancement, but they can also facilitate carrier separation at the metal–semiconductor interface by providing electric forces at the space charge region. Similar to scattering, near field coupling of these metallic nanoparticles depends on the geometrical parameters and the materials.[74] The hot spots are generally formed in nanounits with sharp corners.[75,76] Moreover, ultranarrow metallic gaps are favorable for the creation of these intense local fields.[73] Thus, taking everything into account, these plasmonic nanoantennas can significantly boost semiconductor absorption capacity by either far-field scattering or near-field confinement. In the same time, they can improve the electrical behavior of the cell by improving the carrier separation dynamics.

One of the most prominent factors, defining the effectiveness of using plasmonics in energy conversion applications, is the position of this plasmonic particle in respect to the semiconductor active layer. The initial attempts in this field proposed a configuration in which plasmonic particles are dispersed on top of the cell. Back in 1996, Stuart and co-workers proved the absorption enhancement upon coating them with metallic nanoparticles.[77] Later studies were conducted to enhance the efficiency of bulk solar cells by these plasmonic objects. However, as already mentioned, plasmon induced optical and carrier dynamics improvement is much more pronounced in ultrathin active coatings. In 2006, in one of the pioneer studies, Derkacs et al. used silver nanoparticles in a-Si based solar cell to enhance light absorption and consequently overall conversion efficiency of the solar cell.[78] In this architecture, the plasmonic particles are placed on top of the solar cell, separated with a 20 nm thick indium tin oxide (ITO) conductive coating. Later on, this improvement was recorded for GaAs based PV cells.[79] Similar strategy has also been used for $Cu(In,Ga)Se_2$ (CIGS) based thin solar cell to improve the photovoltaic performance of the design.[80] The use of these plasmonic particles in both front and back sides of ultrathin a-Si based solar cell has been also studied.[81] It was found that the particles at the backside have little to no impact on the device efficiency while the front particles could improve light absorption. However, as stated hereinabove, a part of performance improvement in plasmonic based systems comes from near field coupling. Therefore, it is envisioned that embedding particles within the bulk of the cell could provide a better performance improvement. This has been proved in the case of Ag and Au nanoparticles embedded in an ultrathin Si layer.[82,83] This is also beneficiary in terms of the long-term stability of the design where a lack of contact with air can minimize the formation of native oxide especially in the case of noble metals such Ag, Al, and Cu which have been found as promising and cost-effective alternatives for precious Au metal. This requirement is much more prominent in the case of water splitting where metals could easy undergo corrosion upon their exposure to the water.[84] Koren et al. studied the impact of Au nanoparticles position relative to a semiconductor layer.[85] Their findings showed that Au nanoparticles on

the surface of the Fe_2O_3 active layer experience a redox reaction ($Au + 3OH^- \rightleftharpoons Au(OH)_3 + 3e^-$) that gives rise to a spurious contribution to the current. In a second configuration, where the semiconductor layer has covered dewetted gold nanoparticles, the improvement and photocurrent-voltage characteristics were improved better. Although the second architecture enhanced the absorption capability of the design but wrapping Au plasmonic particles with a high permittivity medium put the plasmonic resonance at 600 nm which is above the Fe_2O_3 band edge. Thus, they concluded that Mie scattering is the dominant process in the absorption enhancement. Their photocurrent improvement was more pronounced in lower applied voltages and almost no difference in larger bias values. They concluded that their activity enhancement is not only due to optical performance, but electrochemical effects are also present and effective in an Au nanoparticle embedded design. Similar results were also found for the case of Au nanorod coated α-Fe_2O_3.[86] While redox reaction related peaks were also present in this case, but the photoactivity of semiconductor film was reinforced by Au nanoparticles. This improvement was negligible for thick layers (≈100 nm) while it was quite distinguishable for thin coatings (≈10 nm). Therefore, an elegant design should have plasmonics particles embedded within ultrathin film thicknesses. Archana and co-workers examined the impact of semiconductor hematite layer thickness on the photoactivity of the plasmonic incorporated photoanode.[87] **Figure 9**a shows the impact of hematite layer thickness in band alignment and the carrier concentration density of the design. In the 110 nm case, due to near-field coupling and Mie scattering, a greater density of photocarriers can be generated. Thus, in such a thin thickness, the whole thickness is effectively depleted. However, as we go toward thicker layers, a larger amount of incident light will be consumed by semiconductor bulk and less will be coupled to Au nanoparticles. Moreover, considering the short diffusion length of holes in this material, decreasing layer thickness will reinforce the collection probability of carriers. Thus, the response of a plasmonically enhanced thin layer can outperform a bare thick slab, if designed properly. They found that the thinnest possible layer that can fully cover the gold particles represents the greatest activity. Stronger absorption and better carrier transport dynamics were the reasons for enhanced activity in thin Au-Fe_2O_3 coating. The EQE was improved to a value as high as 50% for the plasmonic incorporated sample while it was below 30% for the bare sample (at $V_{Ag/AgCl} = 0.6$ V). The similar findings were reported for the case of Ag-$BiVO_4$ where three different configurations of fully embedded, half embedded, and on semiconductor surface were simulated,[88] see Figure 9b. Numerical simulations reveal that the absorption has been reinforced in the first case while the other ones have only surface effects. Moreover, the characterization results demonstrate an improvement in carrier transport and collection efficiency upon the introduction of uniformly dispersed Ag nanoparticles within the bulk of active layer. The maximum EQE has improved by two folds from 10% for pristine sample to 20% for optimum Ag loaded $BiVO_4$ photoanode. Authors[88] have attributed this to better charge generation and separation within the near field coupling region of plasmonic particles. The LSPR-induced electric field at the vicinity of nanometal surface creates a large density of electron–hole pairs within the semiconductor layer. These electron–hole pairs are separated by

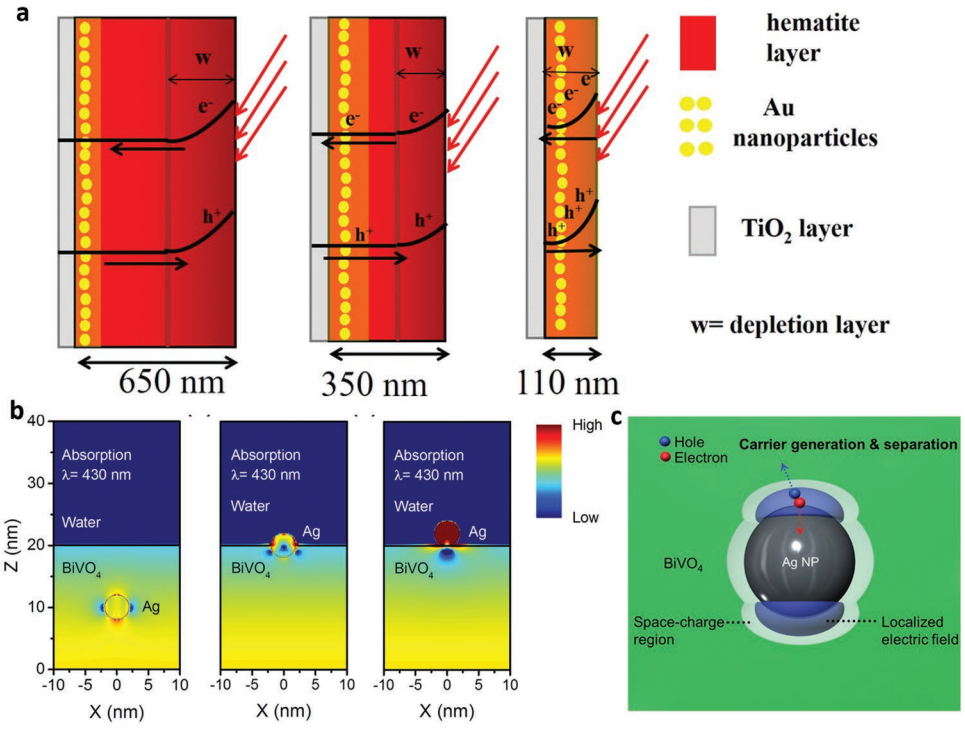

Figure 9. a) Schematic representation of carrier dynamics in different thicknesses of α-Fe_2O_3-coated gold nanoparticles. b) The electric field profiles for different configurations of fully embedded, half embedded, and on semiconductor surface. c) The plasmonic near-field induced charge separation in Ag-$BiVO_4$ design. a) Reproduced with permission.[87] Copyright 2015, American Chemical Society. b,c) Reproduced with permission.[88] Copyright 2018, American Chemical Society.

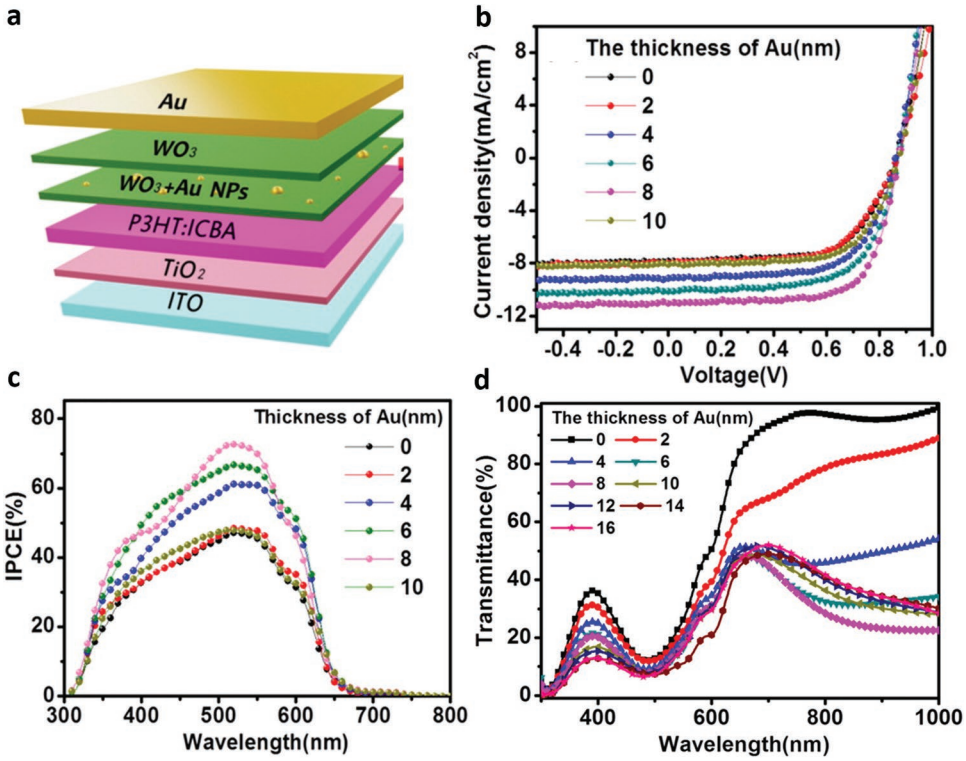

Figure 10. a) The proposed plasmonically enhanced organic solar cell and b) its photocurrent–voltage response. c) The IPCE values for different Au thicknesses and the d) transmittance data of the cell. Reproduced with permission.[92] Copyright 2015, American Chemical Society.

means of Schottky junction formed at metal–semiconductor interface. The formation of the Schottky junction creates a space-charge region in the semiconductor, and this, in turn, enhances the charge separation. These findings have been proven by electrochemical impedance spectroscopy (EIS) measurement. Based on EIS results, the Ag loaded plasmonic $BiVO_4$ photoanode has smaller depletion region resistance compared to the bare one. The intense electric fields around the surface of Ag plasmonic particle not only generate high density of carriers but separate them in an efficient way (Figure 9c). However, these near field evanescent waves significantly decay as we go away from the surface and they are effective just at close vicinity of the particle. On the other hand, the absorption and scattering cross section of plasmonic particles is much larger than their projected geometrical area.[89] Therefore, a moderate loading of nanounits could be enough to fully harvest the incident light. This has been shown in an Au-WO_3 hybrid photoanode where an optimum particle size and weight loading percentage of 10 nm and 1.2 wt% leads to four times improvement in photocurrent at an applied bias of 1 V (vs Ag/AgCl).[89] For the case of the Ag-photosensitizer system, a surface coverage as low as 12–14% was shown to be the optimal condition.[90] Generally speaking, higher metal nanoparticles concentrations will predominantly diminish the electrical transport properties of the semiconductor layer. In other words, in this case, the metallic nanounits act as unwanted trapping sites and limit carrier collection efficiency. Together with all of these parameters, the size of particle should be fine-tuned to maximize the response.[91] Employing the surface energy differences between Au and WO_3, Au nanoparticles can automatically grow up through the process from nucleation in ultrathin coatings.[92] It was determined that the photoconversion efficiency of P3HT based organic solar cell can be improved from 4.67% for bare sample to 6.63% for the optimal gold layer thickness of 8 nm.[92] The proposed design and its *J–V* characteristic have been plotted in **Figure 10**a,b. The incident photon conversion efficiency (IPCE) data have been extracted for bare and plasmonic samples. Figure 10c shows that the IPCE has been substantiated to a value as high as 80% at the incident light wavelength of ≈520 nm. The position of this peak is in accordance with the position of transmission dip in Figure 10d which means that a stronger light trapping is the origin of higher IPCE. As we can see from this panel, the transmission spectra do not significantly change after 12 nm Au thickness. This means that deposition of Au film leads to formation of nanoislands in sub-10 nm thicknesses and thicker layers form continuous film. Thinning down these trapping architectures is not only for boosting their photoconversion efficiency but it can also open up the opportunity to exploit them in flexible, wearable photoelectronics. An ink-printing CIGS based ultrathin flexible solar cell was proposed where the incorporation of nanoplasmonic units in the interface of pn junction have improved efficiency to a relatively high value of 10.36% (while the efficiency for bare structure was 8.31%).[93] This solar cell reveals near 80% flat EQE from 550 to 1100 nm. For a flexible bendable cell, the operation in angular incident lights is also of great importance. These scattering particles have omnidirectional response where the enhancement compared to bare structure becomes more

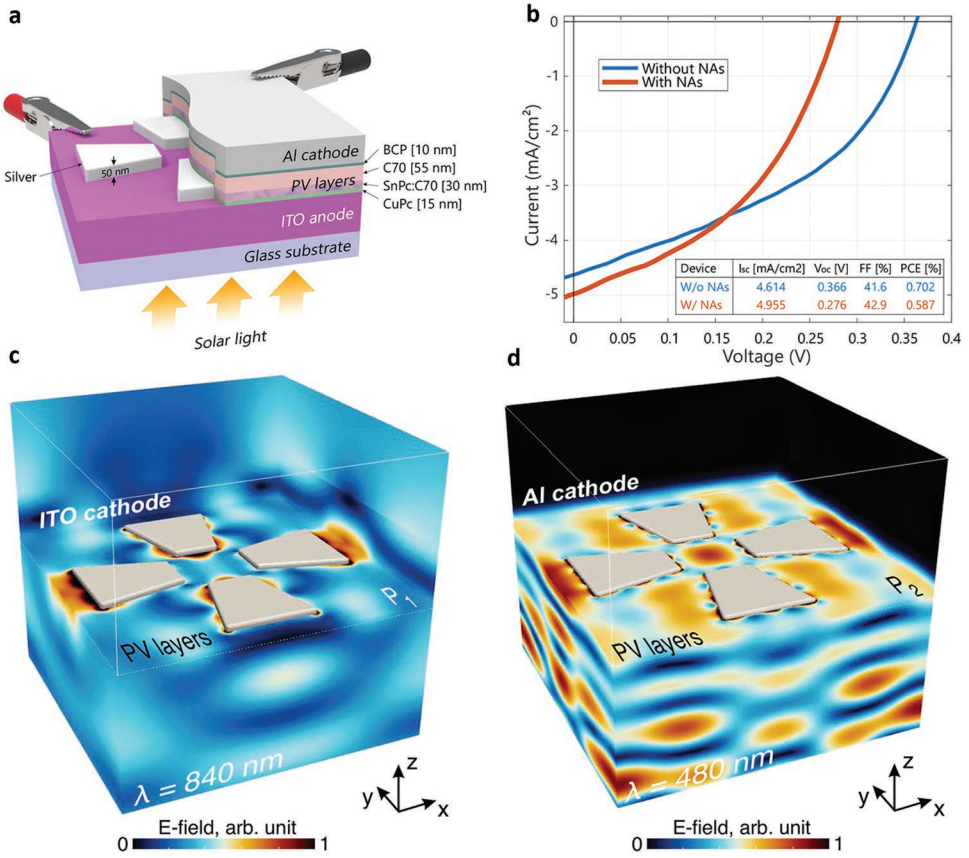

Figure 11. The a) proposed solar cell with nanoantenna design, and its c) *J–V* response compared to a bare cell. Normalized electric field intensity distributions for the solar cell with c) ITO anode and cathode, $\lambda = 840$ nm d) and with ITO anode and Al cathode, $\lambda = 480$ nm. Reproduced with permission.[94] Copyright 2018, American Chemical Society.

distinguishable at wider oblique angles. Besides these subwavelength colloidal nanoplasmonic particles, predesigned metallic nanoantennas can be made using lithography techniques to obtain a specific functionality. Tapered silver nanoantennas were used to couple the incident light into the active layer.[94] The effective trapping in these nano-objects stems from the excitation of collective modes of the plasmonic antenna strips and their coupling into semiconductor photonic modes. These nanostrips can be designated in a way that field localization within the metallic structure is much weaker than the gap between adjacent elements. Upon placing two nanoparticles at a deep subwavelength distance, their optically driven free electrons couple dynamically across the gap, and this causes a large field enhancements in the gap position. For a periodic pattern of nanoplasmonic units, this enhancement has a narrow spectral coverage[95] and this is not desired for photoconversion applications. However, in the random nanopatterns (such as colloidal assemblies or dewetted particles) with multiple gap distances, this light confinement can be achieved in a broad wavelength range.[96] Hence, in such designs, the incident power will be efficiently coupled into the semiconductor layer rather than being lost in metal. This coupling could be further intensified by the use of a reflective metal mirror. In this cavity design, the semiconductor active layer will be sandwiched by a planar mirror and trapping antenna where the formation of gap plasmon resonance can substantially enhance light harvesting inside the semiconductor bulk. Gap plasmon resonance will be discussed in upcoming section. The proposed solar cell design, and its *J–V* response (in comparison with the bare cell) are represented in **Figure 11**a,b. Moreover, Figure 11c,d depicts normalized electric field intensity distributions for the solar cell with ITO anode and cathode ($\lambda = 840$ nm) and with ITO anode and Al cathode ($\lambda = 480$ nm). As these panels clearly illustrate, for the case with ITO cathode, the strong light confinement is mainly achieved in the edges of nanoplasmonic antenna design. However, introduction of the bottom reflecting Al mirror as cathode provides strong field localization within the bulk of solar cell. This essentially stems from excitation of gap plasmonics in the cavity design. Another example of an innovative plasmonic design was to replace ITO layer with plasmonic cavity with subwavelength hole arrays.[97] Incorporation of this plasmonic unit enhances the EQE to a maximum value of 70% at around 600 nm while this value for the bare sample stays below 50% in the whole range. This partially transmissive/reflective plasmonic architecture led to an improvement in device efficiency, η, from 2.9% to 4.4% which was among the highest achieved conversion values for P3HT/PCBM polymer solar cells.

As already stated, a part of light trapping improvement in the semiconductor-based devices is associated with light

scattering. The introduction of a reflective mirror and a spacer below the plasmonic structure (if designed properly) could maximize the optical path length of the scattered light.[94,98–103] This will, in principle, make a "10 nm limit" for efficient ultrathin solar cells possible.[98] A nanocavity based on Al-SiO_2 (55 nm) – Au nanoparticle was uniformly coated with 10 nm tin mono sulfide (SnS) where a broad and near unity absorption was realized for such a thin coating.[101] It was found that this broad absorption behavior is attained via the superposition of two resonance modes; 1) due to the excitation of localized surface plasmons (LSPRs) and 2) first-order FP cavity modes. A wiser architecture is to replace the spacer with a conductive high bandgap metal oxide to enhance the probability of carrier separation. Butun et al. proposed a cavity structure made of an Al-NiO_X-Ag-(monolayer MoS_2) where the plasmonic antenna produces intense local fields and these confined modes are coupled to monolayer MoS_2 to achieve 4 times higher absorption compared to that of a bare none cavity design.[102] The photoluminescence measurements have demonstrated that most of the light absorption has occurred in MoS_2 monolayer. Moreover, injection of hot electrons from a plasmonic nanoantenna into a 2D semiconductor can be utilized for sub-bandgap photodetection.[104] These metallic nanoantennas can be replaced with highly ceramics, such as titanium nitride (TiN).[105]

2.2.2. Plasmonic Nanostructured Mirrors

Another strategy to intensify the absorption capability of an ultrathin semiconductor layer is the utilization of nanostructured back reflector. These metamirrors could be mainly obtained by nanoparticles or periodically patterned subwavelength units on optically thick reflector.[106–113] In the case of nanoparticle-based mirrors, the performance improvement is generally attributed to the scattering property of the plasmonic units. However, their contribution has been found to be weak, as explained in the previous section. The periodic pattern of nanostructures, such as gratings, patches, grooves, and holes, can significantly improve light absorption.[106–112] In one of the pioneer studies, a group of researchers in Atwater lab designed a nanogroove based reflector, tiled to be polarization independent.[114] They demonstrated that a single nanogroove under a 200 nm thick thin Si active layer can make above bandgap absorption 2.5 times stronger over 10 μm^2 area. They found that this enhancement mainly originated from the coupling of the light into surface plasmon polaritons (SPPs) in a semiconductor-metal interface. Coupling to SPPs makes absorption confined in a mode volume which is dramatically smaller compared to the exponential decay profiles occurring in the bulk. It was shown that the right choice of grooves' width and semiconductor layer thickness can maximize absorption in the active layer. It was envisioned that this strategy could be extended to other semiconductor types. A later study proposed a design based on Ag nanogratings filled by ITO and covered by a 100 nm thick Si layer.[115] According to the finite-difference time-domain (FDTD) simulation results, there are three mechanisms responsible for light trapping enhancement in this nanostructured back mirror. The first mechanism was the formation of FP resonances in the metal–semiconductor double layer design. This resonance was red-shifted as we replace the plane metal with a nanograting design. This was due to the fact that the grating structure will effectively change the optical path length within the cavity. The width, height, and periodicity of the design can effectively tune the cavity optical length. While the plane MS structure has only FP resonance as the responsible mechanism for light harvesting, the grating structure can support SPPs in Ag-Si and Ag-ITO interfaces for TM polarization. The third trapping scheme was attributed to the coupling of incident light into the *a*-Si planar waveguide. The excitation of guided mode resonances in a-Si slab waveguide leads to strong filed patterns within the active layer for both TE and TM polarizations. The superposition of these three resonance modes resulted in a broadband light trapping. Therefore, different from previous discussed plasmonic nanoantennas, this nanostructure-based reflector can be used as a mean to tune and widen the spectral position of resonant absorption. One of the most frequently utilized metamirror designs is based on metallic nanogratings on a thick planar bottom mirror. This design was utilized to tailor absorption profile in a thin lossy film. It was theoretically shown that the decrease in the filling fraction of metal gratings (while the grating constant is fixed) will red-shift the FP resonance of the cavity.[116] In this statement, the filling fraction is grating width to grating constant ratio. In fact, as we make the grating narrower (while periodicity is kept constant), the design approaches to a planar MS junction with only the bottom metal as a reflector. This consequently causes the cavity length larger and resonance moves to longer wavelengths. This strategy is of particular interest in narrow bandgap semiconductors in which the absorption coefficient is much smaller in longer wavelengths (in comparison with that of short range). Thus, while the inherent high extinction coefficient in UV and short visible range will provide light perfect absorption, the longer wavelengths will be harvested by the help of this metasurface back mirrors. Alongside with all of these effects, a metasurface mirror can be designed in a way that it acts as a magnetic mirror with near zero reflection phase. In a conventional bulk metal mirror, light takes π phase difference as it hits the metal and thus a destructive phase difference (with a minimum field intensity) will be generated in the metal–semiconductor interface. Esfandyarpour et al. designed a groove shaped metamaterial mirror to tackle this problem.[117] The proposed design has been depicted in **Figure 12**a. As it can be deduced from this panel, the metamaterial-based design has higher absorption strength over a broad wavelength range. It was deduced that, while other metals have constant near π phase for a reflected wave, the groove depth in the metamaterial mirror can be adjusted in a way that any arbitrary phase difference can be achieved. This has been shown in Figure 12b. Besides all these promising optical features, the realization of such a complex design is a challenging task. As depicted in Figure 12a, there is an air gap between the metamirror and the planar active layer. So, in the ideal case, the absorbing layer should be made as a thin coating on top of the grating without diffusing into the grooves. The authors have used spin-coating technique to deposit the active layer and no clear proof has been provided for the formation of a planar semiconductor layer. It has been noted by the authors that epitaxial lift-off and subsequent transfer process can be utilized to obtain the

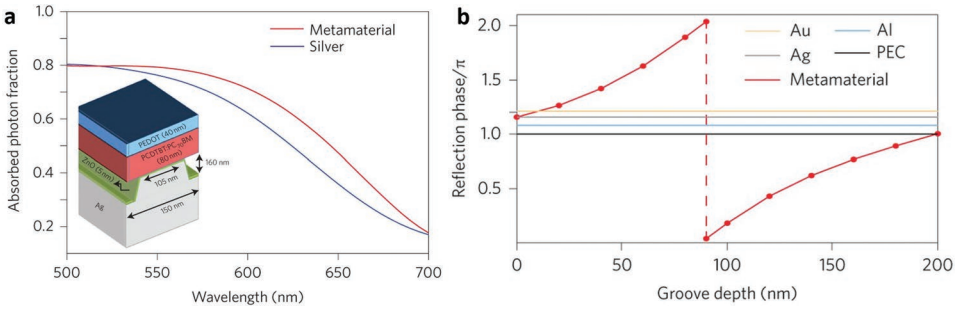

Figure 12. The proposed magnetic metamaterial mirror design. The reflection phase for different metals and metamaterial design at 600 nm light irradiation as a function of groove depth. Reproduced with permission.[117] Copyright 2014, Springer Nature.

proposed ideal design. As an alternative, the grooves can be filled with a transparent dielectric and chemical mechanical polishing (CMP) can be employed to planarize the structure before active layer coating. Apart from all the above-mentioned fabrication complexities, the main drawback with these type of designs is the polarization sensitivity of the grating structure where it can support SPP modes in TM polarization not in TE one. The replacement of this 1D elongated grating with periodic patches, or fishnet-like holes will reinforce the efficient operation of the structure in all light polarizations.[109,118,119] This is important for the practical application of this strategy considering the fact that the incident solar irradiation is also unpolarized. Besides these symmetric designs, the polarization insensitivity can be acquired by arrangement of gratings in a proper way.[120,121] A recent study proposed a metamaterial based mirror based on periodic patterns of Ag nanoparticles on Ag film.[122] Authors employed dark-field scattering spectroscopy to scrutinize the mechanisms responsible for light absorption enhancement. LSPRs, propagating SPPs, and plasmon-absorption-induced scattering were the main mechanisms responsible for light absorption enhancement in this metadesign. A later study demonstrated the applicability of this mirror in the absorption enhancement of MoS_2–Organic van der Waals Heterojunctions.[123] These metamirrors were utilized in flexible polymer solar cells.[124] Ou et al. demonstrated an efficient light trapping scheme based on simultaneous use of a silver mesowire grid-based front transparent electrode (instead of ITO) and a plasmonic meta-mirror-based back reflector electrode (instead of a flat metal coating). As shown in **Figure 13**a, the groove is created on photoactive layer by imprinting quasi-random nanostructures on its surface. Atomic force microscopy (AFM) shows the morphology of the mirror, see Figure 13b. As it can be calculated from *J*–*V* curves in Figure 13c, the use of metamirror has substantiated solar cell

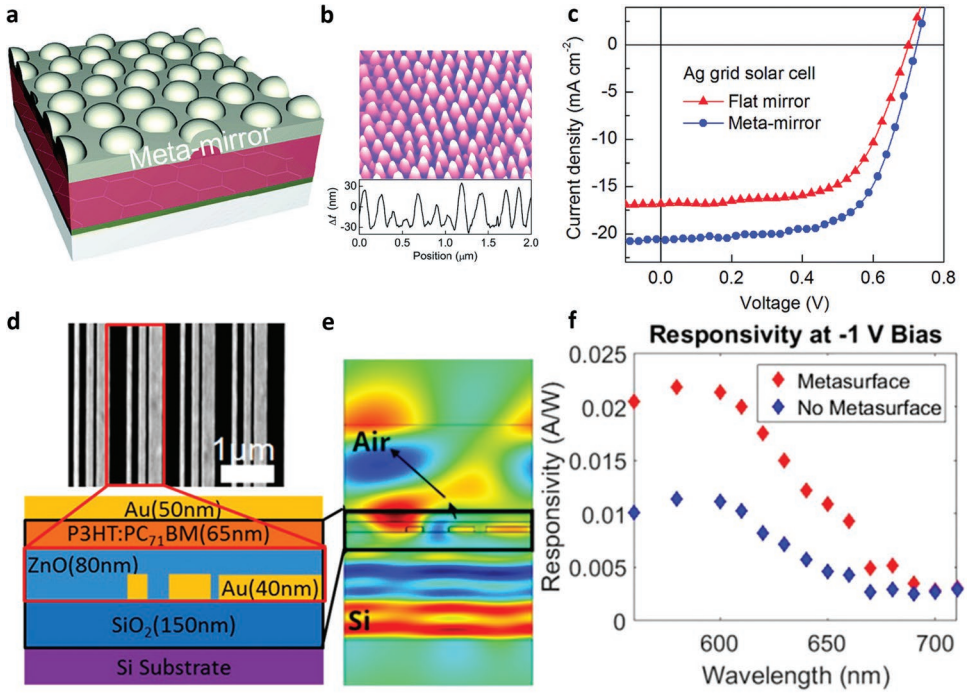

Figure 13. a) The proposed metamirror design, b) its AFM image, and c) *J*–*V* characteristic which shows improvement compared to a flat mirror-based design. d) The proposed metamaterial-based design, and e) its light deflection profile. f) The photoresponsivity of the structure with and without metasurface mirror. a–c) Reproduced with permission.[124] Copyright 2016, Royal Society of Chemistry. d–f) Reproduced with permission.[125] Copyright 2018, American Chemical Society.

efficiency from 7.53% (for flat design) to 9.50%. The proposed design shows an EQE as high as 80% in its optimum geometries. Besides all of these equally spaced patterned nanostructures, an innovative design was recently introduced to improve light trapping in organic solar cells. The distance between multielement gratings was designed in a way that the normal incident light is deflected by an oblique angle of 20°,[125] depicted in Figure 13d–f. This functionality resulted in enhancement in the absorption of light and generated photocurrent throughout a broad range spanning from 560 to 690 nm. A very recent study demonstrated the potential application of these predesigned back reflectors in in solar fuel devices. A 47% improvement in light absorption in the use of Ag nanopatches below ultrathin $CuBi_2O_4$ active layer was recorded.[126] This was mainly attributed to the excitation of SPPs. Topological insulators can be utilized as an alternative for metals. Topological insulators are quantum materials with topologically protected metallic (edge) surface states and insulating (dielectric) bulk states.[127] In these materials, the lossy bulk metal is replaced with a lossless dielectric and therefore parasitic absorption is minimized. Moreover, due to their inherent insulating nature, they do not deteriorate the electrical performance of PV cells. Thus, they can be designed to act as a low-loss and high-performance metamirror for enhancing light absorption in photoconversion devices. Employing topological insulators as inherently core–shell design where the core is high index dielectric and the shell acts as a metal can be excellent alternative for precious and noble metals based plasmonic.[128] The use of nanocone back reflector made of $Bi_{1.5}Sb_{0.5}Te_{1.8}Se_{1.2}$ (BSTS) material has reinforced light absorption in ultrathin a-Si layer by 15%, see **Figure 14**a,b. Due to extremely large refractive index of the BSTS design the light is strongly backscattered and due to its plasmonic shell large near-field enhancements can be coupled to the active layer, Figure 14c.

2.2.3. Gap Plasmon Cavities

As explained in the previous sections, plasmonic nanoantennas are embedded within the bulk of active layer to enhance light scattering and near-field confinement. However, the bottom nanostructured metasurfaces could support SPPs in the bottom MS junction. The combination of these two designs bring us to the concept of gap surface plasmon (GSP) based cavities.[129,130] Gap plasmon resonators are typically made of a thin semiconductor/dielectric layer that has been embedded with a thick bottom mirror and a nanounit plasmonic top layer. In this cavity, light is efficiently coupled into semiconductor layer via excitation of GSPs in the gap between the top nanopatch and the underlying thick metal. This could be seen in the magnetic field profile across the cavity plane.[130] It has been shown that this structure could also support propagation surface plasmons in the bottom metal/dielectric interface.[131] Therefore, this nanocavity design can significantly couple the incident light into semiconductor/dielectric layer in its resonance frequency. The BW of this resonance is a function of spacer thickness and refractive index, top resonator shape, and the type of metal layers.[129,130] The use of lossy metals such as Ti or Cr can lead to wider overall absorption while noble metals have narrower resonance BW.[132] As already stated, the excitation of GSPs lead to intense field localization within the semiconductor and between bottom and top metals. In the case of using lossy metals (compared to noble metals), a larger portion of confined light is dissipated within the metal and consequently weaker absorption in semiconductor will be achieved.[133] Therefore, noble metals, such as Au and Ag, are preferred for energy conversion applications. Multishape/dimensions, elongated units, and structures with sharp corners have been found to broaden the absorption BW of these GSP based cavities.[17] The use of fishnet like nanogrids with subwavelength periodicity has been proposed to provide strong light absorption in a 25 nm thick GaAs based metal–semiconductor–metal (MSM) cavity.[134] The absorption was approximately retained above 0.8 from 400 to ≈850 nm. Substantial extension in the upper absorption edge was attained by the coating of this design using a Si_3N_4 antireflective coating (ARC). Based on the FDTD simulation estimations, a dominant part of the light is coupled to the semiconductor layer and a negligible portion is dissipated in Ag top and bottom coatings. Similar to this study, authors proved the functionality of this MSM cavity for 12 nm thick a-Si using a checkerboard and an aperiodic nanomesh Au top contact morphologies.[135] Similarly, a broadband GSP resonator was designed for PV applications using metal dewetting process which is a large scale compatible route.[136] The effectiveness of this approach is not limited to semiconductors, but also thin organic coatings and dye molecules can also benefit from this strategy.[137–139] Chikkaraddy et al. demonstrated single-molecule strong coupling at room temperature in

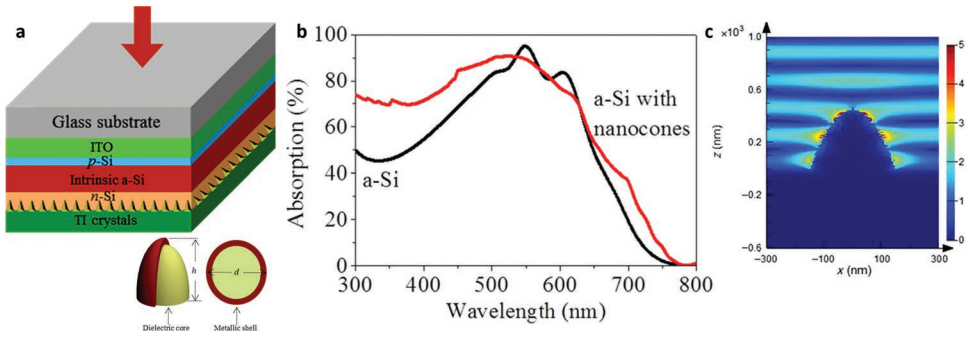

Figure 14. a) Incorporation of topological insulator based nanocones into a-Si based solar cell and b) its impact in absorption enhancement in the active layer. c) The electric field profile around the BSTS nanocone. Reproduced with permission.[128] Copyright 2016, American Association for the Advancement of Science.

plasmonic nanocavities gap.[137] They employed a 0.9 nm thick dye molecule as spacer and 40 nm diameter Au nanoparticles as a top nanopattern. They claimed that the strong interaction among particles and their image results in a dimer-like construct with hot spots having an amplitude enhancement as large as three order of magnitudes. Moreover, a 40 nm thick P3HT:$PC_{60}BM$ organic layer sandwiched between Al thick mirror and top Al nanopatches can offer broadband light absorption covering the whole visible range (400–700 nm).[139] This was further approved in a complete solar cell where the use of taper Ag nanoantennas has coupled the incident light into the bulk of active layer.[94] Rather than PVs, this strong light localization has been actually found as a promising trapping strategy in ultrathin water splitting cells. The confinement of light in ultrathin dimensions will lead to excitation of large density of photocarriers with a minimized transport length and this in turn maximize their participation in water oxidation reaction. Colloidal CdSe nanoplatelets with five atomic layers (i.e., 1.67 nm) was placed within a cavity that is made of sparely distributed Au nanoparticles,[140] **Figure 15**a. The introduction of Au nanoparticles has significantly enhanced light localization on the position of the active layer and this in turn caused a fivefold improvement in the photocurrent value, see Figures 15b,c. This extreme confined hot spot created higher density of photocarrier pairs in the CdSe film and simultaneously, facilitate interfacial charge transport and separation. However, later studies on the use of GSP based MSM design in water splitting application revealed a dominant role for hot electron injection. To prove this, the spacer layer was chosen as a visible transparent high bandgap oxide coating and a cut-off filter was integrated into measurement setup to filter out the semiconductor oxide layer response.[141–143] It was recorded that the Au-TiO_2-Au nanoparticle cavity can propose near unity light absorption over a wide frequency range covering the whole visible spectrum and extending toward the near infrared regime, as shown in **Figure 16**a–c.[143] Figure 16c compares the absorption spectra for Au-TiO_2-Au nanoparticle gap plasmon cavity with that of TiO_2-Au nanoparticle plasmonic design. As we can see from this panel, the absorption has been significantly intensified upon introducing the back reflector. The extracted EQE data proves a broad excitation and collection of hot electrons with a maximum value around 1.4% (at $V = 0.3\ V_{SCE}$). A 20-fold enhancement in the photocurrent values was probed for the MSM cavity compared to the bare TiO_2 under the UV cut-off solar irradiation ($\lambda > 400$ nm).[142] In a quite recent work, Zhu and coauthors successfully constructed an MSM cavity based on 50 nm thick WO_3 coating to acquire photocurrent enhancement in both the UV and visible regime.[144] As shown in **Figure 17**a,b, they demonstrated that, under solar irradiation, this GSP based MSM cavity can significantly enhance anodic photocurrent compared to bare WO_3. Under the optical excitation of gap plasmon resonance in the visible region $\lambda > 480$ nm (where semiconductor layer is transparent for incoming photons), both the top and bottom Schottky barriers can play a positive role in the photocurrent generation. The Schottky barrier, formed in top metal–semiconductor interface, is responsible for injecting hot electrons into WO_3, and the bottom junction can trap injected hot electrons and transport them

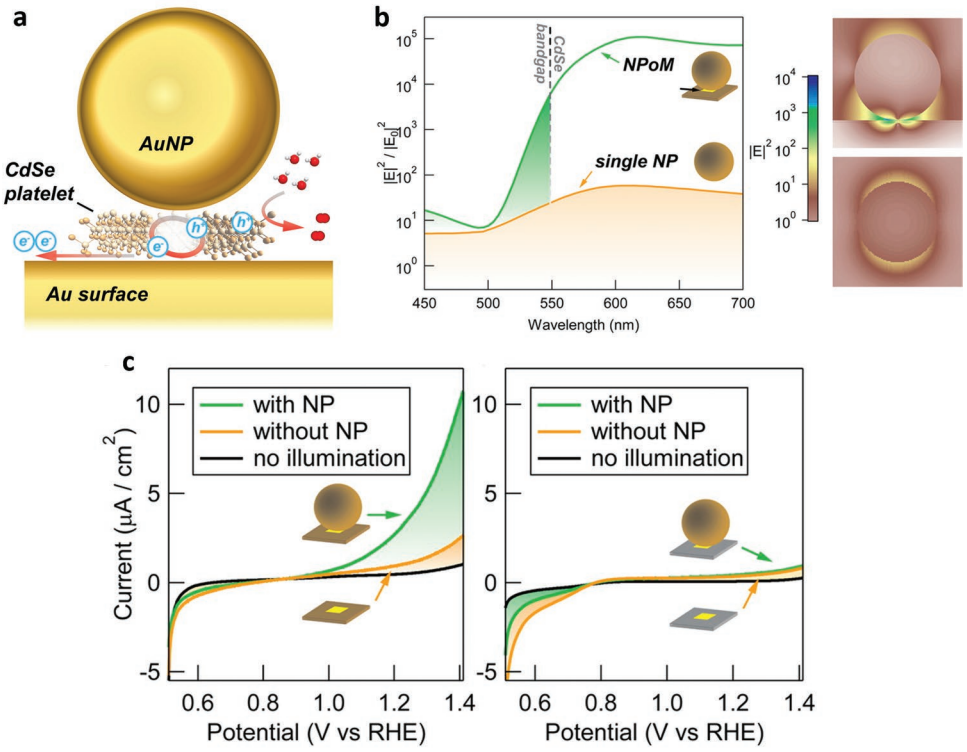

Figure 15. a) The proposed ultrathin MSM cavity, a) its near filed intensity strength compared to a bare nanoparticle, c) and photocurrent–voltage characteristic of different plasmonic and GSP coupled designs. Reproduced with permission.[140] Copyright 2015, American Chemical Society.

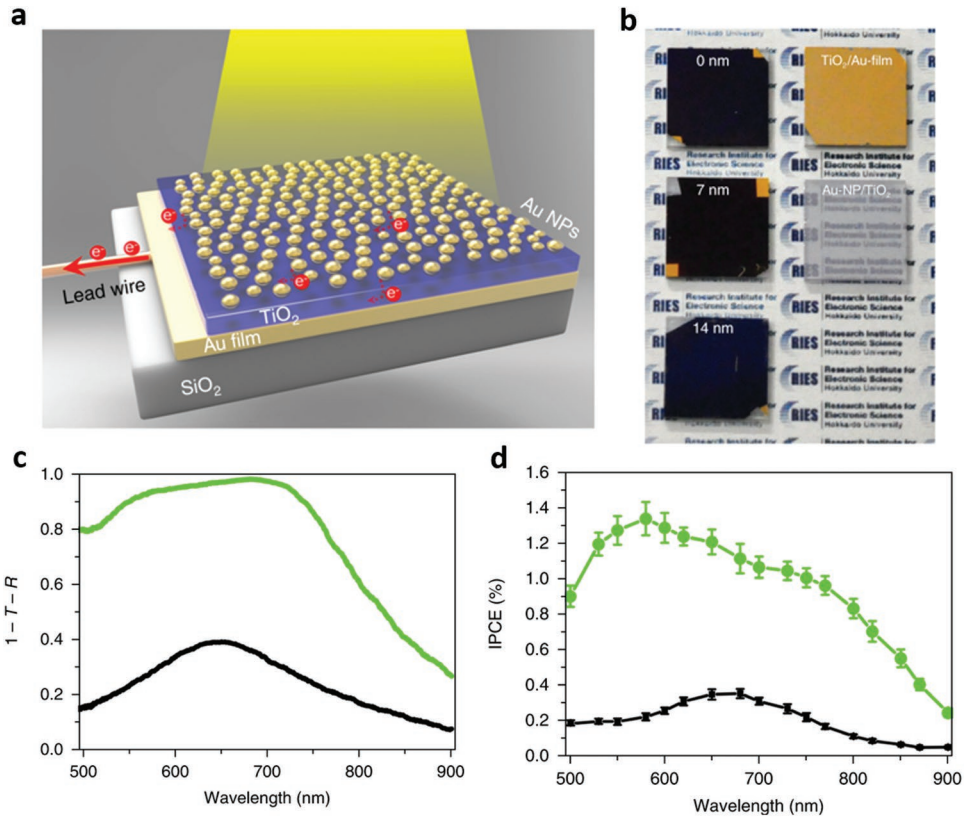

Figure 16. a) Schematic of the proposed MSM cavity with partially inlaid Au nanoparticles. b) Photographs of Au-nanoparticle/TiO_2/Au-film structures with inlaid depths of 0, 7, and 14 nm (left panel). Photographs of the 28 nm TiO_2/Au-film structure without Au nanoparticles and the Au-NP/28 nm TiO_2 structure without the Au film are included for comparison. c) The absorption spectra measured under the same conditions as the photocurrent measurements (aqueous electrolyte solution with an applied potential of 0.3 V_{SCE}) and d) its corresponding IPCE for the Au-NP/TiO_2/Au-film (green) and Au-NP/TiO_2(black) photoelectrodes with the same TiO_2 thickness of 28 nm and Au-NP inlaid depth of 7 nm. Reproduced with permission.[143] Copyright 2018, Springer Nature.

into the Au film, see Figure 17c,d. As depicted in Figure 17e,f, under the direct UV excitation where WO_3 is active, the electron trapping effect at the bottom barrier can contribute to the anodic photocurrent enhancement. Authors further increase the photocurrent response of the system by replacing bottom Au mirror with Pt that has higher work function and can create larger energetic barrier for electrons. A recent study also demonstrated this configuration for an ultrathin hematite case. They showed that the use of multidimension disks will provide GSP modes in a broad wavelength range and this in turn will lead to significant enhancement in the activity of the semiconductor layer.[145]

2.3. Light Trapping Using Dielectric Units

Similar to metals, dielectrics can be also employed to obtain light trapping schemes in ultrathin semiconductor layers. Essentially, metals have three main drawbacks; the first is their inherent high absorption coefficient which leads to higher parasitic absorption and consequently less power is coupled into the semiconductor coating. The second is the narrow spectral BW of plasmonic modes that limits the full usage of incident solar irradiation. The third is possible photocorrosion upon exposing to air and water environment, which is a crucial factor especially for water splitting photoanodes, influencing their long term stability. By analyzing the role of dispersion and dissipation of the nanoparticle material for both metal and dielectric cases it can be envisioned that dielectric particles could have even better performance.[146,147] It has been theoretically proved that the electric field distribution in the vicinity of a plasmonic metal can be mimicked nonplasmonically by a high refractive index dielectric nanoparticle.[148] Thus, in recent years, micro and nanostructured dielectric objects were found as promising low-loss candidates to replace metals for light trapping applications. We have already showed that different parameters including size, type, and configuration can influence the scattering and near field intensity of a metal object. For deep subwavelength particles, the near field enhancement is the dominant mechanism while for particle diameters larger than 100 nm, scattering becomes the most effective light harvesting scheme. Similar, electric field distribution, and scattering behavior can be also presented by dielectric subwavelength objects. However, the story is quite different for wavelength-scale dimensions. For metals, enlarging the particle size to a level comparable with incident light wavelength will cause large reflection for incident light. However, dielectrics can efficiently couple light into active layer in both subwavelength and

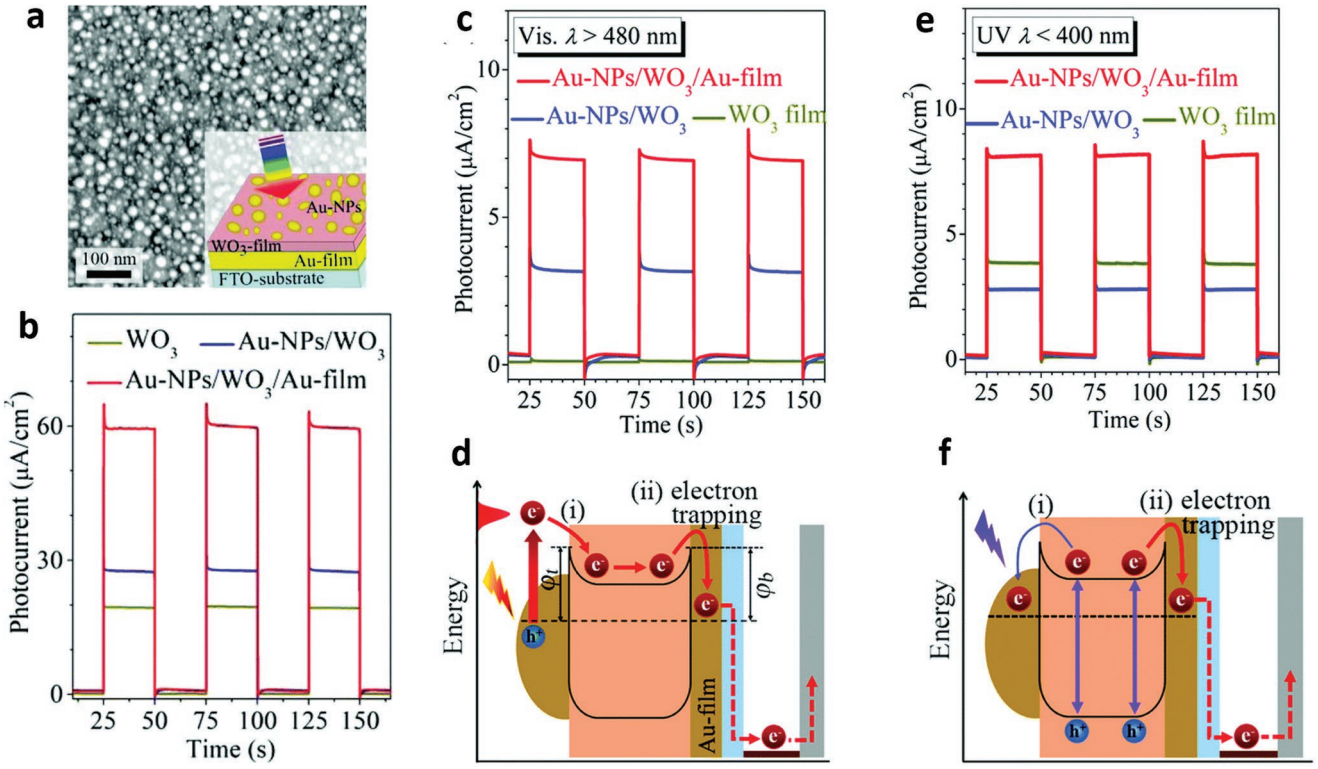

Figure 17. a) The MSM cavity design and b) the *J–t* results for three samples of bare WO_3, Au-nanoparticle-WO_3 and MSM cavity under full solar spectrum irradiation. The *J–t* response of these designs under c) visible and e) UV irradiation and d,f) proposed enhancement mechanisms for each case, respectively. Reproduced with permission.[144] Copyright 2018, Royal Society of Chemistry.

wavelength-scale particle dimensions. **Figure 18**a–c shows the near-field distribution of the square of electric field intensity for three different dielectric particle radii of 50, 500, and 1000 nm.[149] The refractive index of sphere is $n = 1.33$ and the incident light wavelength is $\lambda = 500$ nm. For subwavelength particle, the field distribution is similar to plasmonic metal and it shows dipolar distribution. However, when the dimensions increase to values comparable with light wavelength, the Mie scattering becomes the dominant scattering mechanism. As illustrated in Figure 18b,c, Mie scattering generates a near filed distribution reminiscent of a convex lens. This is the so-called photonic nanojet. The hot spots, created in the bottom part of these microspheres, have significantly larger intensity and they can be diffractively coupled to underlying ultrathin layer.[21] In this section, we will summarize these dielectric unit based ideas in two main parts; 1) subwavelength nanostructures and 2) wavelength-scale microstructures. It should be mentioned that one of the most common approaches in increasing light absorption is to use single or multiple antireflective planar coatings. These coatings provide a gradual impedance matching between air and underlying substrate and consequently reduce the reflection from surface. However, many great works have already covered these ideas.[150–152] Thus, this review essentially focuses on recent innovative designs to maximize light absorption in ultrathin active layers.

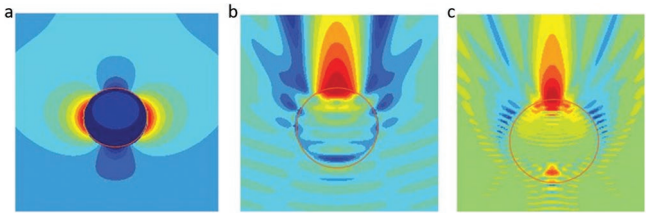

Figure 18. The near-field distribution of the square of electric field intensity for three different dielectric particle radii of 50, 500, and 1000 nm. The refractive index of sphere is $n = 1.33$ and the incident light wavelength is $\lambda = 500$ nm. Reproduced with permission.[149] Copyright 2014, Springer Nature.

2.3.1. Subwavelength Nanostructures

As already stated hereinabove, the near field distribution around a dielectric object with dimensions much smaller than the wavelength is similar to that of a plasmonic nanoparticle. Therefore, these dielectric nanoparticle antennas can be used as light scattering and near field enhancement objects. The use of these Mie scattering nanoantennas in vicinity or in the bulk of active layer could couple light into the active layer and enhance their optical path length. It has been shown that silica nanoparticles can offer a higher efficiency enhancement compared to that of Au particles.[147] A similar result was found in the case of quantum-well solar cell where silica and gold nanoparticles induced 17% and 1% increase in the conversion efficiency of the cell.[153] Similarly, the use of closely packed silica subwavelength nanospheres was demonstrated as a promising

approach to improve light trapping in different solar cells such as CIGS,[154] and perovskite solar cells.[155] These ordered particles are mainly obtained using self-assembly fabrication routes. A recent paper proposed a large scale compatible route to coat complex surfaces with a monolayer of silica particles.[156] However, in most of these designs, the enhancement is generally attributed to the scattering property of the particles rather than their antireflective behavior. In other words, the Mie scattering property of dielectric particles dominate their antireflective behavior when the substrate refractive index is low (because there is already a fine matching between air and substrate refractive index). The antireflection functionality can be added to this system when the substrate is a high refractive index medium such as Si or GaAs. It was shown that the deposition of TiO_2 nanoparticles having a diameter of 65 nm can provide high forward transmission across a broad wavelength range and this can go beyond the Au case.[157] It was shown that Au nanoparticle based ARC have low transmission in $\lambda < 550$ nm, which was attributed to parasitic absorption of these plasmonic metals. However, the TiO_2 case operates efficiently over entire visible and short NIR regimes. The use of periodically patterned tapered TiO_2 nanostructures can simultaneously act as an ARC and Mie scatterer to couple the incident light into the active region of the solar cell. This nanostructured top layer has outperformed conventional Si_3N_4 ARC.

Incorporation of these particles within the solar cell medium could substantiate their optical trapping capability (compared to those introduced on the surface). In this case, Mie scattering enhanced near-infrared light response in a thin-film silicon solar cell will increase the optical path length of the incident light. Embedding optically and electrically lossless particles with high scattering efficiency in forward and lateral directions can significantly improve light trapping in semiconductor slabs.[158] Similarly, authors systematically studied the effect of dielectric embedding for the case of methyl ammonium lead iodide perovskite solar cell.[159] For this purpose, they used three different particle types of SiO_2, TiO_2, and Si. They found that the solar absorption could be boosted by about 6% and 10% for SiO_2 and Si particles, while TiO_2 has no impact in the light harvesting of the active layer. Analyzing the electric field distributions, authors proved that the excitation of collective and hybrid (of both localized and propagating character) resonance modes are the reason for this increase. Moreover, the poor performance of TiO_2 nanoparticles stems from the low refractive index contrast between perovskite film and TiO_2 particle which leads to weak light scattering by the spheres.

On the other side, embedding particles in the bottom and within the cell can add up a new scheme for light trapping which is surface texturing. The deposition of sequential layers on these rough nanoparticles' design induces a surface texturing that further facilitates light trapping. The use of spin-coated silica nanoparticles with a radius of 130 nm has led to a 16% enhancement in short circuit current density of the thin Si solar cell.[160] Further theoretical study showed that this enhancement is mainly attributed to surface texturing rather than Mie scattering.[161] In fact, regardless of being metal or dielectric, surface texturing induced by these embedded particles can increase light optical path via light diffraction in an angular way. Theuring et al. compared a flat Si solar cell with three different structures; Ag nanoparticle based texturing, SiO_2 nanoparticle based texturing and inherent texturing.[162] It was shown that the solar cell efficiency is increased from 6.06% to a value of ≈7% for all three cases. The EQE reached to a maximum value of 80% in the textured case. While the maximum value was same for flat and textured cases, the EQE values were slightly higher in the longer wavelengths for plasmonic sample ($\lambda > 550$ nm). So, from these findings, the authors deduced that the optical light trapping capability is mainly defined by the texture of the design rather than the type of material. Van Lare and co-workers demonstrated the functionality of this strategy in the performance improvement of the CIGS solar cell.[163] For this purpose, they compared scattering from front-patterned TiO_2 nanounits with those of back-patterned SiO_2 particles. While TiO_2 front nanoparticles provided a small enhancement in photoconversion efficiency of the solar cell, patterning the Mo/CIGS back interface using silica nanoparticles can increase the solar cell efficiency from 11.1% to 12.3%. The proposed design has reached to an EQE value as large as 80% and its value covers an ultrabroad range extending from 400 nm to above 1200 nm. It was stated that, although this design configuration reduces parasitic absorption on Mo back mirror, its detrimental effect is still the main limiting factor. The same group later introduced an idea based on periodic 2D silica nanomeshes to minimize parasitic absorption in the Mo back contact. They showed that the efficiency of flat solar cell can increase from 8.8% to 11.4% for nanomeshes based back dielectric pattern.[164] The authors attributed this improvement to both optical and electrical loss passivation. It was shown that the silica coating will partially isolate the active layer from the bottom collector metal and this consequently will reduce the recombination probability.

Besides, all these dielectric based trapping mechanisms, these dielectric nanostructures can be also integrated into the illuminating face of a solar cell to act as ARC. These nanostructured dielectric patterns, so called moth's eye inspired designs, are generally made of tapered geometries to gradually match the air impedance into the underlying substrate.[165–167] Patterning these nanoshapes on both sides of a glass substrate can reduce the reflection to a value below 5% in a broad wavelength range.[165] These patterns were integrated with different type of solar cells including dye sensitized and organic solar cells.[166,167] An improved solar cell efficiency of 6.19% (compared to that of 5.16% for a flat design) was acquired mainly originated from the antireflective response of the inverted moth's eye design.[167] Besides this improvement in the optical response of the solar cell, these nanotextured designs could also act as hydrophobic coatings to provide a self-cleaning character for the solar cell design. However, considering the fact that these nanostructured ARCs are grown on glass substrate which already has a small refractive index, the overall efficiency enhancement is not significant. A better functionality for these designs is to use them in flexible PV cells. They can add a significant functionality to top-illuminated flexible organic solar cells where the ITO layer (which has brittleness under repeated bending and needs high temperature deposition processing) should be replaced with a multilayer design such as frequently reported dielectric–metal–dielectric configuration.[168–170] The most commonly employed dielectrics in this three-layer coating

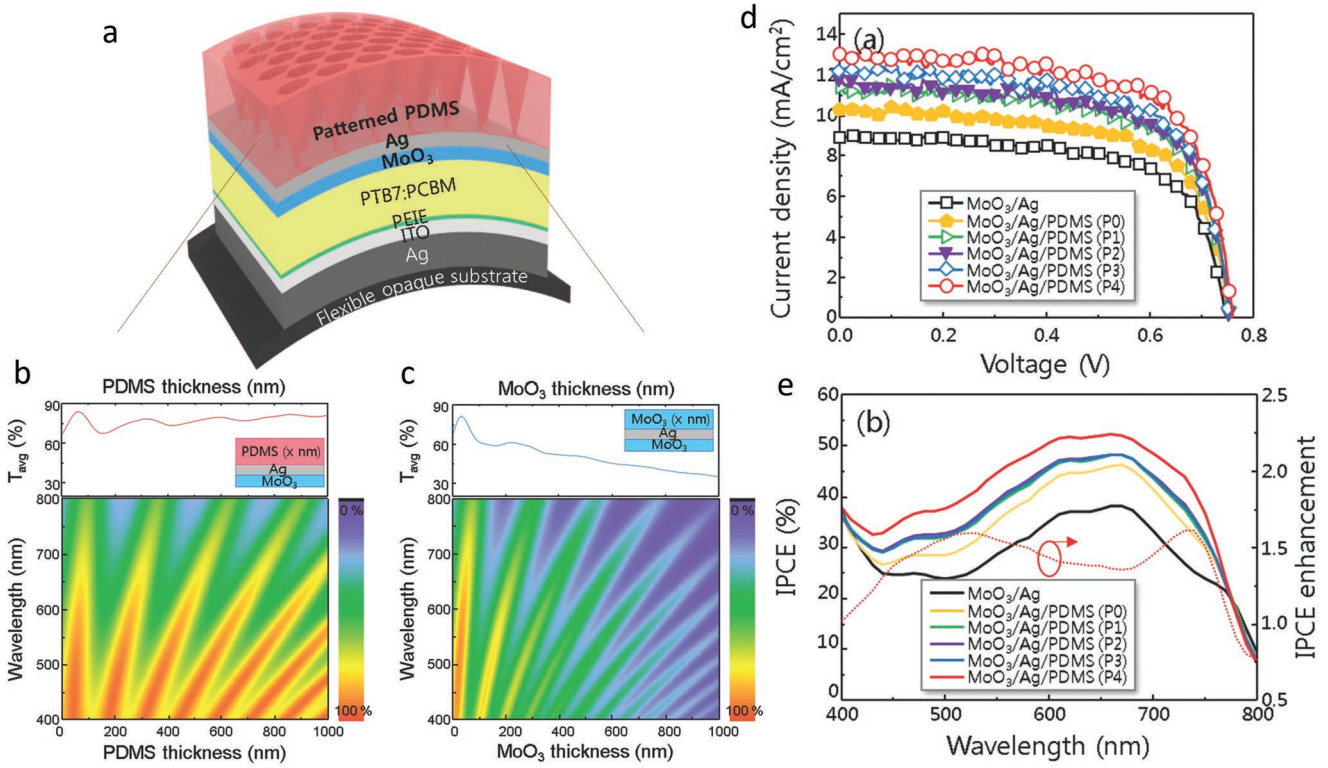

Figure 19. a) Inverted pyramidal polymer texture based organic solar cell. Simulated 2D contour plots of b) MoO_3/Ag/PDMS transmittance as a function of PDMS thickness and c) MoO_3/Ag/MoO_3 transmittance as a function of MoO_3 thickness. Moreover, the average transmittance (T_{avg}) spectra (in the range of 400–800 nm) of each electrode are also plotted. d) photocurrent-voltage characteristics and e) the corresponding IPCE data of the solar cell for different average inverted patterns radii of 160, 230, 270, and 320 nm (denoted as P_1, P_2, P_3, and P_4, respectively) and the case without these patterned PDMS (P_0). Reproduced with permission.[168] Copyright 2015, Wiley-VCH.

are MoO_3, WO_3, and V_2O_5 that have high refractive index dielectrics.[169,170] Therefore, the Fresnel reflection from multiple interfaces will significantly diminish the conversion efficiency of these top-illuminated cells. Ham et al. proposed an elegant design in which the top dielectric is replaced with an inverted pyramidal polymer texture to enhance the transmissivity of the top electrode.[168] This patterned three-layer ARC enhanced solar cell photoconversion efficiency from 4.46% (for a reference conventional cell) to 6.75%. As shown in **Figure 19**a, the proposed design has inverted pyramids as the top layer. To gain a better insight on the functionality of this nanostructured unit, 2D transmittance contour plots of b) MoO_3/Ag/PDMS as a function of PDMS thickness and MoO_3/Ag/MoO_3 as a function of MoO_3 thickness are compared. Moreover, the average transmittance (T_{avg}) spectra (λ = 400–800 nm) of each electrode is also depicted in the same panel, see Figure 19b,c. From this figure, it can be deduced that MoO_3/Ag/MoO_3 multilayer cavity has high transmission at specific layer thickness. However, inverted PDMS based design could maintain its average transmittance high in a wide range of PDMS thickness. Therefore, different pyramidal designs with various radii of 160, 230, 270, and 320 nm (denoted as P_1, P_2, P_3, and P_4, respectively) have been fabricated to find the optimal case. The case without these patterned PDMS is denoted as P_0. As Figure 19d implies, increase in the radius of PDMS inverted patterns will lead to enhancement in the short circuit current and the overall device efficiency. Moreover, the improvement in IPCE values is detected for the sample P_4 compared to P_0 in a wavelength range of 400–800 nm, Figure 19e. This broad enhancement shows the nonresonant nature of absorption enhancement via PDMS antireflective patterns. In dielectric structures, unlike metal units that provide resonant absorption, the absorption improvement is experienced in a broad wavelength regime. This is mainly originated from the ultrabroadband antireflection behavior of these designs.

2.3.2. Wavelength-Scale Microstructures

Besides the previously explained nanodesigns, the use of structures with dimensions close to (or larger than) the incident light wavelength has been proposed as a winning strategy to substantiate light absorption in thin semiconductor layers.[171–175] Dielectric nano- and microspheres are an example of these architectures that have been widely used in different solar cell types and water splitting cells. Similar to other dielectric based designs, these spheres can contribute in device performance enhancement in two main ways; 1) broadband reduction of Fresnel reflection by acting as an ARC and 2) increase in the scattering and optical path length of the light by diffractively coupling of the incident light into the underlying active layer. In the case of thin semiconductor slab, the

reflection from bottom surface also adds FP resonance to further enhance light trapping. In one of the pioneer studies in this field, researchers form Atwater's group demonstrated a significant enhancement in the light absorption of 100 nm thick a-Si based solar cell using hexagonally close-packed SiO_2 monolayer array.[176] FDTD numerical simulations revealed that whispering gallery modes (WGMs) are supported by these spherical objects. Due to the close proximity of these spheres, WGMs couple to each other and form a guided mode resonance. These confined modes cannot be supported with small particles and only spherical objects with wavelength-scale dimensions can excite them. By altering the radius and lattice constant of these spheres, the spectral position of optimal coupling between the WGM and a-Si is tuned. As the size of dielectric sphere becomes larger, a greater number of WGMs will be excited and this will lead to a broader absorption enhancement.[177] Besides the size, other parameters such as shape, refractive index and position of this spherical objects are also prominent to obtain the maximized light trapping. As already stated, these large particles can also contribute in absorption enhancement via reduction in the surface reflection.[171,172] Thus, a better antireflective behavior can be acquired by replacing silica with a higher index dielectric such as TiO_2.[178] This will reduce the impedance mismatch between air and underneath active layer. Moreover, this gradual refractive index change can be attained in a tapered like design. This is the case for a half-spheroid pattern. It was shown that this configuration is the optimum pattern for light enhancement which yields a twofold increase in photocurrent compared to a flat reference cell.[178] The use of periodically patterned polystyrene (PS) half-microspheres with a diameter much larger than the wavelength (≈100 µm) has led to an enhancement as high as 60% in photoconversion efficiency of organic solar cell.[173] All the discussed design architectures utilize these scattering objects at the top surface of the cell. However, they can also be embedded into the bulk of the active semiconductor layer. This has been investigated in a solution-processed solar cell. As shown in **Figure 20**a–e, it was demonstrated that microspheres, embedded within the bulk, can provide a better near field enhancement compared to top and half-embedded designs.[179] A 25% enhancement in photocurrent density was recorded for the case that spheres are fully infiltrated with lead sulfide (PbS) active layer. All the above-mentioned wavelength-scale based spherical scatterers have high Omni-directionality and that makes them practical and large-scale compatible designs for light trapping enhancement in different types of photovoltaic cells. Alongside these optically large spherical objects, other designs such as nanowires, nanorods, and nanocones have been used to simultaneously act as ARC and scattering antenna. These structures can also be combined with spherical geometries.[180] Chao et al. fabricated a tightly packed and randomly oriented ZnO nanorods as a broadband ARC and efficient light scattering scaffold.[181] They showed that the structure has a polarization insensitive and omnidirectional response. The integration of random ZnO nanorods into a CIGS solar cell substantiated the cell performance.[182] A further step on improvement in the ARC behavior of these nanorods have been taken in the ref. [174] The authors have adopted a hydrothermal method to create syringe like nanowires to make the gradual index matching more efficient. Under this nanostructure design, a planar Si_3N_4 ARC has been introduced to get the optimal index matching. Upon this modification, the response of the bare GaAs solar cell has been significantly improved from 14.5% to 19.1%.[174] A more precise control on this refractive index matching can be acquired using random and periodically patterned tapered designs.[183,184] Such nanostructured architectures can offer robust super hydrophobicity and enhanced polarization-independent optical transmission exceeding 98% has over a wide range of wavelength and incidence angles.[184] A flexible, 3D nanocone antireflection film was fabricated to enhance CdTe based solar cell efficiency. The fabricated 3D ARC can be attached to any arbitrary surface which makes it a facial design for enhancing light trapping in other type of thin film solar cells.[185] A similar trapping scheme has been integrated into other types of solar cell. Inverted pyramidal shapes with dimensions in the order of visible light wavelength were prepared using soft elastomeric stamp technique and integrated into organic solar cell as an ARC.[175] Random and patterned V-grooves with dimensions much larger than the wavelength were also employed to enhance the photovoltaic performance of thin organic solar cells.[186–189] These wavelength-scale structured haze films are made using a large-scale compatible route for future printable PVs. They are essentially made on the back surface of substrate to avoid any damage to the organic active layer. They generally use etched molds as a template for soft imprint lithography. The approach, together with large dimensions of the layer, provides us a better route to control the dimension and periodicity of the printed design.

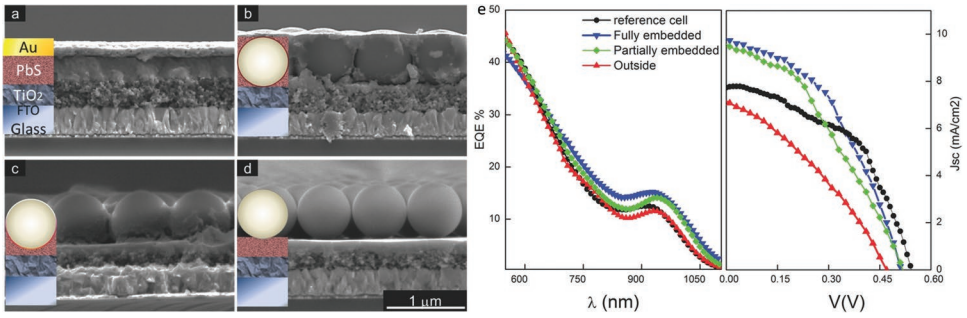

Figure 20. Cross-sectional SEM images of a) planar solar cell design, and the ones with nanospheres. The spheres are b) fully embedded, c) partially embedded or d) outside on the top surface. e) The external quantum efficiency (EQE) and *J–V* characteristics of different configurations under solar irradiation. Reproduced with permission.[179] Copyright 2013, Wiley-VCH.

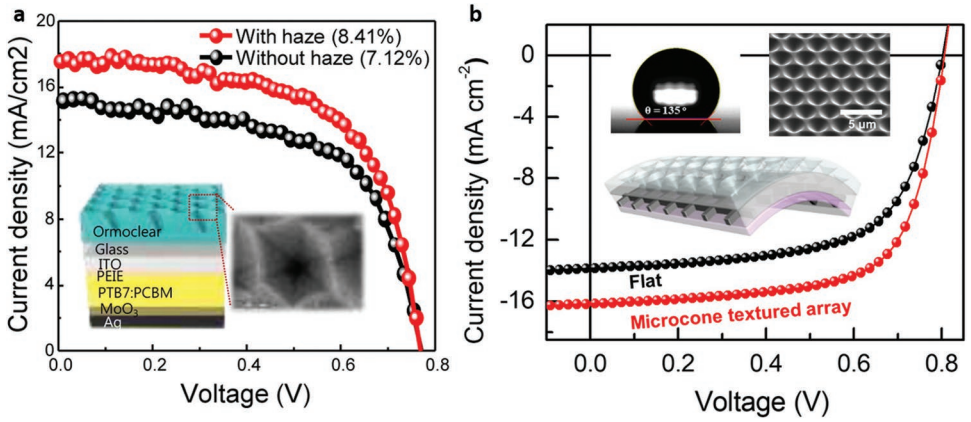

Figure 21. a) The inverted cone ARC coating to increase the organic solar cell efficiency. b) Incorporation of inverted nanocones with dual light trapping and water repellent functionalities. a) Reproduced with permission.[187] Copyright 2016, American Chemical Society. b) Reproduced with permission.[189] Copyright 2018, American Chemical Society.

This could be utilized to tune the resonance peak position by altering the cone dimensions. Thus, the resonance can be placed in the absorption peak of the active layer to maximize the device efficiency. For instance, as shown in,[187] cone dimensions that put resonance at the spectral position of organic layer absorption maximum yields to greatest enhancement in power conversion efficiency. Compared with a flat device (PCE = 7.12%, J_{sc} = 15.6 mA cm^{-2}), improved PCE of 8.41% is achieved in a haze film, **Figure 21**a. Similar to microspheres, these microcones can act as an extreme water-repellent design to add up self-cleaning property to their trapping functionality, as shown in Figure 21b.[189] The efficient light trapping has been also demonstrated in the dimensions orders of magnitude larger than the wavelength. A 1 mm thick polymeric retroreflective textured sheet can be optimized in a way to suppress light escape from the design and a 19% enhancement in efficiency of a thin film polymer solar cell.[190] Alongside these designed structures, organic fiber based paper has been found as an excellent option to enhance light trapping in thin film solar cells.[191–193] This fiber-based paper has ultrahigh haze with high specular light diffraction. Therefore, they can act both as ARC and scattering objects to enhance the optical path length of the incident light. These papers can be easily transferred into any type of solar cell designs. While most of the reports have integrated these micro-scale dielectric scattering objects as top ARC to efficiently couple light into the cavity, they can be used as back-side reflector. A nanoporous anodized aluminum oxide (AAO) template was employed as a back mirror to selectively reflect or transmit the light.[194] In this design, the AAO design reflects light back into cavity in wide viewing angles while it is transparent to normal light incidence. Therefore, this could be a wise design for transparent PV where there is a good trade-off between light absorption and transmission is acquired.

Taking all into account, similar to metals, dielectric objects can be utilized as efficient light trapping schemes. Based on the size, shape, and position of these particles, scattering or antireflective behavior can dominate the enhancement. The use of these nonmetallic objects in both the bottom and top surfaces of the solar cell can provide the most effective trapping condition. In such a hybrid design, top patterned lossless nanounits can diffractively couple incident light into the active layer. This could be substantially improved by introducing a back scattering mirror. Lee et al. realized a highly efficient (η = 16.2%) GaAs based ultrathin solar cell using top contact patterned TiO_2 nanoposts and bottom specular back-side reflector.[195]

2.4. Light Trapping Using Designed Semiconductor Units

One of the recently emerged active research areas is the design of ultrathin nanostructured resonant high index semiconductor metafilms and metasurfaces for broadband light harvesting. Based on the Mie theory, Mie scattering can occur in both metal and dielectric nanospheres and the character of this scattering is defined by particle size and permittivity. Due to strong light decay inside the particle bulk, single metallic object can only support electrical dipoles and quadrupoles.[196] However, a dielectric scatterer can couple light into four main resonant modes of electrical dipole (ed), magnetic dipole (md), electrical quadrupole (eq), and magnetic quadrupole (mq). These modes have been schematically represented in **Figure 22**. Magnetic dipole is created when the light wavelength inside medium (λ/n) becomes comparable with the particle diameter.[196] While md is the only scattering active mode in small particles, enlarging the sphere dimension adds up other major modes to obtain a broad and efficient response. The efficiency and spectral coverage of the scattering can be strengthened by increasing the refractive index value of the sphere that can be the case for Si and GaAs based particles.[197–199] Therefore, a nanostructured

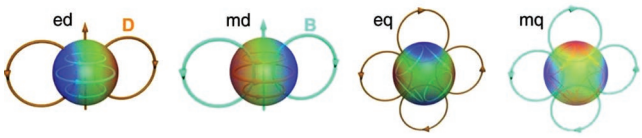

Figure 22. Resonant modes supported by a dielectric nanoparticle unit including electrical dipole (ed), magnetic dipole (md), electrical quadrupole (eq), and magnetic quadrupole (mq). The colors resemble surface charge distribution for ed and eq, and surface current distribution for md and mq modes. Reproduced with permission.[196] Copyright 2016, American Association for the Advancement of Science.

semiconductor design can efficiently couple the free space photons to Mie or leaky mode resonances of these subwavelength units. These high refractive index designs can act as a low-loss plasmonic dielectric nanoresonator.[200] Not only spheres, but also other geometries such as nanowires, nanospheroids, and nanogratings can provide this functionality.[201–205] The spectral position and coverage of this coupling resonance modes is a function of the size, shape, and arrangement of these units and they can be independently tailored to achieve an overall broad response.[197,206] In the case of semiconductor nanowires, it is proven that increasing the wire length will lead to the excitation of a greater number of leaky modes and this in turn causes a broader scattering response. In addition, with this excellent scattering property of high index particles, they can also act as a broadband ARC, if designed properly. Therefore, in recent years, the use of designed semiconductor metasurfaces has been the subject of many studies in energy conversion applications. In this section, we will review some of the recent strategies in this field.

In 2009, a broadband photodetector was made using an individual Ge nanowire.[207] It was shown that leaky mode resonances supported by this high index nanowire are the responsible mechanism for light confinement and harvesting. Generally speaking, in a nanowire design, for the incident angles perpendicular (and oblique) to the nanowire axis, absorption is governed by Mie resonances. While, leaky mode excitation governs light harvesting at grazing incidence angles.[208] In fact, in this case, the nanowire acts as an optical antenna. Thus, upon excitation, incident light is coupled to a leaky mode resonance, and this consequently leads to an enhanced electromagnetic field in the nanowire and substantiates light absorption. It should be noted, leaky mode in a nanowire waveguide is a mode with propagating electromagnetic fields outside the structure. These leaky waves can radiate energy into the surrounding medium and strongly attenuate along the guide axis (causing light absorption within the lossy nanowire). In one of the pioneer studies, Cao et al. demonstrated an unprecedented strong harvesting potential for periodic arrangement of Si nanogratings on top of a glass substrate.[209] This study shows that this array of optical nanoantennas can couple light into their leaky mode resonances and consequently absorb it. It was shown that the response of this grating is a function of array periodicity and at a proper design geometry it can significantly go beyond that of a bulk semiconductor (with the same thickness). Later, this design strategy was utilized for Ge based nanograting on glass substrate.[210] Authors extracted a contour plot to find the optimal real and imaginary parts for ideal semiconductor absorber at a wavelength of 600 nm. While the ideal absorber point is located at low permittivity values, the germanium epsilon data is quite larger. To bring the effective epsilon values to the ideal point, a design made of deep subwavelength gratings was proposed. Based on the effective medium theory, for nanounit dimensions much smaller than the wavelength, the optical permittivity of a semiconductor film can be effectively reduced by its composition with air. As shown in **Figure 23**a, the authors extracted trajectory of epsilon data for different filling fractions (FFs). For an optimal FF of 0.17 and grating width of 50 nm, the effective permittivity values are placed in the optimal point (denoted as point B) and thus metafilm design can have an absorption above 50%, which was an estimated limit for a single layer absorber.[210] The light trapping and concentration inside the nanograting bulk shows a Mie-like behavior that is the responsible mechanism for light absorption in these metafilms. The only drawback with these designs is their polarization sensitivity that limits their usage for practical applications. Infinite-fold symmetric designs, such as nanoshperes, nanodiscs, and nanopillars, can be used to mitigate this deficiency.[211,212] It is worth to note that proper arrangement of particles can also provide this polarization insensitivity, even for elongated asymmetric design units.[114,120,121] Lank et al. demonstrated a strong light absorption using Si nanopillars.[211] As illustrated in Figure 23b, they showed that simultaneous excitation of ed and md resonances is responsible for this strong light absorption. Tuning the pillars' diameter, the spectral position of ed and md resonances were shifted. In smaller radii, the shorter wavelength resonance (ed) was effectively superposed with the longer wavelength mode (which is md) and a broad and flat response was achieved. Increasing this dimension will impose a red-shift in the spectral position of resonance modes and two modes will be split. A recent study utilized these ed and md modes to obtain a near unity absorber in the NIR regime using single layer Ge nanodiscs.[212] They showed that, in a specific disc diameter, both ed and md modes are active and the simultaneous excitation of these modes leads to near perfect light absorption in a narrow wavelength. Moreover, these modes keep their contribution in shorter wavelength regimes where a moderate absorption can be acquired. Similar to previous study, the absorption can be tuned by altering geometrical dimensions. The authors showed that an increase in the height of nanodisc design can induce a red-shift in the absorption profile of the metafilm.[212] The simultaneous excitation of ed and md modes lead to a broad absorption BW using a single layer of Ge patches. These results have been summarized in **Figure 24**a–f. All of the above-mentioned semiconductor based metasurfaces have been fabricated on glass substrate. The introduction of a thin semiconductor layer beneath of the semiconductor unit can make the overall design continuous that can be important for real optoelectronic applications. Moreover, such a structure can support multiple guided mode and Mie resonances in which the superposition of these resonant peak will make overall absorption broad.[213–215] The main mechanism in all of the above-mentioned designs is to couple light into nanostructure to fully harvest it. In the case that these designed particles are brought on top of Si, which is a more practical substrate for photoconversion applications, the structure will also act as a resonant ARC. Therefore, the excitation of electric and magnetic modes will suppress light back-scattering (reflection) and increase its coupling to semiconductor active layer. The use of periodic pattern of Si nanospheres and nanocylinders on a crystalline silicon layer has been proved as a promising resonant ARC layer that enhances silicon solar cell absorption in much smaller dimensions compared to a conventional bulky cell.[216,217] An experimental study utilized silicon nanodiscs on top of a silicon wafer to provide ultrabroadband ARC behavior.[218] Polman and co-workers experimentally demonstrated that dense array of nanodiscs with a 250 nm diameter and a 150 nm height can significantly reduce the reflection from a Si wafer. The average reflectivity of silicon slab was reduced

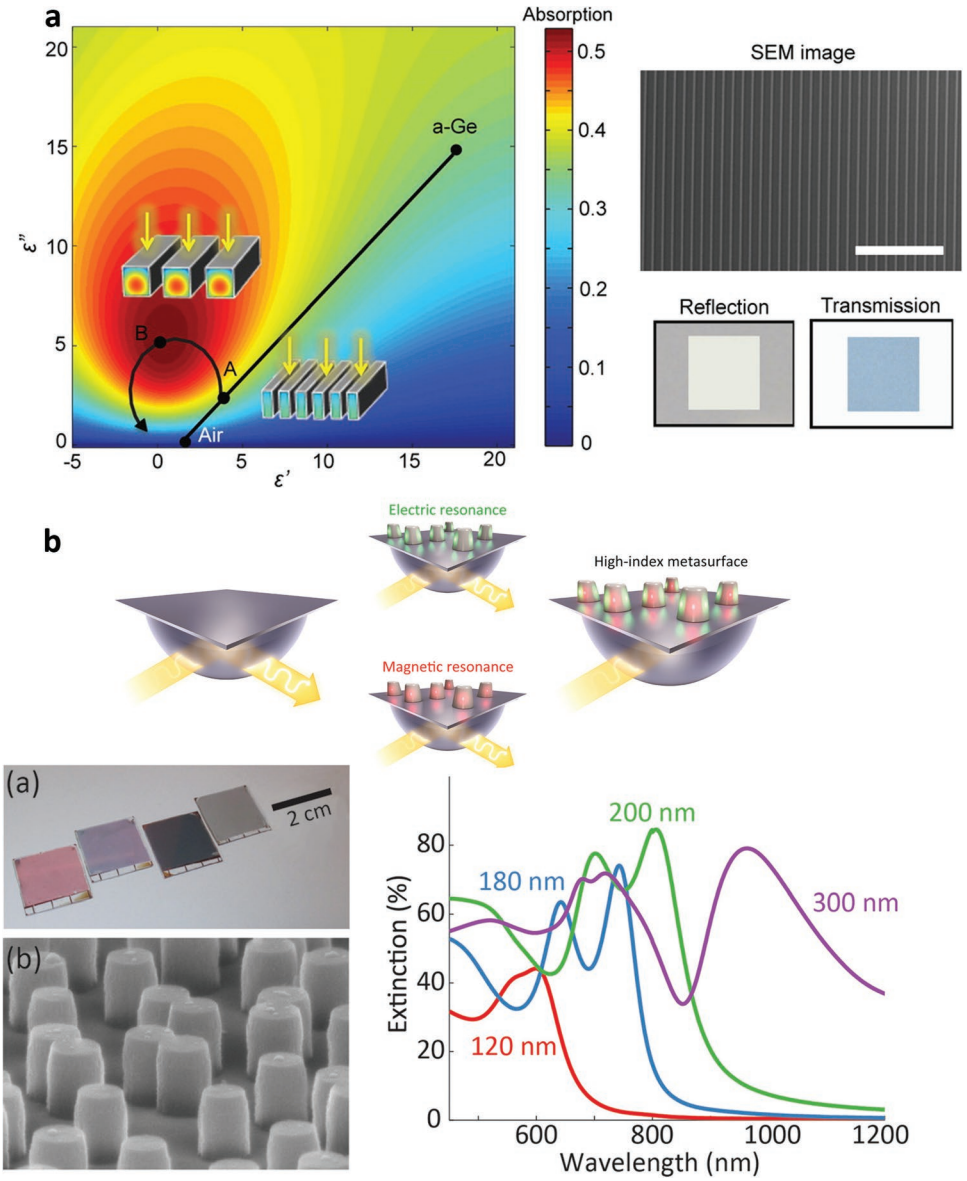

Figure 23. a) The absorption contour plot representing the dependence between the permittivity data for ideal absorber. Solid line represents the permittivity data for a Ge grating with FFs from one (Ge) to zero (air). Points A and B represent an FF of 0.17 for grating widths of 30 and 50 nm, respectively. The SEM and optical images of fabricated samples have also been shown. b) The Si nanopillar design which can simultaneously excite electric and magnetic resonances. The extinction spectra are measured for different pillar radii of 120, 180, 200, and 300 nm. By tuning this geometry, the spectral position of electrical and magnetic resonances can be tuned to obtain a broad response. a) Reproduced with permission.[210] Copyright 2016, American Chemical Society. b) Reproduced with permission.[211] Copyright 2017, American Chemical Society.

from 32.2% to 7.5% in a spectrally broad range from 450 to 900 nm. Coating the design with a 60 nm thick Si_3N_4 ARC further dropped the reflection to a value as low as 1.3%. A recent study realized such behavior using multidimensional/multiresonant nanopillar units.[219] The authors first demonstrated the fact that a judiciously designed, single Mie resonator can represent antireflective behavior at its resonance wavelength. They later showed that a multidimensional design can superpose these resonant responses in which the overall response will be broader compared to single sized sample, see **Figure 25**a. As shown in Figure 25b, FDTD simulations demonstrated that the active pillars are switched in different wavelengths. Therefore, in every wavelength, there is a resonant unit to couple light into the underlying active layer. Therefore, the multidimensional units will lead to a broad anti reflection behavior. Overall, the structure shows less than 4% reflection throughout the whole visible range.

All of the above-mentioned results revealed the potential functionality of semiconductor based metasurfaces for light harvesting applications. This functionality can be strengthened by their integration with metal layer. It has been shown that hybrid metal–semiconductor designs can have high

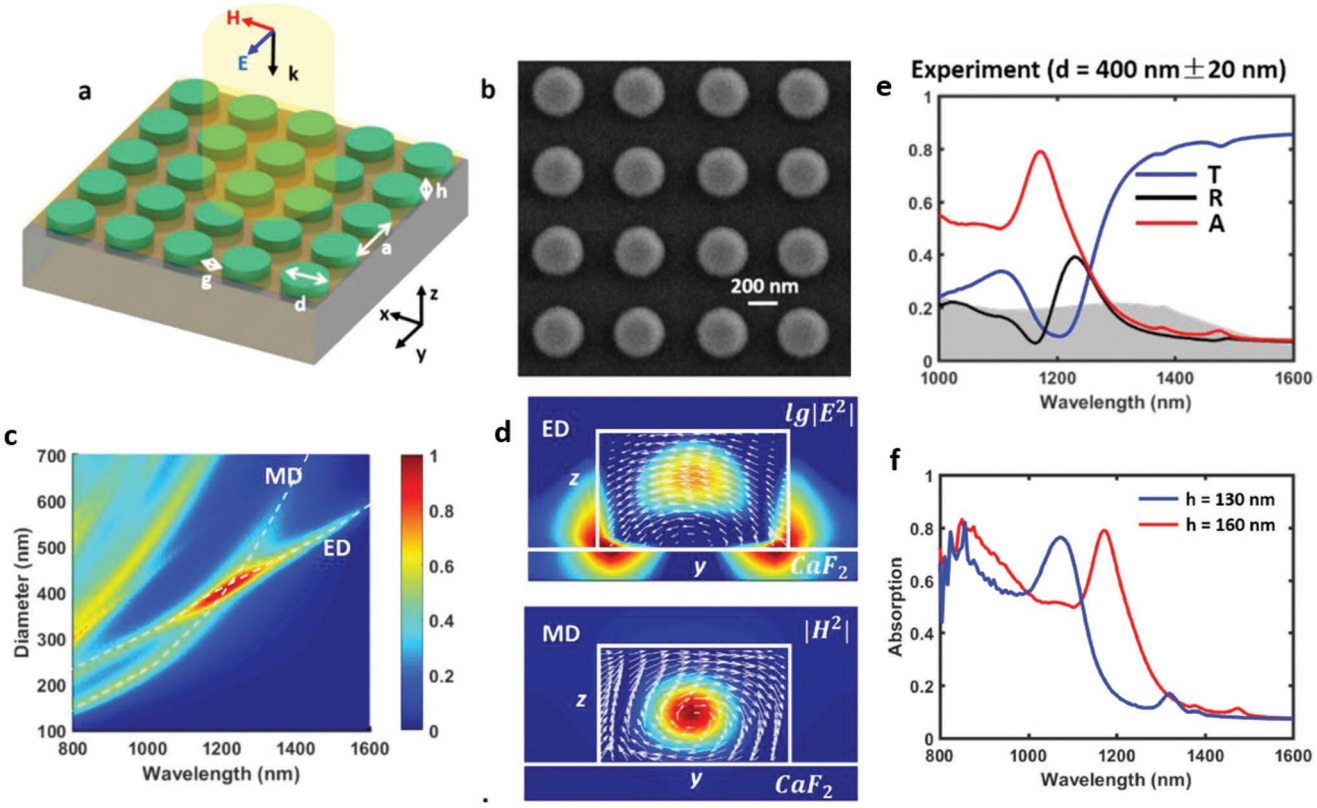

Figure 24. a) The proposed Ge nanodisc metasurface design and b) its SEM image. c) Absorption contour plot as a function of disc diameter and incident light wavelength. d) Field distribution for ed and md resonance modes. e,f) Absorption spectra for the nanodisc designs with different diameter and heights. Reproduced with permission.[212] Copyright 2018, Wiley-VCH.

absorption capacity. This has been shown in nanosphere and nanowire based core–shell designs[220,221] where the core material is metal and the shell is an ultrathin semiconductor layer. According to these studies, when the semiconductor shell layer thickness is thick the structure shows a near unity but narrow absorption response. However, in the case of thin semiconductor, the design performs as an ultrabroadband absorber.[221] In the earlier case, Mie resonance modes are dominant mechanism while in the latter case, FP resonances will be responsible for light near unity absorption. Their use in metal–insulator-semiconductor (MIS) configuration can mimic the field localization of a metal based GSP and their response will be like a low-loss plasmonic.[200,222] Therefore, it can be deduced that the integration of a metallic layer underneath these semiconductor nanounits can intensify their absorption characteristics. This has been proved in many different nanounits' shapes including nanorings, nanoholes, nanopatches, and nanogratings.[223–227] In these designs, the Mie resonances supported by the top semiconductor nanounits are superposed with FP cavity modes of the planar design. Thus, the overall

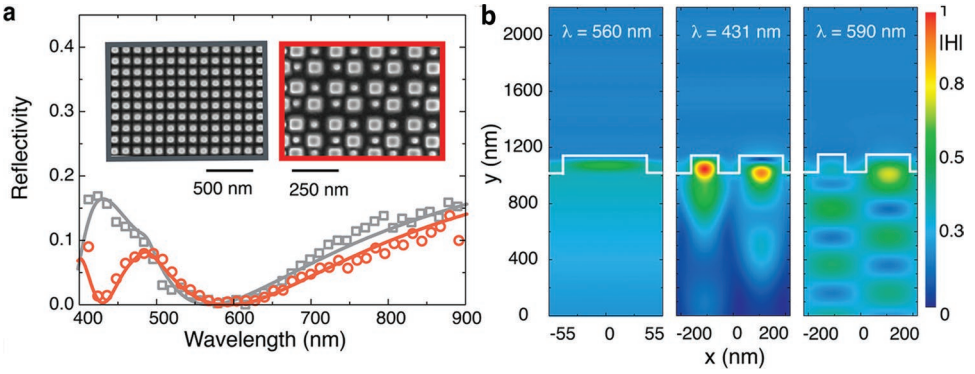

Figure 25. a) The reflection profiles for single and dual sized Mie scattering objects grown on Si wafer. The top SEM images of the sample have been shown in the inset. b) The magnetic field profile across the design at the resonance frequencies of single and dual sized samples. Reproduced with permission.[219] Copyright 2018, American Chemical Society.

structure can act as a dual absorber. To broaden the response, Coupled Mie resonances supported with nanopillar of dissimilar materials (dielectric and metallic) has been recently found as an effective strategy to acquired light near unity absorption in the whole visible light wavelength.[228,229] This broadband response has been demonstrated in Ge nanostructure-based MS design. In looking back at Figure 2, we see that the Ge with a moderate thickness can have proper matching with the ideal data. The matching can be even better if we effectively reduce the n and k data. A team of researcher from Brongersma's group designed a Ge nanograting design on top of gold layer to provide light perfect absorption in a broad wavelength regime,[230] **Figure 26**a–c. This nanograting design can efficiently operate in the TM polarization but it loses its functionality in TE polarized light illumination, Figure 26b,c. This response was further broadened by the utilization of dual-width nanograting beams to provide multiresonance conditions. Figure 26d–f summarizes the above-mentioned results. As these panels imply the absorption response for the proposed dual width grating is superposition of individual structures. A recent study designed a metal–Ge nanodesign to obtain light perfect absorption in an ultrabroadband range covering the whole visible and NIR ranges.[231] In this elegant design, a total average absorption of 81% (69% harvested in active layer) over a broad spectral range, from 400 to 1500 nm, was obtained using a deep wavelength Ge thickness of 80 nm which is built on a gold coating. It was found that the best response is achieved in a nanohole PC design that is fabricated on top of a thin Ge layer, see Figure 26g,h. The authors demonstrated that this ultrabroadband light harvesting stems from the synergy of coupling the incident light to FP resonances hybridized with Brewster modes in the visible spectrum, and with photonic–plasmonic modes sustained by this design in the NIR range. By simultaneously optimizing the Ge layer geometries and PC periodicity, you can put resonance peaks in the spectrally close positions so that the overall response becomes broad.

This semiconductor metasurfaces has exhibited a promising response for PEC-WS applications. Light trapping for solar fuel

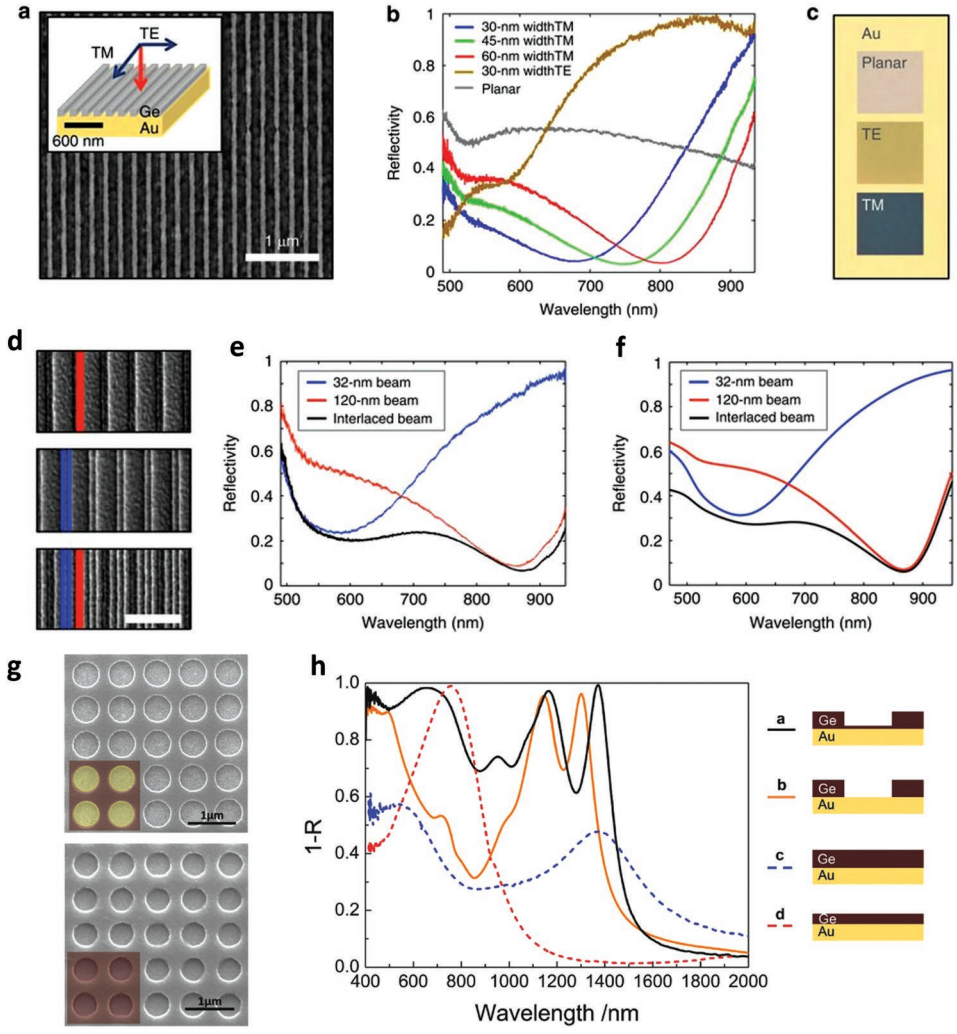

Figure 26. a) The SEM image, b) reflection spectra, and c) optical image of the fabricated Au-Ge nanograting designs with different beam width. d) The SEM image and e,f) the reflection spectra of the multidimensional nanograting design. g) The SEM image and h) reflection spectra of Au-Ge PC based ultrabroadband absorber with different design architectures. a–f) Reproduced with permission.[230] Copyright 2015, Springer Nature. g,h) Reproduced with permission.[231] Copyright 2018, Wiley-VCH.

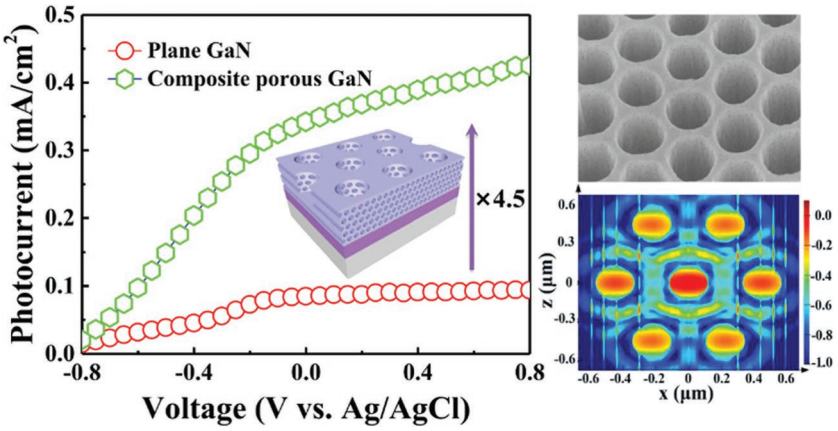

Figure 27. The nanohole GaN based PC for efficient water splitting reaction. Reproduced with permission.[233] Copyright 2018, American Chemical Society.

generation with Mie and guided mode resonances was realized in a thin α-Fe_2O_3 photoanode. The structure is made of gratings that have placed on top of each other to provide a gradual matching between air and underlying substrate.[232] This provides us the opportunity to obtain light strong absorption in dimensions much smaller than the hole diffusion length. Recent studies demonstrated a proper trapping scheme based on semiconductor nanoholes to effectively couple light into photonic modes. As depicted in **Figure 27**, a porous GaN based design with both well-ordered lateral and vertical holes was found as an efficient photoanode compared to that of a planar design.[233] Using this nanohole design, the UV reflectance will be suppressed and the meantime the exposed surface area will be significantly increases. The light will be confined in the hole positions and this intensified light confinement will lead to generation of large density of photocarriers in the vicinity of hole surface. Moreover, the proposed design will introduce a much higher surface area compared to a planar design and this in turn increases the water oxidation activity of the cell. This leads to a 4.5-fold increase in the saturation photocurrent of the structure compared to bare planar GaN photoanode. This strategy is applied for $SrTiO_3$ case where these nanoholes will support LSPR modes to enhance the activity of the design.[234] Similar to Si case, the use of properly designed nanodiscs was found as a promising way to effectively reduce reflection from InP surface. As illustrated in **Figure 28**a–c, a periodic arrangement of InP nanopillars is created at the surface of the photoelectrode to act as resonant ARC.[235] This device displays an unprecedented photocathodic power conversion efficiency of 15.8% for single junction water reduction. Further to improve the layer stability a thin TiO_2 layer was coated on top of the sample without disturbing the antireflective behavior of the metasurface design.[235] Using the self-assembly of lamellar block copolymers, the authors demonstrated a metasurface design that can couple light efficiently to the underlying Si

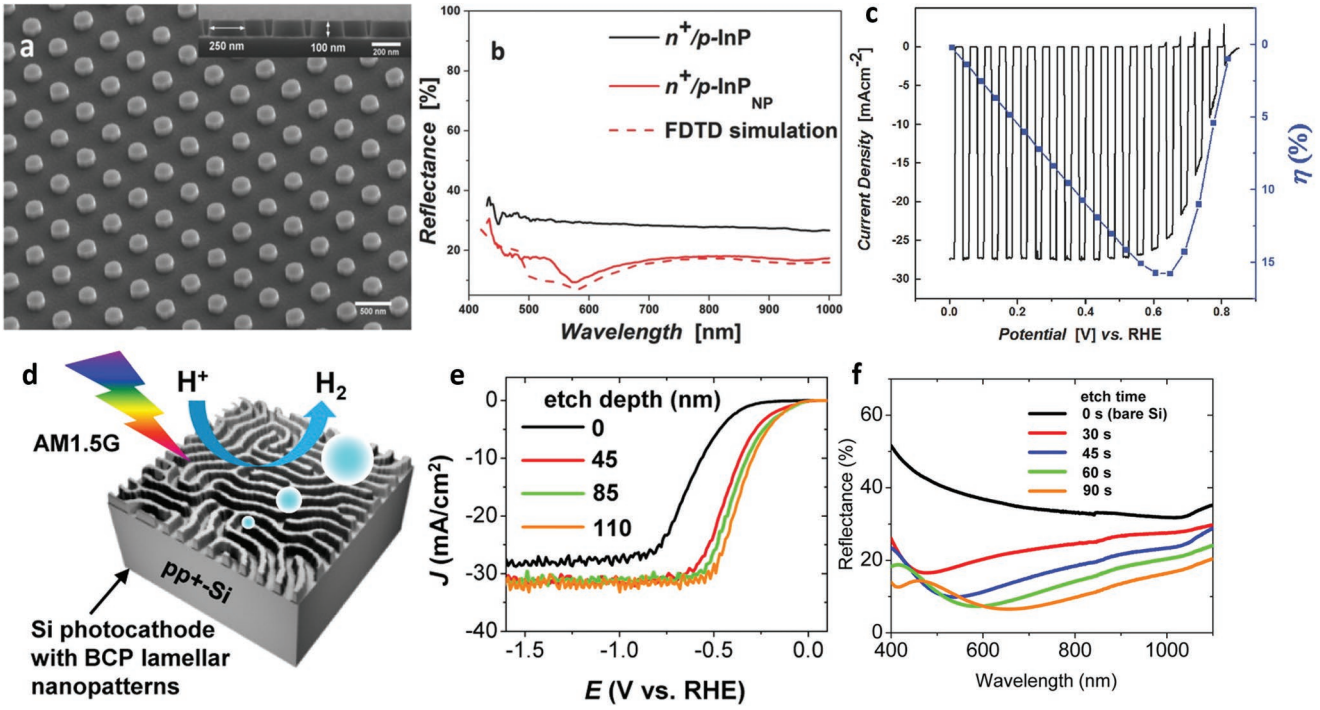

Figure 28. a) The InP nanodisc metasurface design, b) its reflection spectra compared to planar design, and c) its *J*–*V* characteristics. d) Fabrication of Si metasurface based on self-assembly of lamellar block copolymers and e) its activity under solar irradiation as a photocathode with different etch depths. f) The reflection spectra of the bare Si slab and the nanopatterned ones with different etch depths. a–c) Reproduced with permission.[235] Copyright 2016, Wiley-VCH. d–f) Reproduced with permission.[236] Copyright 2015, American Chemical Society.

slab,[236] see Figure 28d. The proposed design can significantly enhance the photocurrent response of the Si photocathode as shown in Figure 28e. This enhancement is mainly attributed into the broadband antireflective behavior of the design. Unlike periodic patterned designs, the proposed design is a random structure with different grooves resonating in different wavelengths. Therefore, the superposition of these resonance modes will lead to near zero reflection in a broad range from 400 to 1100 nm, see Figure 28e. Thus, taking all of this into account, the resonant high index metasurfaces can couple light into the underlying layer through antireflective behavior.

2.5. Impedance Matched Trapping Scaffolds

Another way for coupling light into the ultrathin semiconductor film thicknesses is to employ trapping scaffolds.[237] A trapping scaffold is a designed 3D patterns that provide a gradual matching between air and the device impedance. In previous part, the discussed microstructured dielectric units were placed on top of the sample to efficiently couple incident light into underlying planar device. However, in this 3D architecture, the whole device is grown on a trapping scaffold to enhance light matter interaction in a broad wavelength regime. Moreover, for applications such as PEC-WS, the semiconductor active layer should have interaction with the surrounding environment. Unlike microstructure dielectric units that isolate the active layer from the outside environment, these 3D structures offer both large surface area and strong absorption in ultrathin dimensions. Thus, perfect light absorption can be achieved in ultrathin active layer thicknesses (with large active area and high collection probability) and this consequently leads to efficient operation of a photoconversion device. If nanotexturing of an active material is designed properly, it can improve the device performance in the following ways: i) by increasing the accessible surface area of the system to make reaction more likely to take place, ii) by being effective at multiple angles of incidence (omnidirectionality), and/or iii) by increasing scattering and trapping light inside its scaffold in which light-matter interaction strength is intensified significantly. On the downside, it can adversely affect the carrier dynamics and so cancel out the device performance by introducing optical and electrical recombination sites stemming from i) nonuniform thin film thickness, ii) increased junction area, iii) surface roughness, iv) high aspect ratios, v) parasitic absorptions, vi) localized defects, viii) nonuniform electric field distribution, etc.[237] Functionality of a 2D or 3D textured design greatly depends on the structural, geometrical, and morphological properties of the layer such as film thickness, doping level, surface area, shape, aspect-ratio, periodicity, and surface roughness and they can be varying according to the fabrication processes (dry etching, nanoimprinting lithography, anodization, PECVD, etc.) Therefore, the fabrication route is a crucial factor defining the efficiency of this high aspect ratio trapping design.

All in all, the understanding of efficient light trapping is, therefore, of crucial importance to remarkably improve photon conversion efficiency. In this section, nanostructure designed devices will be categorized into metal and metal oxide-based trapping scaffolds with their incorporating schemes and design guidelines (antireflection coatings, back-reflectors, and surface texturing).

2.5.1. Metal Based Scaffold

To achieve aforementioned purposes, several different morphologies have been utilized. Nanorod (NR), nanowire (NW), nanocone (NC), nanopillar (NPL), nanospike (NSP), nanosheet (NS), nanodendritic (ND), and other 3D structures are among the proposed nanostructures. The main motivation on using these configurations is to increase light absorption efficiency and BW in ultrathin semiconductor layer dimensions. Moreover, structures with tapered feature such as NCs and NWs can act as a broadband impedance-matched designs to couple light into a thin absorbing layer throughout an ultrabroadband range.[238] Therefore, the 3D NC design will be coated with a metal layer which simultaneously acts as an optical mirror and electrical conductor. This configuration has been successfully employed for PEC-WS applications using low extinction coefficient visible active semiconductor layers.[239–241] As an example, Iron oxide (hematite, α-Fe_2O_3) with a relatively small optical bandgap (E_g = 2.0–2.2 eV) can ensure light absorption not only in the UV regime but also in the visible portion of the spectrum which contains about 40% of the solar spectrum. Although hematite has good chemical stability, suitable bandgap, and abundance, it suffers from poor electrical performance with short hole diffusion length. Thus, carriers get recombined before reaching to the semiconductor surface. The use of ultrathin α-Fe_2O_3 film deposited on conductive 3D nanophotonic structure was proposed as a winning strategy to absorb light in a broad range with an intensity near unity, and to keep carrier collection efficiency and surface-active area high. It was shown that the deposition of a thin α-Fe_2O_3 layer on periodically patterned Au nanopillars can improve the response compared to a flat MS junction.[239] The authors have contributed this enhancement to the increased light absorption stemming from both surface plasmon resonances and photonic-mode light trapping in the nanostructured topography. Similar results have been demonstrated for other plasmonic metal–semiconductor combinations where the simultaneous utilization of plasmonic and photonic modes will enhance the absorption of the system.[240,241] Ferry et al. designed and fabricated periodic and random arrays of nanoscatterers placed in the back contact of an ultrathin (<100 nm absorber thickness) a-Si:H solar cell and explained the findings correlated with surface topography and spatial correlations.[242] Similar to the previous design, it was deduced that Ag nanostructured plasmonic back reflector gives photocurrent rising in both the blue and the red portions of the spectrum due to plasmonic and Mie scattering. This back contact ensures i) coupling in the waveguide modes of thin photoabsorber, ii) elongating light path, and consequently iii) increasing short circuit current density. One question that needs to be asked, however, is whether periodic or random nanostructures provide better light trapping in solar cells. In the light of waveguide theory,[243] performance limited-factors was scrutinized for the periodic nanocavity, random pyramidal texture, and the flat substrates in the α-Si based solar cell with an absorber layer of only 250 nm. In the case of periodicity, light is distributed

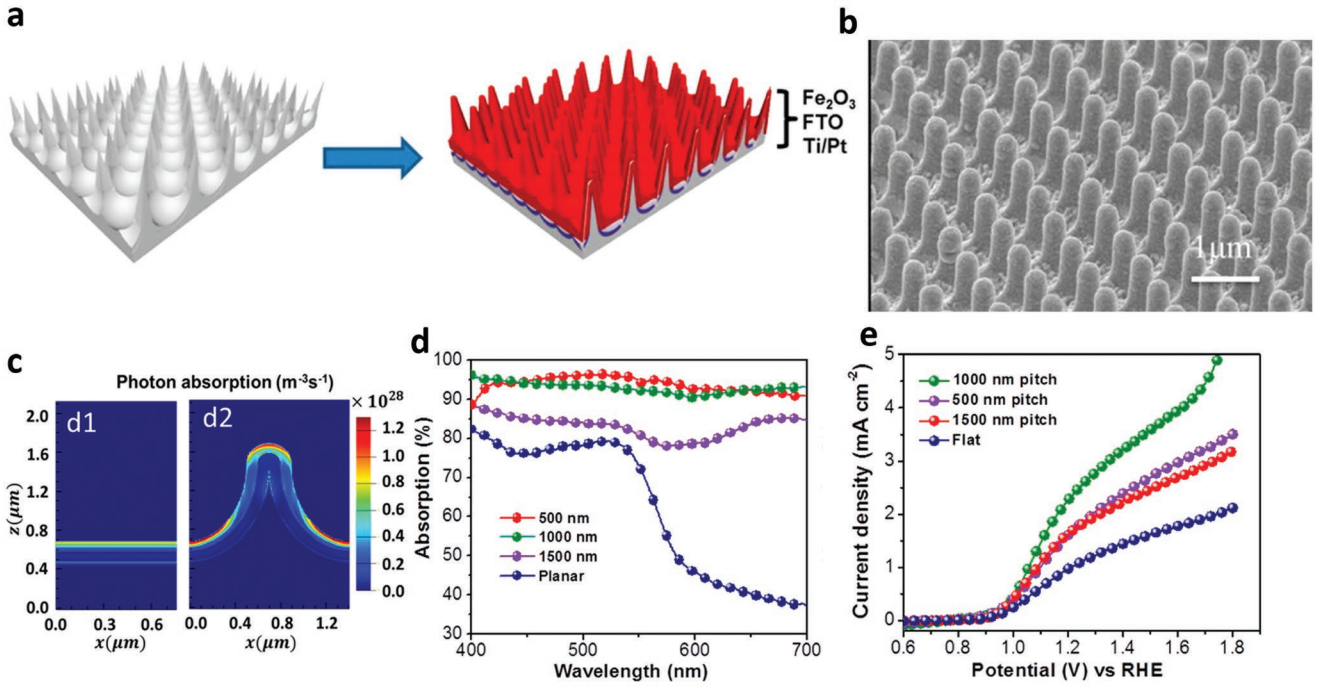

Figure 29. a) The schematic representation of Al NSPs coated with multilayer active design and b) its SEM image. c) The absorption profile across a planar and NSP design. d) The absorption and e) *J–V* profiles for planar and NSP designs with different pitch dimensions. Reproduced with permission.[244] Copyright 2014, American Chemical Society.

equally over its individual diffracting orders and light can be coupled into guided modes at only certain energies. For the random case, however, the Lambertian scatterer is prevailing and it can couple light at any energy, so it distributes light in all directions. However, the strong trapping nature of this designs revealed that there has been almost no difference in the performance of both solar cells with 10.9% efficiencies including periodic nanocavity and the random pyramid substrate.

While these plasmonic designs have subwavelength dimensions, nonplasmonic metals based designs with higher aspect ratios can be used to intensify light trapping in an ultrabroadband spectral range. As a 3D scaffold, Al NSPs are fabricated utilizing anodic aluminum oxide (AAO) in different anodization time, then removed by wet-etching. Afterward, the successive deposition of a Ti-Pt-FTO-α-Fe_2O_3 multilayer was conducted to make the photoanode, as depicted in **Figure 29**a,b.[244] The proposed structure can have much stronger absorption response compared to that of a planar design, Figure 29c. Further improvement was achieved by doping hematite layer with Ti dopants. From Figure 29d, Ti-doped α-Fe_2O_3 on the 3D substrate exhibits much better absorption compared to planar design and consequently they should have higher photocurrent values. As expected, Ti-doped α-Fe_2O_3 on the NSP substrates with three different pitches exhibits much more photocurrent amount as opposed to planar configurations (Figure 29e). The response of such 3D design can be further improved by use of a multilayer shell with proper band alignment. The composite thin films of $ZnFe_2O_4$/α-Fe_2O_3 on 3D NSP design shows a photocurrent density which is 3.4 and 1.9 times greater than that of planar pure α-Fe_2O_3 and $ZnFe_2O_4$/α-Fe_2O_3 on FTO substrate, respectively.[245] In a similar study, AAO template based scaffold was made using an alumina inverted nanocone (i-cone) substrates to grow high-quality crystalline, nanotextured InP thin film to be used in PV and PEC-WS applications.[246] This study merges the benefits of thin film vapor–liquid–solid growth technique (TF-VLS) and AAO to make the structure coating conformally, scalable, low-cost and large grain size (>100 μm), thereby creating high external luminescence efficiency and high open-circuit voltage compared to thin film counterparts. Although a higher aspect ratio provides a better and spectrally broader impedance matching, it is not the only parameter that defines the overall photoconversion response of a system. Lin et al. utilized inverted nanocone (i-cone) nanostructures as a 3D trapping scaffold, due to their gradually tuned refractive index (antireflection effect), self-cleaning, superior mechanical robustness, etc.[247] They built up an αSi:H based solar cell on this 3D pattern with various depth and pitches via nanoimprinting technique instead of costly lithographic and etching processes. Comparing the *J–V* characteristics of designs with three different aspect ratios of 0.25, 0.5, and 1, they found that the optimal case is 0.5 where the photoconversion efficiency is improved to a value of 7.58% (from 5.66% in the case of flat cell). Looking at SEM images of these three cases, it was found that 0.5 aspect ratio i-cones have the most conformal layer with antireflection effect that shows the highest light absorption capability. Therefore, increasing the length of nanostructures does not always make the efficiency higher but also fabrication concerns should be considered. To tackle with this coverage issue, the nanocones can be fully buried using semiconductor active layer.[248] However, this will make the semiconductor layer a bulk design rather than a thin film and this in turn leads to higher recombination and trapping probability. A wise approach can be transfer of light absorbing thin film structure on a predesigned surface-textured substrate. This

not only mitigates coverage issue, but also it provides a big step forward toward the use of variety of materials to convert solar energy into chemical energy or photovoltaic energy. Substantial improvement in PEC-WS performance could be attained by engineering the photoanode design in order to have high light absorption and high charge transfer efficiency simultaneously. In a recent study, a predesigned $BiVO_4$ (≈2.4 eV) based MIS nanocavity was synthesized and transferred on textured polydimethylsiloxane (PDMS) substrates.[249] The thickness of active layer was only ≈80 nm, which is much smaller than its light absorption depth (≈200–500 nm). However, transferring this MIS cavity on a trapping pattern has significantly improved its water oxidation activity. For this aim, modified water assisted transfer printing (WTP) method was utilized and it seems more advantageous than other surface textured methods in terms of process cost, material choices as textured substrates, and ability to being coated conformal by light absorbers. As illustrated in **Figure 30**a,b, $BiVO_4$ integration on the patterned PDMS, causes an increment of the surface roughness, and introduces light trapping strategy in two ways; i) *resonant light trapping*: Au film is added as a back reflector for $BiVO_4/SnO_2$ multilayer to create an optical cavity and to introduce strong interference effects for light perfect absorption, ii) *light retrapping*: some escaped back-reflected photons from surface textured $Au/SnO_2/BiVO_4$ film will be redirected and trapped with the design. In fact, the textured pattern has a wavelength-scale periodicity, so it operates as a 2D grating that diffracts light in angular directions. As shown in Figure 30c,d, the textured $BiVO_4$ photoelectrode fabricated by WTP method and it improves the photocurrent value from 0.34 mA cm^{-1} at 1.23 V_{RHE} (for SnO_2/ $BiVO_4$ thin film) to 0.86 (for $Au/SnO_2/BiVO_4$ on flat substrate) and 1.37 mA cm^{-1} (for $Au/SnO_2/BiVO_4$ on patterned PDMS) and further to 2 mA cm^{-1} at 1.23 V_{RHE} when iron oxyhydroxide oxygen evolution catalyst was added (for $Au/SnO_2/BiVO_4$+FeOOH on patterned PDMS). Thus, a hybrid design that combines cavity enhanced strong interference and scaffold enhanced light trapping is an elegant way to boost the activity of a thin film based photoconversion system. A recent paper demonstrated an efficient PEC-WS photoanode where a $WO_3/BiVO_4$ double layer is sandwiched with an Au nanosphere trapping scheme on bottom, and Au nanoparticles on top.[250] Thus, the structure can benefit from multiple light trapping mechanisms including strong interference of MIS cavity, scaffold induced light trapping, and top gold nanoparticles originated gap plasmon excitation. All these optical benefits, together with proper carrier separation (in double layer junction) and collection, will lead to a significant increase in the water oxidation capability of the photoanode. Another example of such a hybrid design that utilizes multiple trapping strategies is provided in ref. [251] Lin and co-workers developed a flexible α-Si:H based solar cell in which 3D nanodent (ND) array is employed as a back reflector to enhance optical path length through exciting hybrid optical modes. The 3D patterned substrate is fabricated by the anodization of flexible and low-cost Ti foil. Moreover, to suppress the light reflection from the top surface, a PDMS based nanopillar membrane is stacked on top of the cell that performs as a broadband and omnidirectional ARC that scatters light into the active layer. While the trapping ND scaffold can significantly improve light absorption in longer wavelengths (compared to planar design), ND covered pillar (NDP) structure will further enhance light harvesting in shorter wavelength values due to ARC behavior of PDMS nanopillars. Thus, solar cell efficiency will be improved from 5.68% (for planar design) to 8.05% (for NDP based design) under AM 1.5 irradiation. The discussed

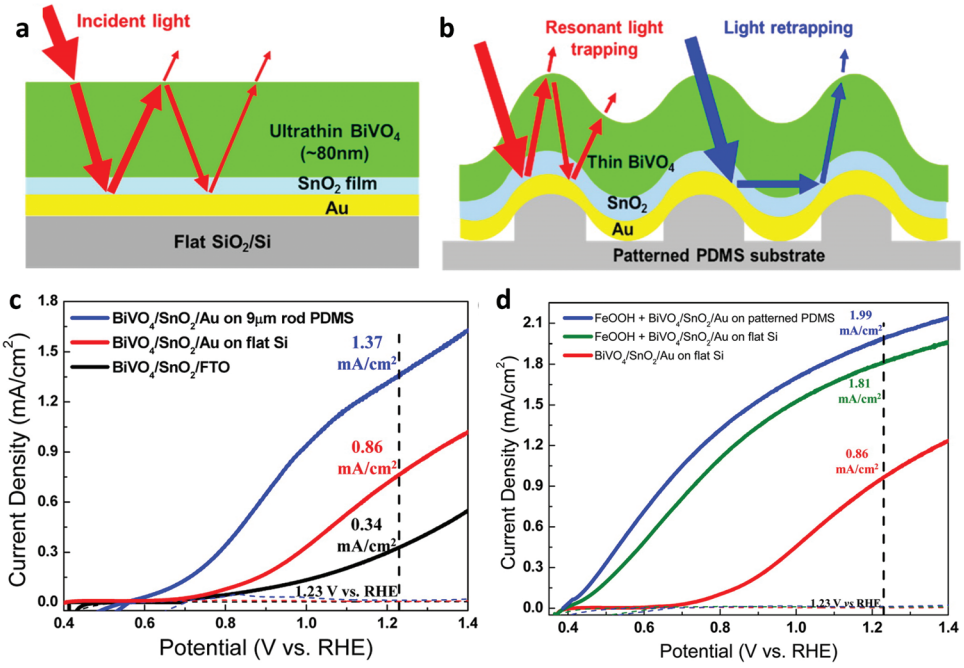

Figure 30. The proposed MIS cavity on a) flat and b) textured design. c) The linear sweep voltammetry of different configurations and d) their response upon adding a catalyst on top of the active $BiVO_4$ layer. Reproduced with permission.[249] Copyright 2016, American Chemical Society.

trapping scaffolds can be also made using semiconductor layers, such as Si, which has a mature processing route. Using Si NCs, we can couple light into ultrathin semiconductor layers or create efficient junctions. Ultrathin transition-metal dichalcogenides (TMDs) (MX_2; M = Ti, V, Ta, Mo, Re, W and X = S, Se, Te) are one of the most promising 2D layered materials as next-generation atomically thin devices and have recently become popular due to their unique electrical, optical, and electrochemical characteristics that do not exist in their bulk counterparts. Unlike other materials, the thickness of 2D layered materials also limited their optical absorption. As revealed in a recent study,[252] trilayers of CVD-grown molybdenum disulfide (MoS2) integrated into light trapping SiO_2/Si nanocone arrays (SiNCs) show great enhancement in the photoresponsivity of photodetectors. The findings indicate that this 3D architecture of SiNCs minimize the reflection via a FP resonance in SiO_2 thin layers (50 nm) and concentrate the light across the whole visible spectrum through Mie-like resonance modes supported by NC design. Recently, Fan et al. utilized this trapping scheme in water PEC-WS application. They fabricated highly efficient and stable photocathodes by integrating a crystalline MoS_2 catalyst with ≈2 nm Al_2O_3 protected n^+p-Si NCs.[253] Sputtering method using a MoS_2 target along with a post annealing step led to a vertically standing, conformal, and crystalline nano-MoS_2 layer on Al_2O_3/n^+p-Si photocathode. The designed photocathode shows promising features including 0.4 V versus RHE onset potential and 35.6 mA cm^{-2} saturated current density.

2.5.2. Metal Oxide Based Scaffold

As can be clearly seen, all of these lossy material-based scaffolds such as metal nanostructures have improved light absorption significantly in ultrathin coating thicknesses. However, the substantial improvement in photocurrent density is less compared to its absorption capability. The reason is the high lossy nature of metals (such as Ti and Pt) compared to low-loss semiconductor layers. In an impedance-matched trapping photonic design such as NC, light is strongly confined between cones where both metal and semiconductor layers have the capability to absorb this light. However, metals have much larger extinction coefficients compared to semiconductors and, therefore, most of the light is dissipated in the metal layer and semiconductor active layer cannot fully utilize the incoming broadband solar irradiation. In other words, parasitic absorption by metal host is quite significant in this architecture. Therefore, it is envisioned that a better strategy is employing lossless gradual index variant photonic designs to provide this trapping mechanism so the whole incident light will be harvested by the semiconductor layer.[254–257] In this design configuration, the predesigned host is made of transparent conductive oxides (TCOs) such as ZnO, ITO, and FTO. Thus, it would serve as an electrical collector for photogenerated electron/hole pairs. The use of high aspect ratio cones coated with an ultrathin Fe_2O_3 layer was designed to orthogonalize the photon propagation and carrier transport by nanostructuring close pack.[258] In the meantime, in this architecture, there needs to be a wise ARC due to the refractive index mismatching (Fe_2O_3 > water) without hampering the water splitting reactions. To tackle this problem, the periodicity of nanocone lattice was designed smaller than the wavelength of the incident light and their height sufficiently large to be able to make a smooth transition. A square lattice of core–shell ITO/(20 nm) Fe_2O_3 NCs, placed on aluminum mirror, yields to perfect optical impedance matching between the water (tip) and nanocones (the bottom of the nanocones). In the same logic, both cone and pyramid have better antireflection than inverted pyramid (tips has better impedance matching than the ridges), but inverted pyramid absorb light most in longer wavelengths due to packing more hematite in such geometry, in other words, the volume of hematite shell in pyramid is higher. Assuming near ideal carrier collection (due to layer thickness below hole diffusion length), it has been estimated that such structure can reach to a theoretical maximum photocurrent value of 12.5 mA cm^{-2} for a cone length above 1 μm, **Figure 31**a,b. This configuration was also experimentally verified as an efficient architecture for water splitting.[259]

A similar modeling approach has been utilized for ZnO NW scaffold based solar cell, see Figure 31c,d. It was theoretically proved that radiative losses can be increased by making core–multishell heterostructures with nonabsorbing/dielectric materials to obtain minimum impedance mismatch. In this 3D pattern, superabsorber of α-Si ultrathin layer with an ultrathin thickness (<10 nm) was designed and engineered to have an absorption above 90% in solar spectrum.[260] As shown in Figures 31d, α-Si (10 nm) is sandwiched between the rectangular shaped, nonabsorber ZnO NWs and multilayer nonabsorbing shells of SiC (30 nm), ZnO (30 nm), and SiO_2 (50 nm). Thus, the increased radiative loss of leaky modes of α-Si results in enhanced solar absorption in this design that pushes the Lambertian limit in the same spectrum, Figure 31e. This nonabsorbing core and nonabsorbing multishell layer with gradually refractive index matching design can be also applied to other type of solar cells such as CdTe, as depicted in Figure 31f. These trapping lossless scaffolds were found as a promising architecture for a-Si based solar cell where an efficiency as high as 9.4% can be achieved using glass microcones as the host.[256,257] Taking inspiration from low-cost a-Si solar cells (α-Si, ~1.7 eV), its ultrathin low-cost photocathode was built for PEC-WS application. The a-Si based cell was grown on a 1.8 μm thick pyramidally textured ZnO transparent front electrode on a glass substrate by low-pressure chemical vapor deposition using diethylzinc and H_2O as precursor gases. The design is capped with a thin TiO_2 as a protection layer.[261] To substantiate the activity of the cell, Ni-Mo alloy as earth-abundant cocatalyst is assembled onto the TiO_2, and the PEC device performances are compared with the state-of-the-art hydrogen evolution catalyst, Pt. According to the obtained results in both cases, the current densities are similar of ≈11 mA cm^{-2} at 0 V_{RHE}, and the hydrogen evolution efficiency of 5.5%, which is almost equal to that of Pt as catalyst. However, the photocathode thickness is overall ≈300 nm, and the performance of this cell can compete with precious metal based PEC devices.

3. Summary, Challenges, and Outlook

Taking all of the above-mentioned studies into account, the main goal in these light harvesting devices such as PV and PEC-WS

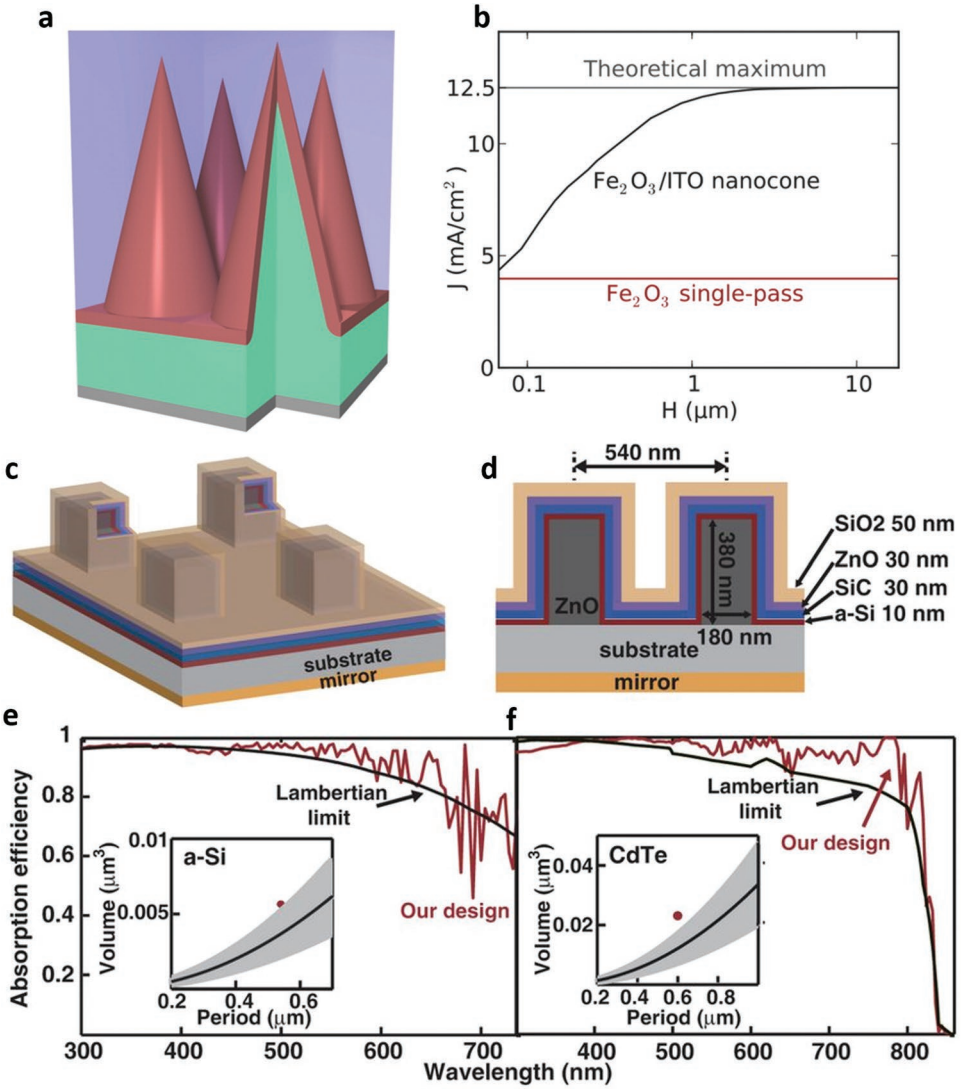

Figure 31. a) Core–shell ITO/(20 nm) Fe_2O_3 NC design and b) its estimated saturated current density as a function of cone length. c,d) Proposed ZnO NW based multilayer ideal absorber and comparison between Lambertian limit and the absorption responses of this ideal design for e) a-Si and f) CdTe based solar cells. a,b) Reproduced with permission.[258] Copyright 2014, American Chemical Society. c–f) Reproduced with permission.[260] Copyright 2014, Springer Nature.

cells is to obtain near perfect light absorption in dimensions smaller or comparable with carrier's diffusion length. Another requirement is the absorption BW that should be maximized to be able to use most of the solar spectrum power. This goal has been already accomplished in commercial single crystalline solar cells such as GaAs and Si based ones, with hundreds of micrometers of thickness. However, for most of the semiconductors, there is a large mismatch between LD and LPD and this limits their photoconversion efficiency and their further up scaling. This mismatch becomes more significant for noncrystalline designs where the LD reduces to nanometer scale dimensions. Moreover, the fabrication of single crystalline layers requires complex and high-cost processing. Thus, briefly, an optically thick and electrically thin photoconversion design with a broad absorption response is our ultimate goal. In this review, a wide variety of light trapping strategies were comprehensively studied to find a proper configuration for efficient coupling of incident light into ultrathin semiconductor active layers. Generally speaking, the main purpose in use of these light trapping schemes was simultaneous suppression of Fresnel reflection and the enhancement of light optical path length within the semiconductor active area. Light trapping was realized by strong interference in planar multilayer configurations, incorporation of plasmonic and dielectric objects, semiconductor nanounits with designer absorption, and 3D trapping scaffolds. From the optical performance perspective, it was demonstrated that all these strategies can be effective and efficient. In summary, the highest conversion efficiencies were attained in hybrid designs where two or more trapping strategies have been added to the cell design to maximize its performance. From the electrical performance perspective, bringing active layer thickness down to carriers' diffusion length will maximize their collection probability. However, the layers' crystallinity and the junction properties are two crucial factors

that define the cell performance. Therefore, the ideal case is the epitaxial growth of single crystalline layers with good junction properties. As an alternative, a proper transfer process can be adopted for this purpose. From the fabrication perspective, among all these methods, the use of a lithography-free planar structure is favorable. These cavity designs are large scale compatible and they can be fabricated by common cleanroom processing. From this point of view, large dielectric trapping units are also suitable choices for upscaling. Moreover, predesigned trapping templates can be attached to conventional PV cells to enhance device efficiency without adding an extra processing step. Thus, the advancement of ultrathin metamaterials based absorbers is anticipated to be a fruitful area of research to pave the way for design of highly efficient photoconversion devices in a wide variety of semiconductor materials.

Acknowledgements

This work was supported by the projects DPT-HAMIT and TUBITAK under Project Nos. 113E331, 114E374, and 115F560. E.O. acknowledges partial support from the Turkish Academy of Sciences. F.K. thanks TÜBA-GEBİP for the young investigator award and BAGEP for the young scientist award.

Conflict of Interest

The authors declare no conflict of interest.

Keywords

light trapping, metamaterials, metasurfaces, photovoltaics, water splitting

Received: January 6, 2019
Revised: April 10, 2019
Published online: May 27, 2019

[1] G. G. Yadav, Y. Wu, G. Zhang, D. Liang, S. Finefrock, H. Yang, H. Fang, *Nanoscale* **2011**, *3*, 2430.
[2] Y. Lin, S. Zhou, D. Wang, G. Yuan, R. Liu, S. W. Sheehan, *Chem. Phys. Lett.* **2011**, *507*, 209.
[3] P. V. Kamat, K. Tvrdy, D. R. Baker, J. G. Radich, *Chem. Rev.* **2010**, *110*, 6664.
[4] F. Stellacci, C. M. Leroy, M. Cornuz, C. Hébert, K. Voïtchovsky, H. Dotan, M. Grätzel, A. Rothschild, S. C. Warren, *Nat. Mater.* **2013**, *12*, 842.
[5] K. Sivula, F. Le Formal, M. Grätzel, *ChemSusChem* **2011**, *4*, 432.
[6] Z. Li, E. Palacios, S. Butun, H. Kocer, K. Aydin, *Sci. Rep.* **2015**, *5*, 1.
[7] N. Mattiucci, M. J. Bloemer, N. Aközbek, G. D'Aguanno, *Sci. Rep.* **2013**, *3*, 3203.
[8] H. Deng, Z. Li, L. Stan, D. Rosenmann, D. Czaplewski, *Opt. Lett.* **2015**, *40*, 2592.
[9] M. Chirumamilla, A. S. Roberts, F. Ding, D. Wang, P. K. Kristensen, S. I. Bozhevolnyi, K. Pedersen, *Opt. Mater. Express* **2016**, *6*, 2704.
[10] G. Kajtár, M. Kafesaki, E. N. Economou, C. M. Soukoulis, *J. Phys. D: Appl. Phys.* **2016**, *49*, 055104.
[11] A. Ghobadi, H. Hajian, M. Gokbayrak, B. Butun, E. Ozbay, *Nanophotonics* **2019**, *1*, 1.
[12] Y. K. Zhong, Y.-C. Lai, M.-H. Tu, B.-R. Chen, S. M. Fu, P. Yu, A. Lin, *Opt. Express* **2016**, *24*, A832.
[13] A. Ghobadi, S. A. Dereshgi, H. Hajian, B. Bozok, B. Butun, *Sci. Rep.* **2017**, *7*, 4755.
[14] A. Ghobadi, H. Hajian, A. R. Rashed, B. Butun, E. Ozbay, *Photonics Res.* **2018**, *6*, 168.
[15] A. Ghobadi, H. Hajian, S. A. Dereshgi, B. Bozok, B. Butun, E. Ozbay, *Sci. Rep.* **2017**, *7*, 1.
[16] S. A. Dereshgi, A. Ghobadi, H. Hajian, B. Butun, *Sci. Rep.* **2017**, *7*, 14872.
[17] A. Ghobadi, H. Hajian, B. Butun, E. Ozbay, *ACS Photonics* **2018**, *5*, 4203.
[18] M. A. Kats, F. Capasso, *Laser Photonics Rev.* **2016**, *10*, 735.
[19] M. A. Kats, R. Blanchard, P. Genevet, F. Capasso, *Nat. Mater.* **2013**, *12*, 20.
[20] A. Ghobadi, H. Hajian, M. C. Soydan, B. Butun, E. Ozbay, *Sci. Rep.* **2019**, *9*, 1.
[21] A. Ghobadi, S. A. Dereshgi, B. Butun, E. Ozbay, *Sci. Rep.* **2017**, *7*, 14538.
[22] J. Park, J. Kang, A. P. Vasudev, D. T. Schoen, H. Kim, E. Hasman, M. L. Brongersma, *ACS Photonics* **2014**, *1*, 812.
[23] Y. Zhang, W. Liu, Z. Li, H. Cheng, Y. Zhang, G. Jia, S. Chen, *Appl. Phys. Lett.* **2017**, *111*, 1.
[24] D. Jariwala, A. R. Davoyan, G. Tagliabue, M. C. Sherrott, J. Wong, H. A. Atwater, *Nano Lett.* **2016**, *16*, 5482.
[25] D. Liu, H. Yu, Y. Duan, Q. Li, Y. Xuan, *Sci. Rep.* **2016**, *6*, 1.
[26] F. F. Schlich, R. Spolenak, *Appl. Phys. Lett.* **2013**, *103*, 213112.
[27] S. S. Mirshafieyan, H. Guo, J. Guo, *IEEE Photonics J.* **2016**, *8*, 1.
[28] B. H. Woo, I. C. Seo, E. Lee, S. Y. Kim, T. Y. Kim, S. C. Lim, H. Y. Jeong, C. K. Hwangbo, Y. C. Jun, *ACS Photonics* **2017**, *4*, 1138.
[29] B. Ding, M. Qiu, R. J. Blaikie, *Opt. Express* **2014**, *22*, 25965.
[30] K.-T. Lee, S. Seo, J. Y. Lee, L. J. Guo, *Adv. Mater.* **2014**, *26*, 6324.
[31] H. Song, L. Guo, Z. Liu, K. Liu, X. Zeng, D. Ji, N. Zhang, H. Hu, S. Jiang, Q. Gan, *Adv. Mater.* **2014**, *26*, 2737.
[32] Z. Xia, H. Song, M. Kim, M. Zhou, T. H. Chang, D. Liu, X. Yin, K. Xiong, H. Mi, X. Wang, F. Xia, Z. Yu, Z. Ma, Q. Gan, *Sci. Adv.* **2017**, *3*, e1602783.
[33] D. Liu, L. Wang, arXiv:1710.06550 [physics.app-ph] **2017**.
[34] D. Liu, H. Yu, Z. Yang, Y. Duan, *Nano Res.* **2016**, *9*, 2354.
[35] D. Liu, Q. Li, *Nano Energy* **2017**, *34*, 172.
[36] S. Kment, F. Riboni, S. Pausova, L. Wang, L. Wang, H. Han, Z. Hubicka, J. Krysa, P. Schmuki, R. Zboril, *Chem. Soc. Rev.* **2017**, *46*, 3716.
[37] A. K. K. Kyaw, D. H. Wang, D. Wynands, J. Zhang, T. Q. Nguyen, G. C. Bazan, A. J. Heeger, *Nano Lett.* **2013**, *13*, 3796.
[38] J. T. Liu, X. H. Deng, W. Yang, J. Li, *Phys. Chem. Chem. Phys.* **2015**, *17*, 3303.
[39] A. Ingenito, O. Isabella, M. Zeman, *ACS Photonics* **2014**, *1*, 270.
[40] H. Hajian, A. Ghobadi, B. Butun, E. Ozbay, *Opt. Express* **2017**, *25*, 31970.
[41] H. Lu, X. Gan, D. Mao, Y. Fan, D. Yang, J. Zhao, *Opt. Express* **2017**, *25*, 21630.
[42] J. D. Ryckman, *ACS Photonics* **2018**, *5*, 574.
[43] J. Zheng, R. A. Barton, D. Englund, *ACS Photonics* **2014**, *1*, 768.
[44] Y. Ben Wu, W. Yang, T. B. Wang, X. H. Deng, J. T. Liu, *Sci. Rep.* **2016**, *6*, 1.
[45] L. Jiang-Tao, C. Yun-Kai, T. Hong, W. Dai-Qiang, W. Zhen-Hua, *Nanotechnology* **2018**, *29*, 144001.
[46] H. Dotan, O. Kfir, E. Sharlin, O. Blank, M. Gross, I. Dumchin, G. Ankonina, A. Rothschild, *Nat. Mater.* **2013**, *12*, 158.
[47] X. Yang, R. Liu, C. Du, P. Dai, Z. Zheng, D. Wang, *ACS Appl. Mater. Interfaces* **2014**, *6*, 12005.
[48] J. P. McClure, K. N. Grew, D. R. Baker, E. Gobrogge, N. Das, D. Chu, *Nanoscale* **2018**, *10*, 7833.

[49] Y. Piekner, H. Dotan, A. Tsyganok, K. Deo Malviya, D. A. Grave, O. Kfir, A. Rothschild, *ACS Photonics* **2018**, *5*, 5068.
[50] A. G. Tamirat, J. Rick, A. A. Dubale, W. N. Su, B. J. Hwang, *Nanoscale Horiz.* **2016**, *1*, 243.
[51] A. Kay, B. Scherrer, Y. Piekner, K. D. Malviya, D. A. Grave, H. Dotan, A. Rothschild, *Adv. Mater.* **2018**, *30*, 1802781.
[52] Y. H. Lee, J. Kim, J. Oh, *ACS Appl. Mater. Interfaces* **2018**, *10*, 33230.
[53] V. Steenhoff, M. Theuring, M. Vehse, K. Von Maydell, *Adv. Opt. Mater.* **2015**, *3*, 182.
[54] Q. Li, K. Du, K. Mao, X. Fang, D. Zhao, H. Ye, M. Qiu, *Sci. Rep.* **2016**, *6*, 29195.
[55] S. Y. Myong, S. S. Kim, K. S. Lim, *J. Appl. Phys.* **2004**, *95*, 1525.
[56] K. T. Lee, J. Y. Lee, S. Seo, L. J. Guo, *Light: Sci. Appl.* **2014**, *3*, 1.
[57] A. Bidiville, T. Koida, M. Kondo, K. Saito, K. Maejima, M. Matsumoto, H. Sai, T. Matsui, T. Suezaki, I. Yoshida, *Jpn. J. Appl. Phys.* **2015**, *54*, 08KB10.
[58] D. Liu, L. Wang, Q. Cui, L. J. Guo, *Adv. Sci.* **2018**, *5*, 1.
[59] Q. Liu, P. Romero-Gomez, P. Mantilla-Perez, S. Colodrero, J. Toudert, J. Martorell, *Adv. Energy Mater.* **2017**, *7*, 1.
[60] A. Ghobadi, T. Gamze, U. Ghobadi, A. K. Okyay, E. Ozbay, *Photonics Res.* **2018**, *6*, 244.
[61] T. G. Ulusoy Ghobadi, A. Ghobadi, T. Okyay, K. Topalli, A. K. Okyay, *RSC Adv.* **2016**, *6*, 112520.
[62] A. Ghobadi, H. I. Yavuz, T. G. Ulusoy, K. C. Icli, M. Ozenbas, A. K. Okyay, *Electrochim. Acta* **2015**, *157*, 23.
[63] A. Ghobadi, T. G. Ulusoy, R. Garifullin, M. O. Guler, A. K. Okyay, *Sci. Rep.* **2016**, *6*, 30587.
[64] A. Ghobadi, T. G. U. Ghobadi, F. Karadas, E. Ozbay, *Sci. Rep.* **2018**, *8*, 16322.
[65] T. G. U. Ghobadi, A. Ghobadi, E. Ozbay, F. Karadas, *ChemPhotoChem* **2018**, *2*, 161.
[66] W. R. Erwin, H. F. Zarick, E. M. Talbert, R. Bardhan, *Energy Environ. Sci.* **2016**, *9*, 1577.
[67] M. Wang, M. Ye, J. Iocozzia, C. Lin, Z. Lin, *Adv. Sci.* **2015**, *3*, 14.
[68] S. K. Cushing, J. Li, F. Meng, T. R. Senty, S. Suri, M. Zhi, M. Li, A. D. Bristow, N. Wu, *J. Am. Chem. Soc.* **2012**, *134*, 15033.
[69] S. K. Cushing, A. D. Bristow, N. Wu, *Phys. Chem. Chem. Phys.* **2015**, *17*, 30013.
[70] H. A. Atwater, A. Polman, *Nat. Mater.* **2010**, *9*, 205.
[71] J. J. Mock, D. R. Smith, S. Schultz, *Nano Lett.* **2003**, *3*, 485.
[72] P. K. Jain, K. S. Lee, I. H. El-Sayed, M. A. El-Sayed, *J. Phys. Chem. B* **2006**, *110*, 7238.
[73] T. Ishida, T. Tatsuma, *J. Phys. Chem. C* **2018**, *122*, 26153.
[74] C. Deeb, X. Zhou, J. Plain, G. P. Wiederrecht, R. Bachelot, M. Russell, P. K. Jain, *J. Phys. Chem. C* **2013**, *117*, 10669.
[75] W. R. Erwin, A. Coppola, H. F. Zarick, P. Arora, K. J. Miller, R. Bardhan, *Nanoscale* **2014**, *6*, 12626.
[76] A. Sousa-Castillo, M. Comesana-Hermo, B. Rodriguez-Gonzalez, M. Perez-Lorenzo, Z. Wang, X. T. Kong, A. O. Govorov, M. A. Correa-Duarte, *J. Phys. Chem. C* **2016**, *120*, 11690.
[77] H. R. Stuart, D. G. Hall, *Appl. Phys. Lett.* **1996**, *69*, 2327.
[78] D. Derkacs, S. H. Lim, P. Matheu, W. Mar, E. T. Yu, *Appl. Phys. Lett.* **2006**, *89*, 093103.
[79] K. Nakayama, K. Tanabe, H. A. Atwater, *Appl. Phys. Lett.* **2008**, *93*, 1.
[80] P. U. Londhe, A. B. Rohom, N. B. Chaure, *Nanosci. Nanotechnol.* **2016**, *6*, 43.
[81] J. D. Winans, C. Hungerford, K. Shome, L. J. Rothberg, P. M. Fauchet, *Opt. Express* **2015**, *23*, A92.
[82] P. Spinelli, A. Polman, *Opt. Express* **2012**, *20*, A641.
[83] G. Faraone, R. Modi, S. Marom, A. Podestà, M. Di Vece, *Opt. Mater.* **2018**, *75*, 204.
[84] M. Lee, J. U. Kim, K. J. Lee, S. Ahn, Y. B. Shin, J. Shin, C. B. Park, *ACS Nano* **2015**, *9*, 6206.
[85] M. Gross Koren, H. Dotan, A. Rothschild, *J. Phys. Chem. C* **2016**, *120*, 15042.
[86] J. Wang, S. Pan, M. Chen, D. A. Dixon, *J. Phys. Chem. C* **2013**, *117*, 22060.
[87] P. S. Archana, N. Pachauri, Z. Shan, S. Pan, A. Gupta, *J. Phys. Chem. C* **2015**, *119*, 15506.
[88] S. Y. Jeong, H. M. Shin, Y. R. Jo, Y. J. Kim, S. Kim, W. J. Lee, G. J. Lee, J. Song, B. J. Moon, S. Seo, H. An, S. H. Lee, Y. M. Song, B. J. Kim, M. H. Yoon, S. Lee, *J. Phys. Chem. C* **2018**, *122*, 7088.
[89] F. Xu, Y. Yao, D. Bai, R. Xu, J. Mei, D. Wu, Z. Gao, K. Jiang, *RSC Adv.* **2015**, *5*, 60339.
[90] K. Leonard, J. You, Y. Takahashi, H. Yonemura, J. Kurawaki, S. Yamada, *J. Phys. Chem. C* **2015**, *119*, 8829.
[91] L. Zhang, L. O. Herrmann, J. J. Baumberg, *Sci. Rep.* **2015**, *5*, 12.
[92] M. Yao, X. Jia, Y. Liu, W. Guo, L. Shen, S. Ruan, *ACS Appl. Mater. Interfaces* **2015**, *7*, 18866.
[93] S. C. Chen, Y. J. Chen, W. T. Chen, Y. T. Yen, T. S. Kao, T. Y. Chuang, Y. K. Liao, K. H. Wu, A. Yabushita, T. P. Hsieh, M. D. B. Charlton, D. P. Tsai, H. C. Kuo, Y. L. Chueh, *ACS Nano* **2014**, *8*, 9341.
[94] P. M. Voroshilov, V. Ovchinnikov, A. Papadimitratos, A. A. Zakhidov, C. R. Simovski, *ACS Photonics* **2018**, *5*, 1767.
[95] J. A. Schuller, E. S. Barnard, W. Cai, Y. C. Jun, J. S. White, M. L. Brongersma, *Nat. Mater.* **2010**, *9*, 193.
[96] N. Zhang, Z. Ji, A. R. Cheney, H. Song, D. Ji, X. Zeng, B. Chen, T. Zhang, A. N. Cartwright, K. Shi, Q. Gan, *Sci. Rep.* **2017**, *7*, 1.
[97] S. Y. Chou, W. Ding, *Opt. Express* **2013**, *21*, A60.
[98] C. Hägglund, S. P. Apell, *J. Phys. Chem. Lett.* **2012**, *3*, 1275.
[99] C. Hägglund, G. Zeltzer, R. Ruiz, I. Thomann, H. B. R. Lee, M. L. Brongersma, S. F. Bent, *Nano Lett.* **2013**, *13*, 3352.
[100] Y. Wang, T. Sun, T. Paudel, Y. Zhang, Z. Ren, K. Kempa, *Nano Lett.* **2012**, *12*, 440.
[101] C. Hägglund, G. Zeltzer, R. Ruiz, A. Wangperawong, K. E. Roelofs, S. F. Bent, *ACS Photonics* **2016**, *3*, 456.
[102] S. M. Bahauddin, H. Robatjazi, I. Thomann, *ACS Photonics* **2016**, *3*, 853.
[103] V. Gusak, B. Kasemo, C. Hägglund, *ACS Nano* **2011**, *5*, 6218.
[104] W. Wang, A. Klots, D. Prasai, Y. Yang, K. I. Bolotin, J. Valentine, *Nano Lett.* **2015**, *15*, 7440.
[105] D. Huo, J. Zhang, H. Wang, X. Ren, C. Wang, H. Su, H. Zhao, *Nanoscale Res. Lett.* **2017**, *12*, 1.
[106] W. B. Shi, R. H. Fan, K. Zhang, D. H. Xu, X. Xiong, R. W. Peng, M. Wang, *J. Appl. Phys.* **2015**, *117*, 065104.
[107] J. Poursafar, M. Bashirpour, M. Kolahdouz, A. Vakilipour Takaloo, M. Masnadi-Shirazi, E. Asl-Soleimani, *Sol. Energy* **2018**, *166*, 98.
[108] P. Prabhathan, V. M. Murukeshan, *Plasmonics* **2016**, *11*, 253.
[109] D. Liu, D. M. Bierman, A. Lenert, H.-T. Yu, Z. Yang, E. N. Wang, Y.-Y. Duan, *Opt. Express* **2015**, *23*, A1491.
[110] H. Heidarzadeh, A. Rostami, M. Dolatyari, G. Rostami, *Appl. Opt.* **2016**, *55*, 1779.
[111] M. Schmid, J. Klaer, R. Klenk, M. Topič, J. Krč, *Thin Solid Films* **2013**, *527*, 308.
[112] F. Enrichi, A. Quandt, G. C. Righini, *Renewable Sustainable Energy Rev.* **2018**, *82*, 2433.
[113] S. Jain, V. Depauw, V. D. Miljkovic, A. Dmitriev, C. Trompoukis, I. Gordon, P. Van Dorpe, O. El Daif, *Prog. Photovoltaics* **2016**, *9*, 261.
[114] V. E. Ferry, L. A. Sweatlock, D. Pacifici, H. A. Atwater, *Nano Lett.* **2008**, *8*, 4391.
[115] W. Wang, S. Wu, K. Reinhardt, Y. Lu, S. Chen, *Nano Lett.* **2010**, *10*, 2012.
[116] J. Park, J. H. Kang, S. J. Kim, E. Hasman, M. L. Brongersma, *IEEE Photonics Technol. Lett.* **2015**, *27*, 1617.
[117] M. Esfandyarpour, E. C. Garnett, Y. Cui, M. D. McGehee, M. L. Brongersma, *Nat. Nanotechnol.* **2014**, *9*, 542.
[118] J. Goffard, F. Mollica, A. Cattoni, C. Sauvan, P. Lalanne, C. Colin, F. Mollica, A. Cattoni, C. Sauvan, P. Lalanne, J. F. Guillemoles, N. Naghavi, S. Collin, *IEEE J. Photovoltaics* **2017**, *7*, 1433.

[119] H. L. Chen, A. Cattoni, N. Vandamme, J. Goffard, A. Lemaitre, A. Delamarre, B. Behaghel, K. Watanabe, M. Sugiyama, J. F. Guillemoles, S. Collin, in *2017 IEEE 44th Photovolt. Spec. Conf. PVSC 2017*, IEEE, Portland, OR, USA **2016**, 3506.
[120] A. Ghobadi, H. Hajian, M. Gokbayrak, S. A. Dereshgi, A. Toprak, B. Butun, E. Ozbay, *Opt. Express* **2017**, *25*, 27624.
[121] D. U. Yildirim, A. Ghobadi, E. Ozbay, *Sci. Rep.* **2018**, *8*, 1.
[122] C. E. Petoukhoff, D. M. O'Carroll, *Nat. Commun.* **2015**, *6*, 1.
[123] C. E. Petoukhoff, M. B. M. Krishna, D. Voiry, I. Bozkurt, S. Deckoff-Jones, M. Chhowalla, D. M. O'Carroll, K. M. Dani, *ACS Nano* **2016**, *10*, 9899.
[124] Q. D. Ou, H. J. Xie, J. De Chen, L. Zhou, Y. Q. Li, J. X. Tang, *J. Mater. Chem. A* **2016**, *4*, 18952.
[125] X. Xu, H. Kwon, B. Gawlik, N. Mohammadi Estakhri, A. Alù, S. V. Sreenivasan, A. Dodabalapur, *Nano Lett.* **2018**, *18*, 3362.
[126] P. Manley, F. F. Abdi, S. Berglund, A. T. M. N. Islam, S. Burger, R. van de Krol, M. Schmid, *ACS Appl. Energy Mater.* **2018**, *1*, 5810.
[127] M. Z. Hasan, C. L. Kane, *Rev. Mod. Phys.* **2010**, *82*, 3045.
[128] Z. Yue, B. Cai, L. Wang, X. Wang, M. Gu, *Sci. Adv.* **2016**, *2*, e1501536.
[129] F. Ding, Y. Yang, R. A. Deshpande, S. I. Bozhevolnyi, *Nanophotonics* **2018**, *7*, 1129.
[130] M. G. Nielsen, A. Pors, O. Albrektsen, S. I. Bozhevolnyi, *Opt. Express* **2012**, *20*, 13311.
[131] M. G. Nielsen, D. K. Gramotnev, A. Pors, O. Albrektsen, S. I. Bozhevolnyi, *Opt. Express* **2011**, *19*, 19310.
[132] F. Ding, J. Dai, Y. Chen, J. Zhu, Y. Jin, S. I. Bozhevolnyi, *Sci. Rep.* **2016**, *6*, 39445.
[133] A. Vora, J. Gwamuri, N. Pala, A. Kulkarni, J. M. Pearce, D. O. Güney, *Sci. Rep.* **2014**, *4*, 1.
[134] N. Vandamme, N. Bardou, C. Dupuis, *ACS Photonics* **2014**, *1*, 878.
[135] T. Sun, C. F. Guo, F. Cao, E. M. Akinoglu, Y. Wang, M. Giersig, Z. Ren, K. Kempa, *Appl. Phys. Lett.* **2014**, *104*, 1.
[136] M. Choi, G. Kang, D. Shin, N. Barange, C. W. Lee, D. H. Ko, K. Kim, *ACS Appl. Mater. Interfaces* **2016**, *8*, 12997.
[137] R. Chikkaraddy, B. De Nijs, F. Benz, S. J. Barrow, O. A. Scherman, E. Rosta, A. Demetriadou, P. Fox, O. Hess, J. J. Baumberg, *Nature* **2016**, *535*, 127.
[138] X. Chen, Y. H. Chen, J. Qin, D. Zhao, B. Ding, R. J. Blaikie, M. Qiu, *Nano Lett.* **2017**, *17*, 3246.
[139] K. Liu, H. Hu, H. Song, X. Zeng, D. Ji, S. Jiang, Q. Gan, *IEEE Photonics Technol. Lett.* **2013**, *25*, 1266.
[140] D. O. Sigle, L. Zhang, S. Ithurria, B. Dubertret, J. J. Baumberg, *J. Phys. Chem. Lett.* **2015**, *6*, 1099.
[141] Y. Lu, W. Dong, Z. Chen, A. Pors, Z. Wang, S. I. Bozhevolnyi, *Sci. Rep.* **2016**, *6*, 1.
[142] F. Tan, N. Wang, D. Y. Lei, W. Yu, X. Zhang, *Adv. Opt. Mater.* **2017**, *5*, 1.
[143] X. Shi, K. Ueno, T. Oshikiri, Q. Sun, K. Sasaki, H. Misawa, *Nat. Nanotechnol.* **2018**, *13*, 953.
[144] L. Zhu, K. Liu, T. Hu, W. Dong, Z. Chen, Z. Wang, *Nanoscale* **2018**, *10*, 12848.
[145] A. Dutta, A. Naldoni, F. Malara, A. O. Govorov, V. Shalaev, A. Boltasseva, *Faraday Discuss.* **2018**, https://doi.org/10.1039/c8fd00148k.
[146] Y. A. Akimov, W. S. Koh, S. Y. Sian, S. Ren, *Appl. Phys. Lett.* **2010**, *96*, 073111.
[147] P. Matheu, S. H. Lim, D. Derkacs, C. McPheeters, E. T. Yu, *Appl. Phys. Lett.* **2008**, *93*, 113108.
[148] A. Devilez, X. Zambrana-Puyalto, B. Stout, N. Bonod, *Phys. Rev. B* **2015**, *92*, 24.
[149] X. Fan, W. Zheng, D. J. Singh, *Light: Sci. Appl.* **2014**, *3*, e179.
[150] H. K. Raut, V. A. Ganesh, A. S. Nair, S. Ramakrishna, *Energy Environ. Sci.* **2011**, *4*, 3779.
[151] J. Zhao, M. A. Green, *IEEE Trans. Electron Devices* **1991**, *38*, 1925.
[152] W.-L. Min, B. Jiang, P. Jiang, *Adv. Mater.* **2008**, *20*, 3914.
[153] D. Derkacs, W. V. Chen, P. M. Matheu, S. H. Lim, P. K. L. Yu, E. T. Yu, *Appl. Phys. Lett.* **2008**, *93*, 091107.
[154] G. Yin, P. Manley, M. Schmid, *Sol. Energy Mater. Sol. Cells* **2016**, *153*, 124.
[155] Q. Luo, X. Deng, C. Zhang, M. Yu, X. Zhou, Z. Wang, X. Chen, S. Huang, *Sol. Energy* **2018**, *169*, 128.
[156] K. Askar, Z. Gu, C. J. Leverant, J. Wang, C. Kim, B. Jiang, P. Jiang, *Opt. Lett.* **2018**, *43*, 5238.
[157] D. Wan, H. L. Chen, T. C. Tseng, C. Y. Fang, Y. S. Lai, F. Y. Yeh, *Adv. Funct. Mater.* **2010**, *20*, 3064.
[158] J. R. Nagel, M. A. Scarpulla, *Opt. Express* **2010**, *18*, A139.
[159] A. Jiménez-Solano, S. Carretero-Palacios, H. Míguez, *Opt. Express* **2018**, *26*, A865.
[160] S. Nunomura, A. Minowa, H. Sai, M. Kondo, *Appl. Phys. Lett.* **2010**, *97*, 063507.
[161] M. A. S. James, R. Negal, *Appl. Phys. Lett.* **2013**, *102*, 033106.
[162] M. Theuring, P. H. Wang, M. Vehse, V. Steenhoff, K. Von Maydell, C. Agert, A. G. Brolo, *J. Phys. Chem. Lett.* **2014**, *5*, 3302.
[163] C. Van Lare, G. Yin, A. Polman, M. Schmid, *ACS Nano* **2015**, *9*, 9603.
[164] G. Yin, M. Song, S. Duan, P. Manley, D. Greiner, C. A. Kaufmann, M. Schmid, *ACS Appl. Mater. Interfaces* **2016**, *8*, 31646.
[165] H. K. Raut, S. S. Dinachali, A. Y. He, V. A. Ganesh, M. S. M. Saifullah, J. Law, S. Ramakrishna, *Energy Environ. Sci.* **2013**, *6*, 1929.
[166] S. Y. Heo, J. K. Koh, G. Kang, S. H. Ahn, W. S. Chi, K. Kim, J. H. Kim, *Adv. Energy Mater.* **2014**, *4*, 1300632.
[167] J. W. Leem, S. Kim, S. H. Lee, J. A. Rogers, E. Kim, J. S. Yu, *Adv. Energy Mater.* **2014**, *4*, 1301315.
[168] J. Ham, W. J. Dong, J. Y. Park, C. J. Yoo, I. Lee, J. L. Lee, *Adv. Mater.* **2015**, *27*, 4027.
[169] S. Schubert, M. Hermenau, J. Meiss, L. Müller-Meskamp, K. Leo, *Adv. Funct. Mater.* **2012**, *22*, 4993.
[170] H. W. Lin, S. W. Chiu, L. Y. Lin, Z. Y. Hung, Y. H. Chen, F. Lin, K. T. Wong, *Adv. Mater.* **2012**, *24*, 2269.
[171] P. M. Voroshilov, C. R. Simovski, P. A. Belov, A. S. Shalin, *J. Appl. Phys.* **2015**, *117*, 203101.
[172] D. Ha, C. Gong, M. S. Leite, J. N. Munday, *ACS Appl. Mater. Interfaces* **2016**, *8*, 24536.
[173] J. D. Myers, W. Cao, V. Cassidy, S. H. Eom, R. Zhou, L. Yang, W. You, J. Xue, *Energy Environ. Sci.* **2012**, *5*, 6900.
[174] L. K. Yeh, K. Y. Lai, G. J. Lin, P. H. Fu, H. C. Chang, C. A. Lin, J. H. He, *Adv. Energy Mater.* **2011**, *1*, 506.
[175] J. K. Hyun, C. Ahn, H. Kang, H. J. Kim, J. Park, K. H. Kim, C. W. Ahn, B. J. Kim, S. Jeon, *Small* **2013**, *9*, 369.
[176] J. Grandidier, D. M. Callahan, J. N. Munday, H. A. Atwater, *Adv. Mater.* **2011**, *23*, 1272.
[177] J. Zhang, X. Jin, P. I. Morales-Guzman, X. Yu, H. Liu, H. Zhang, L. Razzari, J. P. Claverie, *ACS Nano* **2016**, *10*, 4496.
[178] M. J. Mendes, A. Araújo, A. Vicente, H. Águas, I. Ferreira, E. Fortunato, R. Martins, *Nano Energy* **2016**, *26*, 286.
[179] A. Mihi, M. Bernechea, D. Kufer, G. Konstantatos, *Adv. Opt. Mater.* **2013**, *1*, 139.
[180] G. Kang, H. Park, D. Shin, S. Baek, M. Choi, D. H. Yu, K. Kim, W. J. Padilla, *Adv. Mater.* **2013**, *25*, 2617.
[181] Y. C. Chao, C. Y. Chen, C. A. Lin, J. H. He, *Energy Environ. Sci.* **2011**, *4*, 3436.
[182] L. Aé, D. Kieven, J. Chen, R. Klenk, T. Rissom, Y. Tang, M. Ch Lux-Steiner, *Prog. Photovoltaics* **2010**, *18*, 209.
[183] J. Yun, W. Wang, S. M. Kim, T. S. Bae, S. Lee, D. Kim, G. H. Lee, H. S. Lee, M. Song, *Energy Environ. Sci.* **2015**, *8*, 932.
[184] K. C. Park, H. J. Choi, C. H. Chang, R. E. Cohen, G. H. McKinley, G. Barbastathis, *ACS Nano* **2012**, *6*, 3789.
[185] K. H. Tsui, Q. Lin, H. Chou, Q. Zhang, H. Fu, P. Qi, Z. Fan, *Adv. Mater.* **2014**, *26*, 2805.
[186] C. Cho, H. Kim, S. Jeong, S. W. Baek, J. W. Seo, D. Han, K. Kim, Y. Park, S. Yoo, J. Y. Lee, *Sol. Energy Mater. Sol. Cells* **2013**, *115*, 36.

[187] J. Ham, W. J. Dong, G. H. Jung, J. L. Lee, *ACS Appl. Mater. Interfaces* **2016**, *8*, 5990.
[188] I. Hwang, D. Choi, S. Lee, J. H. Seo, K. H. Kim, I. Yoon, K. Seo, *ACS Appl. Mater. Interfaces* **2017**, *9*, 21276.
[189] R. T. Ginting, E. B. Jeon, J. M. Kim, W. Y. Jin, J. W. Kang, *ACS Appl. Mater. Interfaces* **2018**, *10*, 31291.
[190] S. Esiner, T. Bus, M. M. Wienk, K. Hermans, R. A. J. Janssen, *Adv. Energy Mater.* **2013**, *3*, 1013.
[191] L. Hu, G. Zheng, J. Yao, N. Liu, B. Weil, M. Eskilsson, E. Karabulut, Z. Ruan, S. Fan, J. T. Bloking, M. D. McGehee, L. Wågberg, Y. Cui, *Energy Environ. Sci.* **2013**, *6*, 513.
[192] D. Ha, Z. Fang, L. Hu, J. N. Munday, *Adv. Energy Mater.* **2014**, *4*, 1301804.
[193] Z. Fang, H. Zhu, Y. Yuan, D. Ha, S. Zhu, C. Preston, Q. Chen, Y. Li, X. Han, S. Lee, G. Chen, T. Li, J. Munday, J. Huang, L. Hu, *Nano Lett.* **2014**, *14*, 765.
[194] D. M. N. M. Dissanayake, B. Roberts, P. C. Ku, *Appl. Phys. Lett.* **2012**, *101*, 063302.
[195] S. M. Lee, A. Kwong, D. Jung, J. Faucher, R. Biswas, L. Shen, D. Kang, M. L. Lee, J. Yoon, *ACS Nano* **2015**, *9*, 10356.
[196] A. I. Kuznetsov, A. E. Miroshnichenko, M. L. Brongersma, Y. S. Kivshar, B. Luk'yanchuk, *Science* **2016**, *354*, aag2472.
[197] Y. Zhang, M. Nieto-Vesperinas, J. J. Sáenz, *J. Opt.* **2015**, *17*, 1.
[198] A. B. Evlyukhin, C. Reinhardt, A. Seidel, B. S. Luk'Yanchuk, B. N. Chichkov, *Phys. Rev. B* **2010**, *82*, 1.
[199] A. Garcia-Etxarri, R. Gomez-Medina, L. S. Froufe-Perez, C. Lopez, L. Chantada, F. Scheffold, J. Aizpurua, M. Nieto-Vesperinas, J. J. Saenz, *Opt. Express* **2010**, *19*, 4815.
[200] Y. Yang, O. D. Miller, T. Christensen, J. D. Joannopoulos, M. Soljačić, *Nano Lett.* **2017**, *17*, 3238.
[201] Y. H. Fu, A. I. Kuznetsov, A. E. Miroshnichenko, Y. F. Yu, B. Luk'yanchuk, *Nat. Commun.* **2013**, *4*, 1.
[202] E. K. Lee, J. H. Song, K. Y. Jeong, J. H. Kang, H. G. Park, M. K. Seo, *Sci. Rep.* **2015**, *5*, 1.
[203] H. S. Ee, J. H. Kang, M. L. Brongersma, M. K. Seo, *Nano Lett.* **2015**, *15*, 1759.
[204] R. Paniagua-Domínguez, Y. F. Yu, A. E. Miroshnichenko, L. A. Krivitsky, Y. H. Fu, V. Valuckas, L. Gonzaga, Y. T. Toh, A. Y. S. Kay, B. Lukyanchuk, A. I. Kuznetsov, *Nat. Commun.* **2016**, *7*, 1.
[205] U. Zywietz, A. B. Evlyukhin, C. Reinhardt, B. N. Chichkov, *Nat. Commun.* **2014**, *5*, 1.
[206] I. Staude, A. E. Miroshnichenko, M. Decker, N. T. Fofang, S. Liu, E. Gonzales, J. Dominguez, T. S. Luk, D. N. Neshev, I. Brener, Y. Kivshar, *ACS Nano* **2013**, *7*, 7824.
[207] L. Cao, J. S. White, J. S. Park, J. A. Schuller, B. M. Clemens, M. L. Brongersma, *Nat. Mater.* **2009**, *8*, 643.
[208] D. R. Abujetas, R. Paniagua-Domínguez, J. A. Sánchez-Gil, *ACS Photonics* **2015**, *2*, 921.
[209] L. Cao, P. Fan, A. P. Vasudev, J. S. White, Z. Yu, W. Cai, J. A. Schuller, S. Fan, M. L. Brongersma, *Nano Lett.* **2010**, *10*, 439.
[210] S. J. Kim, J. Park, M. Esfandyarpour, E. F. Pecora, P. G. Kik, M. L. Brongersma, *Nano Lett.* **2016**, *16*, 3801.
[211] N. Odebo Länk, R. Verre, P. Johansson, M. Käll, *Nano Lett.* **2017**, *17*, 3054.
[212] J. Tian, H. Luo, Q. Li, X. Pei, K. Du, M. Qiu, *Laser Photonics Rev.* **2018**, *12*, 1.
[213] J. A. Giese, J. W. Yoon, B. R. Wenner, J. W. Allen, M. S. Allen, R. Magnusson, *Opt. Lett.* **2014**, *39*, 486.
[214] R. A. Pala, S. Butun, K. Aydin, H. A. Atwater, *Sci. Rep.* **2016**, *6*, 1.
[215] J. Wu, *Opt. Laser Technol.* **2016**, *79*, 95.
[216] K. V. Baryshnikova, M. I. Petrov, V. E. Babicheva, P. A. Belov, *Sci. Rep.* **2016**, *6*, 1.
[217] P. Spinelli, M. A. Verschuuren, A. Polman, *IEEE J. Photovoltaics* **2014**, *4*, 554.
[218] P. Spinelli, M. A. Verschuuren, A. Polman, *Nat. Commun.* **2012**, *3*, 692.
[219] E. F. Pecora, A. Cordaro, P. G. Kik, M. L. Brongersma, *ACS Photonics* **2018**, *5*, 4456.
[220] S. A. Mann, E. C. Garnett, *Nano Lett.* **2013**, *13*, 3173.
[221] T. Gollisch, A. V. M. Herz, *ACS Photonics* **2015**, *2*, 653.
[222] Z. Huang, J. Wang, Z. Liu, G. Xu, Y. Fan, H. Zhong, B. Cao, C. Wang, K. Xu, *J. Phys. Chem. C* **2015**, *119*, 28127.
[223] G. Liu, J. Chen, P. Pan, Z. Liu, *IEEE J. Sel. Top. Quantum Electron.* **2019**, *25*, 1.
[224] S. Roy, *Plasmonics* **2018**, *13*, 1499.
[225] G. Liu, Y. Nie, G. Fu, X. Liu, Y. Liu, L. Tang, Z. Liu, *Nanotechnology* **2017**, *28*, 1.
[226] B. C. P. Sturmberg, T. K. Chong, D.-Y. Choi, T. P. White, L. C. Botten, K. B. Dossou, C. G. Poulton, K. R. Catchpole, R. C. McPhedran, C. Martijn de Sterke, *Optica* **2016**, *3*, 556.
[227] F. Pratesi, M. Burresi, F. Riboli, K. Vynck, D. S. Wiersma, *Opt. Express* **2013**, *21*, A460.
[228] Q. Qian, T. Sun, Y. Yan, C. Wang, *Adv. Opt. Mater.* **2017**, *5*, 1.
[229] V. K. Narasimhan, T. M. Hymel, R. A. Lai, Y. Cui, *ACS Nano* **2015**, *9*, 10590.
[230] S. J. Kim, P. Fan, J. H. Kang, M. L. Brongersma, *Nat. Commun.* **2015**, *6*, 1.
[231] P. Molet, J. L. Garcia-Pomar, C. Matricardi, M. Garriga, M. I. Alonso, A. Mihi, *Adv. Mater.* **2018**, *30*, 1705876.
[232] S. J. Kim, I. Thomann, J. Park, J. H. Kang, A. P. Vasudev, M. L. Brongersma, *Nano Lett.* **2014**, *14*, 1446.
[233] C. Yang, X. Xi, Z. Yu, H. Cao, J. Li, S. Lin, Z. Ma, L. Zhao, *ACS Appl. Mater. Interfaces* **2018**, *10*, 5492.
[234] L. Shi, W. Zhou, Z. Li, S. Koul, A. Kushima, Y. Yang, *ACS Nano* **2018**, *12*, 6335.
[235] L. Gao, Y. Cui, R. H. J. Vervuurt, D. Van Dam, R. P. J. Van Veldhoven, J. P. Hofmann, A. A. Bol, J. E. M. Haverkort, P. H. L. Notten, E. P. A. M. Bakkers, E. J. M. Hensen, *Adv. Funct. Mater.* **2016**, *26*, 679.
[236] L. Shen, C. He, J. Qiu, S. M. Lee, A. Kalita, S. B. Cronin, M. P. Stoykovich, J. Yoon, *ACS Appl. Mater. Interfaces* **2015**, *7*, 26043.
[237] S. F. Leung, Q. Zhang, M. M. Tavakoli, J. He, X. Mo, Z. Fan, *Small* **2016**, *12*, 2536.
[238] A. Ghobadi, S. A. Dereshgi, H. Hajian, G. Birant, B. Butun, A. Bek, E. Ozbay, *Nanoscale* **2017**, *9*, 16652.
[239] H. Gao, C. Liu, H. E. Jeong, P. Yang, *ACS Nano* **2012**, *6*, 234.
[240] V. Gusak, B. Kasemo, C. Hägglund, *J. Phys. Chem. C* **2014**, *118*, 22840.
[241] J. Y. Lu, S. H. Nam, K. Wilke, A. Raza, Y. E. Lee, A. AlGhaferi, N. X. Fang, T. J. Zhang, *Adv. Opt. Mater.* **2016**, *4*, 1255.
[242] V. E. Ferry, M. A. Verschuuren, M. C. Van Lare, R. E. I. Schropp, H. A. Atwater, A. Polman, *Nano Lett.* **2011**, *11*, 4239.
[243] C. Battaglia, C. M. Hsu, K. Söderström, J. Escarré, F. J. Haug, M. Charrière, M. Boccard, M. Despeisse, D. T. L. Alexander, M. Cantoni, Y. Cui, C. Ballif, *ACS Nano* **2012**, *6*, 2790.
[244] Y. Qiu, S. F. Leung, Q. Zhang, B. Hua, Q. Lin, Z. Wei, K. H. Tsui, Y. Zhang, S. Yang, Z. Fan, *Nano Lett.* **2014**, *14*, 2123.
[245] S. Hussain, S. Hussain, A. Waleed, M. M. Tavakoli, S. Yang, M. K. Rauf, Z. Fan, M. A. Nadeem, *J. Phys. Chem. C* **2017**, *121*, 18360.
[246] Q. Lin, D. Sarkar, Y. Lin, M. Yeung, L. Blankemeier, J. Hazra, W. Wang, S. Niu, J. Ravichandran, Z. Fan, R. Kapadia, *ACS Nano* **2017**, *11*, 5113.
[247] Q. Lin, S. F. Leung, L. Lu, X. Chen, Z. Chen, H. Tang, W. Su, D. Li, Z. Fan, *ACS Nano* **2014**, *8*, 6484.
[248] Y. Qiu, W. Liu, W. Chen, W. Chen, G. Zhou, P.-C. Hsu, R. Zhang, Z. Liang, S. Fan, Y. Zhang, Y. Cui, *Sci. Adv.* **2016**, *2*, e1501764.
[249] J. Zhao, Y. Guo, L. Cai, H. Li, K. X. Wang, I. S. Cho, C. H. Lee, S. Fan, X. Zheng, *ACS Energy Lett.* **2016**, *1*, 68.

[250] B. Chen, Z. Zhang, M. Baek, S. Kim, W. Kim, K. Yong, *Appl. Catal., B* **2018**, *237*, 763.
[251] Y. Lin, Z. Xu, D. Yu, L. Lu, M. Yin, M. M. Tavakoli, X. Chen, Y. Hao, Z. Fan, Y. Cui, D. Li, *ACS Appl. Mater. Interfaces* **2016**, *8*, 10929.
[252] Y. Cho, B. Cho, Y. Kim, J. Lee, E. Kim, T. T. T. Nguyen, J. H. Lee, S. Yoon, D. H. Kim, J. H. Choi, D. W. Kim, *ACS Appl. Mater. Interfaces* **2017**, *9*, 6314.
[253] R. Fan, J. Mao, Z. Yin, J. Jie, W. Dong, L. Fang, F. Zheng, M. Shen, *ACS Appl. Mater. Interfaces* **2017**, *9*, 6123.
[254] D. Liang, Y. Huo, Y. Kang, K. X. Wang, A. Gu, M. Tan, Z. Yu, S. Li, J. Jia, X. Bao, S. Wang, Y. Yao, H. S. P. Wong, S. Fan, Y. Cui, J. S. Harris, *Adv. Energy Mater.* **2012**, *2*, 1254.
[255] C. M. Hsu, C. Battaglia, C. Pahud, Z. Ruan, F. J. Haug, S. H. Fan, C. Ballif, Y. Cui, *Adv. Energy Mater.* **2012**, *2*, 628.
[256] J. Kim, A. J. Hong, J. W. Nah, B. Shin, F. M. Ross, D. K. Sadana, *ACS Nano* **2012**, *6*, 265.
[257] J. Kim, C. Battaglia, M. Charrière, A. Hong, W. Jung, H. Park, C. Ballif, D. Sadana, *Adv. Mater.* **2014**, *26*, 4082.
[258] K. X. Wang, Z. Yu, V. Liu, M. L. Brongersma, T. F. Jaramillo, S. Fan, *ACS Photonics* **2014**, *1*, 235.
[259] J. Li, Y. Qiu, Z. Wei, Q. Lin, Q. Zhang, K. Yan, H. Chen, S. Xiao, Z. Fan, S. Yang, *Energy Environ. Sci.* **2014**, *7*, 3651.
[260] Y. Yu, L. Huang, L. Cao, *Sci. Rep.* **2014**, *4*, 1.
[261] Y. Lin, C. Battaglia, M. Boccard, M. Hettick, Z. Yu, C. Ballif, J. W. Ager, A. Javey, *Nano Lett.* **2013**, *13*, 5615.